2019-11-01

# Groundwater Level Mapping Tool: Development of a Web Application to Effectively Characterize Groundwater Resources

Steven William Evans
*Brigham Young University*

Groundwater Level Mapping Tool: Development of a Web Application to Effectively

Characterize Groundwater Resources

Steven William Evans

A thesis submitted to the faculty of
Brigham Young University
in partial fulfillment of the requirements for the degree of

Master of Science

Norman L. Jones, Chair
Daniel P. Ames
Gus P. Williams

Department of Civil and Environmental Engineering

Brigham Young University

ABSTRACT

Groundwater Level Mapping Tool: Development of a Web Application to Effectively
Characterize Groundwater Resources

Steven William Evans
Department of Civil and Environmental Engineering, BYU
Master of Science

Groundwater is used worldwide as a major source for agricultural irrigation, industrial processes, mining, and drinking water. An accurate understanding of groundwater levels and trends is essential for decision makers to effectively manage groundwater resources throughout an aquifer, ensuring its sustainable development and usage. Unfortunately, groundwater is one of the most challenging and expensive water resources to characterize, quantify, and monitor on a regional basis. Data, though present, are often limited or sporadic, and are generally not used to their full potential to aid decision makers in their groundwater management.

This thesis presents a solution to this under-utilization of available data through the creation of an open-source, Python-based web application used to characterize, visualize, and quantify groundwater resources on a regional basis. This application includes tools to extrapolate and interpolate time series observations of groundwater levels in monitoring wells through multi-linear regression, using correlated data from other wells. It is also possible to extrapolate time series observations using machine learning techniques with Earth observations as inputs. The app also performs spatial interpolation using GSLIB Kriging code. Combining the results of spatial and temporal interpolation, the app enables the user to calculate changes in aquifer storage, and to produce and view aquifer-wide maps and animations of groundwater levels over time. This tool will provide decision makers with an easy to use and easy to understand method for tracking groundwater resources. Thus far, this tool has been used to map groundwater in Texas, Utah, South Africa, Colombia, and the Dominican Republic.

# ACKNOWLEDGEMENTS

I would like to thank my parents, Richard and Claudia Evans, for their love and support throughout my entire life. They taught me how to work hard, how to think, how to learn, and to follow the Lord Jesus Christ. Anything that I accomplish or achieve is because of the foundation laid for me by my wonderful parents. I would like to thank Dr. Wood Miller and Dr. Rollin Hotchkiss for convincing me to stay at BYU and complete a master's degree. I would also like to thank Dr. Norm Jones for guiding my research, and teaching me about groundwater and interpolation. I would like to thank Dr. Dan Ames for teaching me how to program web applications with Python, and how to set up and use databases, which was essential for my research. I would like to thank Dr. Gus Williams for guiding me through the use of machine learning and other statistical techniques in this research. I would also like to thank NASA GEO for funding and supporting this research.

TABLE OF CONTENTS

# LIST OF TABLES

## LIST OF FIGURES

x

# 1 INTRODUCTION

Groundwater is depended on worldwide as a major source for agricultural irrigation, industrial processes, mining, and drinking water. The USGS reports that 30.1% of the Earth's fresh water consists of groundwater, while 1.2% consists of surface water in lakes, rivers, and streams (Gleick, 1993). Although fresh groundwater is so abundant, its responsible and sustainable use poses a significant challenge. Due in part to the difficulties associated with quantifying groundwater, many areas worldwide have severely and irreversibly depleted vast amounts of their groundwater resources, sometimes in complete ignorance. Worldwide examples of this depletion include the San Joaquin Valley in California, USA, where excessive groundwater pumping has resulted in land subsidence up to 28 feet since 1920 (Galloway & Riley, 1999), Mexico City, Mexico (Ortega‐Guerrero, Rudolph, & Cherry, 1999), and Jakarta, Indonesia (Abidin, Andreas, Djaja, Darmawan, & Gamal, 2008). These and other areas have permanently reduced potential aquifer storage volume as excessive groundwater withdrawal results in lower pore pressures and increased effective stress, which leads to the compaction of the aquifer system.

The case of California's San Joaquin Valley demonstrates the role of human activity in aquifer sustainability. Between the early 1900s and the late 1960s, the area relied almost exclusively on groundwater for agricultural irrigation. As of 1960, water levels in the deep aquifer system were declining at a rate of about 10 feet per year. During this time period, the

USGS began an intensive investigation into groundwater and land subsidence in the area. Later, as surface water from the Delta-Mendota Canal, the Friant-Kern Canal, and the California Aqueduct largely supplanted groundwater for irrigation of the valley in the late 1960s, water levels in the aquifer system made a dramatic recovery and land subsidence began to abate (Galloway & Riley, 1999). This case demonstrates that policies and practices can be implemented to improve the sustainable use of groundwater when decision makers are informed and aware of the past and present conditions of their aquifer.

## 1.1    Past Research and Background

One of the great challenges of groundwater sustainability is the ability to accurately characterize the state of an aquifer, so as to implement practices, procedures, and regulations to promote its sustainable use. Although fresh groundwater is often abundant, and prevalently used in some areas, it is difficult and expensive to accurately quantify groundwater compared to surface water resources. The state of surface water resources is readily visible to the naked eye, can be measured easily, and is straightforward to quantify. This is not the case for groundwater, which generally requires drilling a monitoring well in order to measure the location of the phreatic surface. While surface storage in a waterbody reaches approximately the same elevation throughout the body, groundwater surface elevations may vary significantly, by hundreds of feet in some cases, throughout an aquifer, depending on the overlying land use, pumping of irrigation wells, aquifer recharge, and other factors. Groundwater levels are heavily influenced by climatic, geographic, lithological, and human factors. For these reasons, it is difficult to quantify and map aquifer water levels and storage volumes.

2

Even when data on water surface elevations are available from monitoring wells drilled into an aquifer, these data are generally not harnessed to their full potential to aid in decision-making. These data are available at point locations scattered in time and space throughout an aquifer, and it is difficult to piece these segments of data together into a complete picture of aquifer-wide behavior. Point data from monitoring wells are typically sparse and give only a limited sampling of the spatial distribution of water levels in the aquifer, and the data observations from these monitoring wells are often temporally sporadic, including large gaps in the time series data, as demonstrated in Figure 1-1.
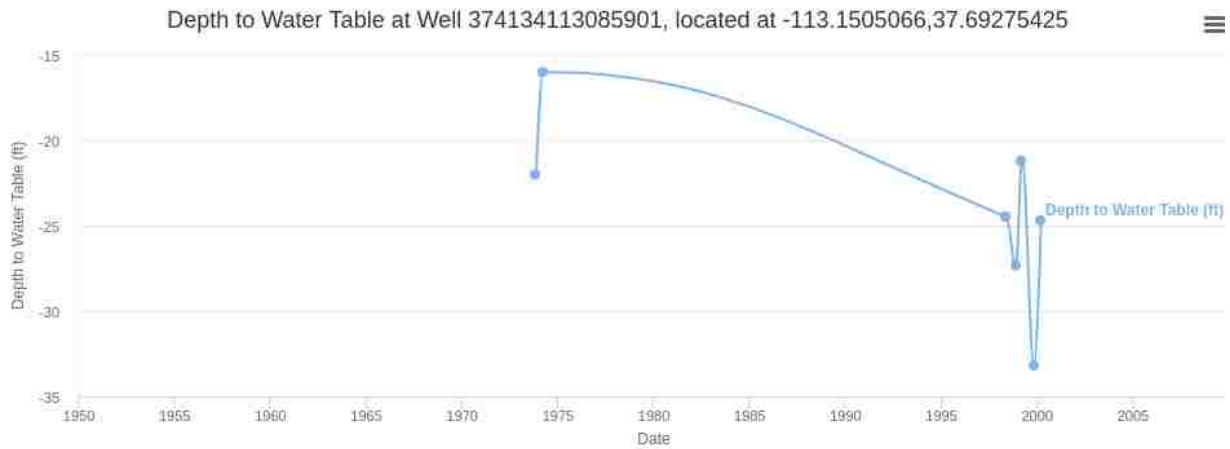


**Figure 1-1: Depth to Water Table at Well 374134113085901 near Cedar City, UT**

### 1.1.1 Spatial Interpolation of Groundwater Data

To solve these problems with data management and visualization of groundwater data, researchers have developed methods for interpolating, extrapolating, and visualizing existing data. One of the most widely used computer programs used for spatial interpolation in this and other fields is the Geostatistical Software Library (GSLIB), developed at Stanford University (Deutsch & Journel, 1992). This program performs spatial interpolation using the Kriging

3

technique pioneered by the South African statistician and mining engineer, Danie G. Krige. This Kriging interpolation technique is used by many researchers in groundwater when attempting to interpolate spatial data. Ahmadi and Sedghamiz (2007) used Kriging interpolation to estimate unknown depths to water table in an aquifer in Iran to a high level of accuracy. Other researchers demonstrated that the accuracy of groundwater surface elevation maps could be improved in some cases by introducing topography to the interpolation using Kriging with an external drift (Boezio, Costa, & Koppe, 2006).

### 1.1.2   Extension of Groundwater Data Through Earth Observations

Efforts have also been made to extend groundwater data through the use of satellite Earth observations. In March, 2002, NASA launched the GRACE (Gravity Recovery and Climate Experiment) mission, which includes two identical satellites that map variations in the gravitational pull of the Earth. The data collected by these satellites are used to calculate changes in the terrestrial water storage of the Earth, which accounts for a large portion of these gravitational anomalies (Tapley, Bettadpur, Ries, Thompson, & Watkins, 2004). Data from the GRACE mission have been used to estimate monthly changes in water storage over large regions, and researchers indicate that GRACE will provide a useful, direct measure of seasonal water storage for river-basin water balance analysis (Swenson, Wahr, & Milly, 2003). GRACE data have also been used to improve the accuracy of interpolated groundwater surface elevation maps in the Indo-Gangetic Basin by using cokriging with GRACE anomaly and TRMM (Tropical Rainfall Measuring Mission) precipitation data (M. Sahoo, Dhar, Kasot, & Kar, 2018). Other models pertinent to groundwater estimation have also been developed using earth observations, such as the Palmer Drought Severity Index, which uses temperature and precipitation observations to estimate relative dryness, and the Soil Moisture liquid water

4

equivalent thickness, which is obtained using a one-layer hydrological model using precipitation and temperature measurements as inputs (J. Huang, van den Dool, & Georgarakos, 1996).

### 1.1.3   Temporal Interpolation of Groundwater Data

Several techniques have been developed and used in an effort to improve the temporal interpolation and estimation of well time series observations. Rouhani and Wackernagel (1990) used Kriging to perform temporal interpolation of depth to water table time series measurements in a basin south of Paris, France. Bidwell (2005) forecasted groundwater levels one month ahead in Canterbury, New Zealand using an ARMAX model based on the eigenstructure of aquifer dynamics. Others have used classical time series models including auto-regressive (AR), moving-average (MA), auto-regressive moving-average (ARMA), auto-regressive integrated moving-average (ARIMA), and seasonal auto-regressive integrated moving-average (SARIMA), and multiple linear regression to predict groundwater levels (Khorasani, Ehteshami, Ghadimi, & Salari, 2016; Mirzavand & Ghazavi, 2015; S. Sahoo & Jha, 2013)

Researchers have also used GRACE satellite observations (Sun, 2013) and data from nearby wells (Sethi, Kumar, Sharma, & Verma, 2010) to predict groundwater levels using an artificial neural network approach. These neural networks vary in size, complexity, and training and computation time requirements. One neural network that has demonstrated extremely fast training time is the Extreme Learning Machine, (Zhu, Miao, & Qing, 2014) which could potentially be applied to groundwater.

## 1.2 Research Objectives

The purpose of this research is to develop an open-source web application that will synthesize and interpolate in-situ groundwater data, together with Earth observations, creating and displaying aquifer-wide maps and animations of groundwater levels, allowing decision makers easy, informative, and accurate access to important groundwater data. This web application, the Groundwater Level Mapping Tool, is built on Tethys Platform, an open source platform for lowering the barrier for environmental web app development (Swain et al., 2016). This application is generalized to allow its use world-wide, and allows decision makers to accomplish the following:

1) View time series and other data for each well within an aquifer.

2) View maps of aquifer-wide groundwater levels at different time periods.

3) Calculate and view estimates of changes in total aquifer storage.

These maps and time series can be created using several different techniques, including Kriging for spatial interpolation, and multi-linear regression, simple PCHIP interpolation, or neural networks using earth observations for temporal interpolation.

This thesis will detail the methods and mathematics used in developing these different techniques and will demonstrate their application and use in aquifers located in Utah, Texas, South Africa, Colombia, and the Dominican Republic. This application can be used to help decision makers sustainably manage groundwater resources in any area throughout the world.

## 2 METHODS

The Groundwater Level Mapping Tool enables users to view groundwater levels and quantify changes in groundwater storage aquifer-wide. To enhance this application, I developed and implemented several techniques for temporally and spatially interpolating groundwater data. Temporal interpolation methods include basic PCHIP interpolation, prediction using multi-linear regression with correlated wells, and prediction using Extreme Learning Machine harnessing Earth observations. Spatial interpolation methods include Inverse Distance Weighted interpolation and Kriging interpolation using GSLIB. The Groundwater Level Mapping Tool uses these spatial and temporal interpolation methods to estimate changes in total aquifer storage volume over time.

### 2.1 The Groundwater Level Mapping Tool

The Groundwater Level Mapping Tool is written mainly in the Python programming language, with supporting JavaScript and html, and is built using the Tethys Platform, a development and hosting environment for environmental web apps aimed at lowering the barrier to water resource web app development (Swain et al., 2016). The app is an extremely visual tool, and can be used to display data for any number of regions with a number of aquifers. Figure 2-1 shows a view of the Groundwater Level Mapping Tool in a web browser, where the user can view all the aquifers of a specified region.

7
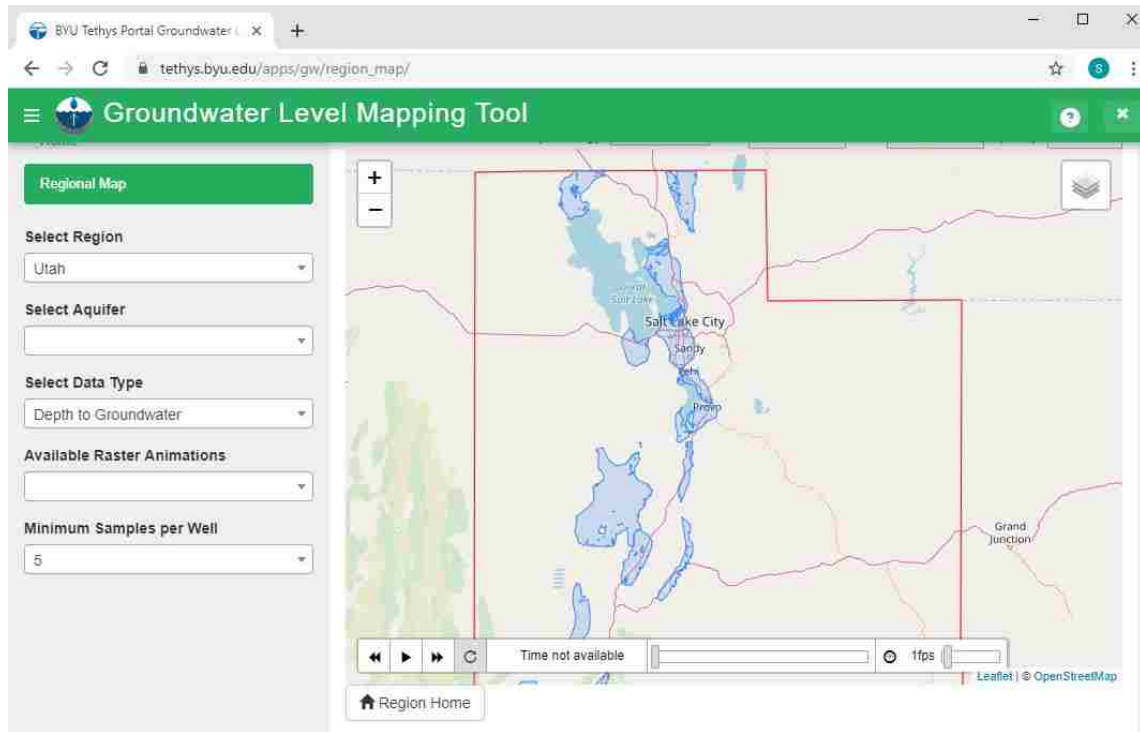
**Figure 2-1: View of Utah Aquifers in Groundwater Level Mapping Tool**

The app enables the user to view data for any of each region's aquifers. The user simply selects an aquifer and is then able to interactively view well time series data for any well in that aquifer, see Figure 2-2. The user may toggle between viewing depth to groundwater, groundwater surface elevation, and drawdown in the well over a specified time period. This method of time series visualization improves upon existing applications by allowing the user to easily associate the time series data with a geographic location, and to quickly and easily navigate from one well to another without needing to refresh, reload, or open another browser window.
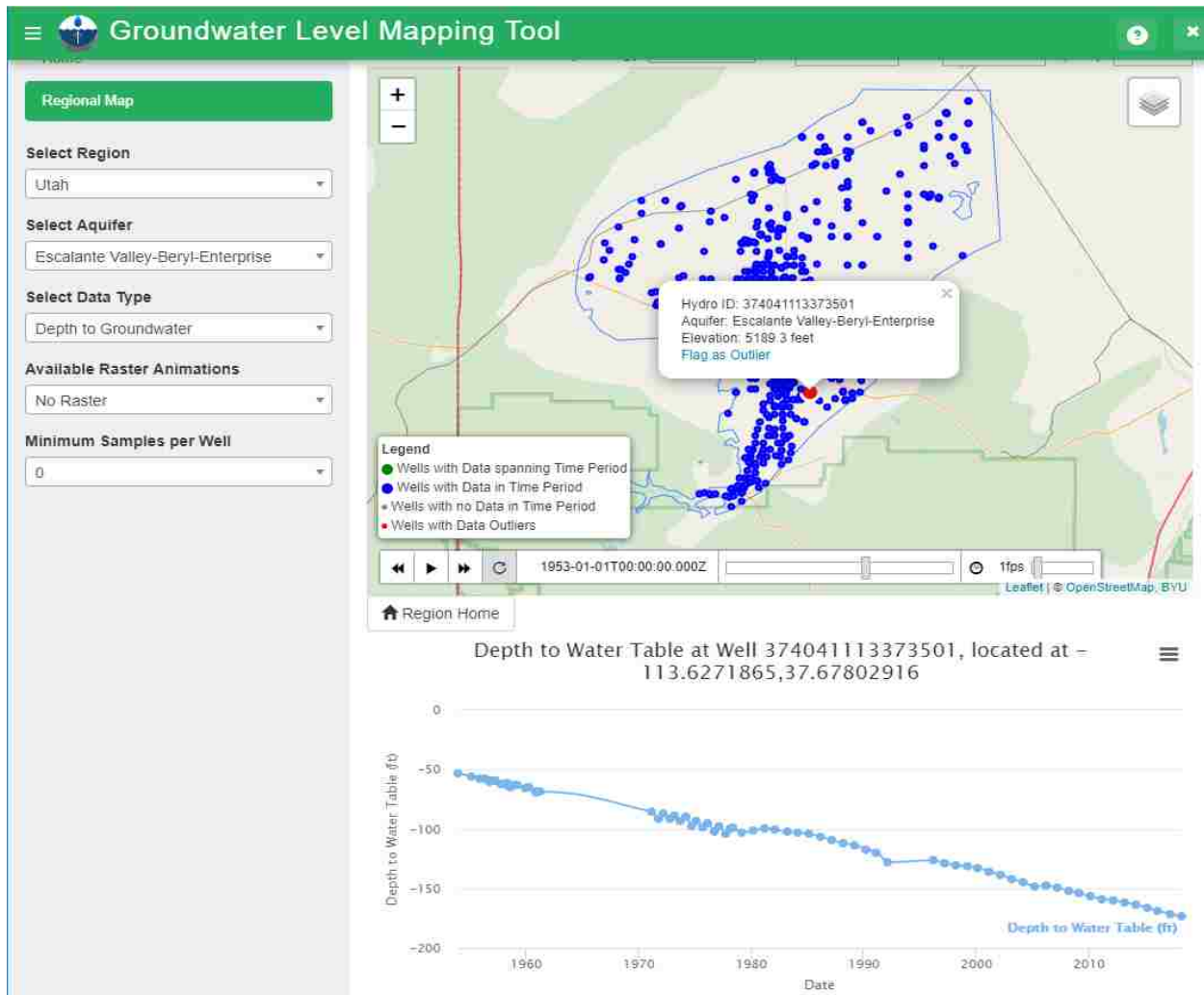
**Figure 2-2: Time Series View in Groundwater Level Mapping Tool**

The Groundwater Level Mapping Tool also allows the user to create and view maps of aquifer-wide groundwater levels, and to easily view changes in groundwater levels over time. Figure 2-3 shows the Groundwater Level Mapping Tool visualization of depth to groundwater (ft) throughout the Beryl-Enterprise aquifer in southern Utah in December, 1949. Figure 2-4 shows the same aquifer 65 years later in December, 2014, demonstrating significant groundwater drawdown, which can also be visualized in Figure 2-5, which shows drawdown between December of 1944 and 2014, in the same aquifer.

9
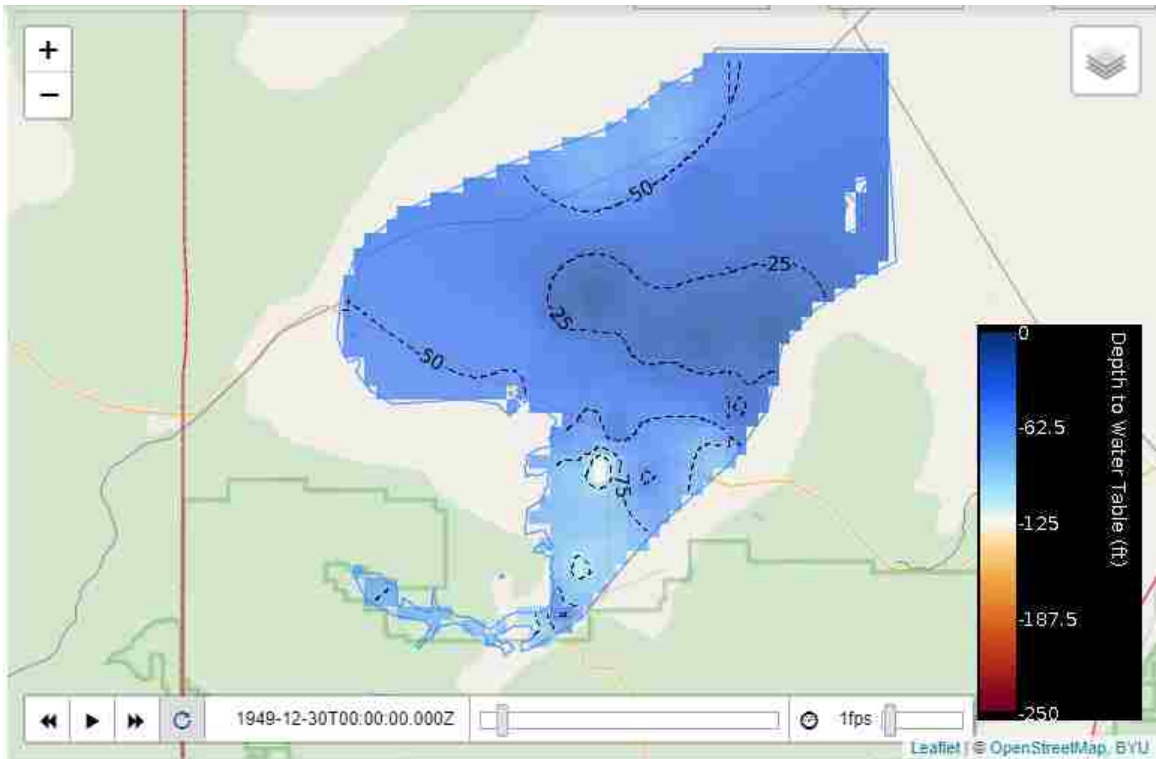
**Figure 2-3: Depth to Water Table in Beryl-Enterprise Aquifer in December, 1949**
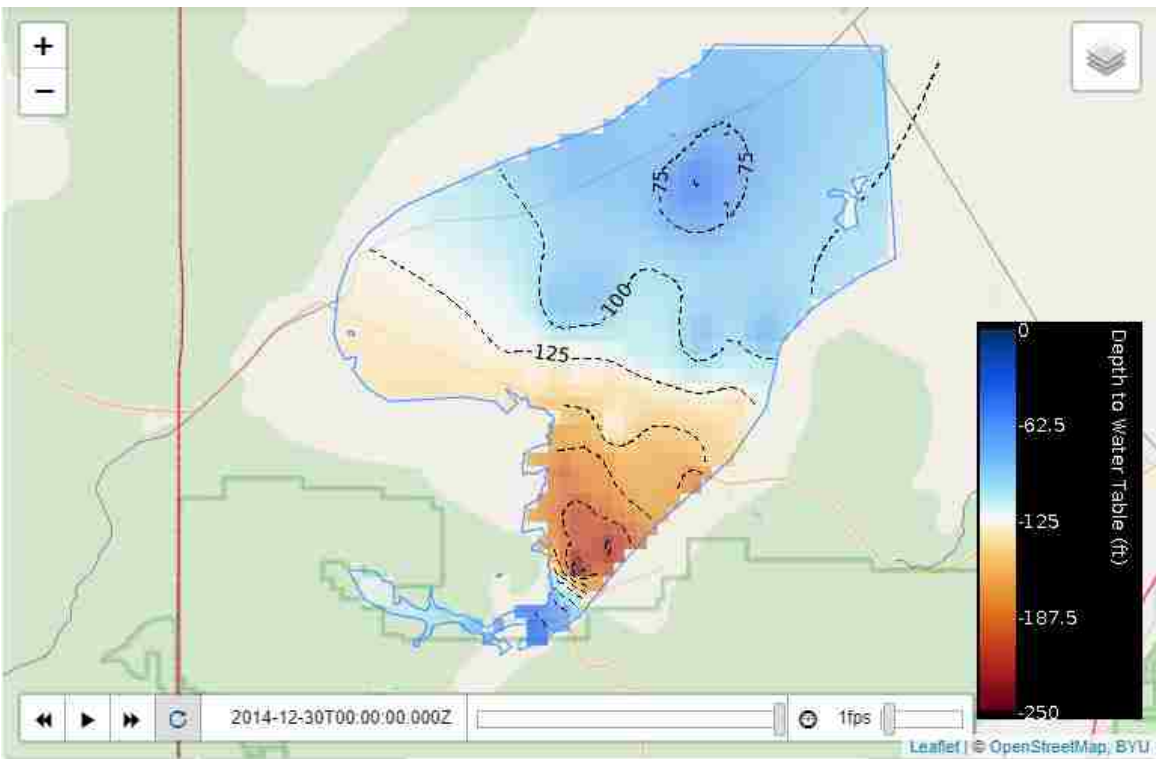


**Figure 2-4: Depth to Water Table in Beryl-Enterprise Aquifer in December, 2014**

10
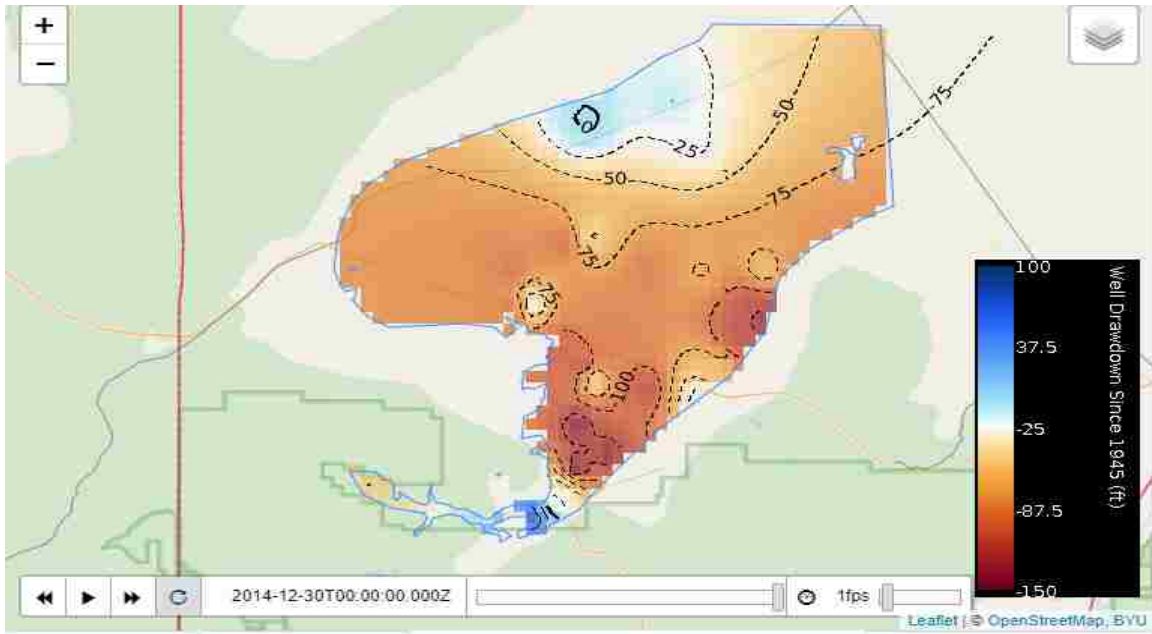
**Figure 2-5: Drawdown from December, 1944 to 2014 in Beryl-Enterprise Aquifer**

The groundwater level maps are stored in NetCDF format on a THREDDS server and displayed using the Leaflet JavaScript library for interactive maps. In addition to the water level maps, the web app also allows the user to calculate and view changes in total aquifer storage based on an aquifer storage coefficient, as shown in Figure 2-6, and detailed in Section 2.4. The methods for creating these maps and storage curves are detailed in the ensuing sections.
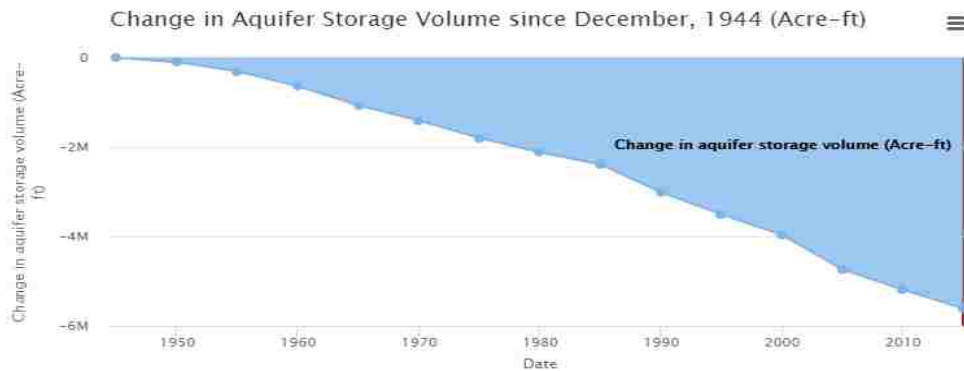


**Figure 2-6: Aquifer Storage Curve for Beryl-Enterprise Aquifer**

11

## 2.2    Temporal Interpolation Techniques

Depth to groundwater measurements from wells throughout an aquifer are generally sampled inconsistently over time. These samples may be recorded monthly, semi-annually, annually, bi-annually, or at other irregular intervals. I found the data collected from South Africa, Utah, Texas, Colombia, South Africa, and the Dominican Republic that I analyzed during this research were quite irregular and inconsistent in sampling rates. Sampling rates varied over time in most wells, and sampling rates were quite inconsistent between wells in the same aquifer. Figure 2-7 demonstrates the inconsistent sampling rate common for many wells: there are long periods of time with no samples, a brief period of semi-annual sampling, and another longer period of annual sampling.



**Figure 2-7: Inconsistent Sampling Rate at Well 374248113075201 near Cedar City, UT**

In order to map groundwater levels throughout an aquifer at a specific time, it is necessary to first perform temporal interpolation on individual wells to the selected time. For wells with significant gaps as described above, this process has the potential to introduce significant error or uncertainty in the process. In this research, I developed three different methods to perform temporal interpolation: PCHIP Interpolation, Multi-Linear Regression Harnessing Correlated Wells, and Extreme Learning Machine Harnessing Earth Observations. I

used these methods to resample the data from each well to a specific time interval, in order to map aquifer-wide groundwater levels over time.

### 2.2.1   PCHIP Interpolation

The simplest interpolation method I used for temporal interpolation is the PCHIP (Piecewise Cubic Hermite Interpolating Polynomial) method. I accomplished this interpolation for each well using the PCHIP interpolation functionality in the Pandas Python library (McKinney, 2010). The PCHIP method interpolates data using a piecewise cubic polynomial P(x) with continuous first derivatives P'(x). The PCHIP method preserves the shape of the data and respects monotonicity. On intervals where the data are monotonic (neither increasing or decreasing), so is P(x), and at points where the data have local minima or maxima, so does P(x). Thus, the second derivative P''(x) is likely not continuous (Fritsch & Carlson, 1980).  Figure 2-8 shows an example of PCHIP interpolation, Figure 2-9 shows in black the resampled data at 5-year intervals obtained through the PCHIP method.



**Figure 2-8: Example PCHIP Interpolation**

13

**Figure 2-9: Resampled Values Obtained from PCHIP Interpolation**

For consistently sampled wells, PCHIP interpolation is a simple, accurate, effective method of resampling data to a specified time interval. This technique is less accurate when there are large gaps in the data (such as the gap from 1984 to 1998 shown in Figure 2-8), or when the target time is outside the range of the sampled data (e.g. we wish to obtain the depth to groundwater in 2005 when recorded data ends in 2001). When the target time is outside the range of sampled data, the PCHIP method assumes the value is the same as the nearest sampled data point.

### 2.2.2 Multi-Linear Regression Harnessing Correlated Wells

To overcome the challenges of data gaps and to accurately extend data beyond its sampled range, I developed a new method of temporal interpolation, Multi-Linear Regression Harnessing Correlated Wells. This method was developed based on the assumption that wells within the same aquifer will likely exhibit similar characteristics in depth to water table fluctuations and trends. This similarity between wells located in the same aquifer is demonstrated in Figure 2-10. The three wells shown are all located in the Cedar Valley Aquifer in southern

14

Utah. Well 37342113100801 (green) is located near the southern end of the aquifer, while the two other wells are located near the center. There is a clear correlation between these wells; the water levels rise and fall following the same general pattern throughout the aquifer. The correlation demonstrated in the Cedar Valley aquifer was typical of other aquifers studied in this research. Figure 2-11 shows correlation between two wells separated by 81 km both located in the Inkomati Water Management Unit of South Africa. The correlation is not as strong in this case due to the greater distance between wells, but the wells exhibit similar behavior due to the similar conditions in the region.
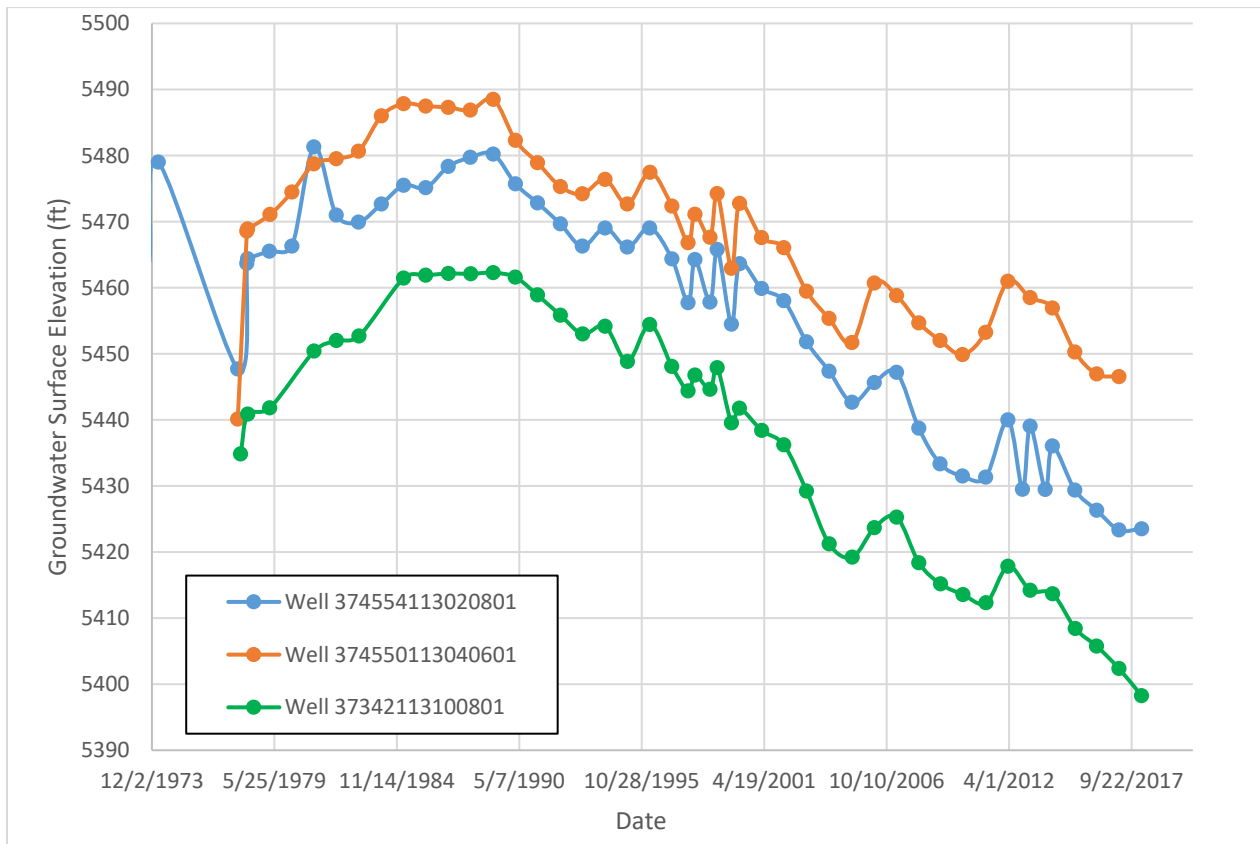


**Figure 2-10: Correlation between Wells in the Cedar Valley Aquifer**
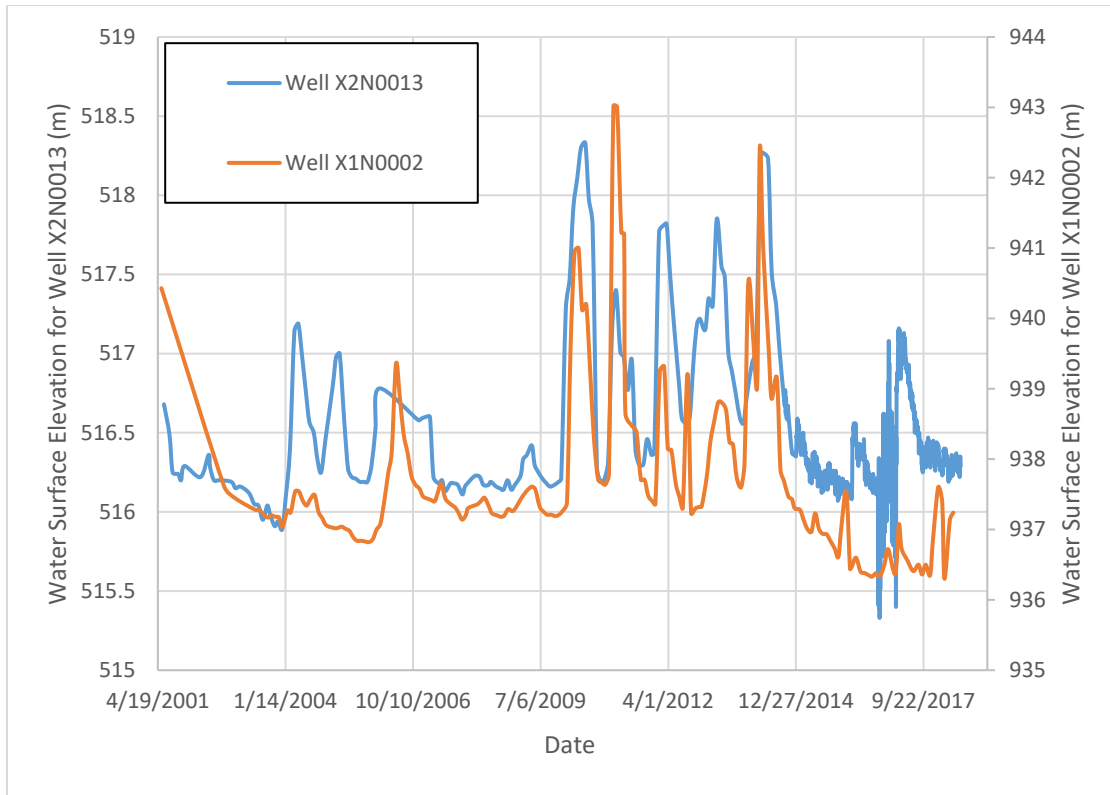
**Figure 2-11: Correlation between Wells in the Inkomati Water Management Unit**

The Multi-Linear Regression method of time series interpolation utilizes this inner-aquifer correlation to yield accurate estimates of water surface elevation for a well at specific times outside the sampling range of the well. This method is useful when the times series data for a well does not thoroughly cover the time(s) of interest. Figure 2-12 shows the time series data for Well 374210113044801 located in the Cedar Valley Aquifer, which has data from 1998 to 2008, which does not span the period of interest from 1985 to 2015. Using Multi-Linear Regression, this wells' time series data can be extended to span the period of interest.

16
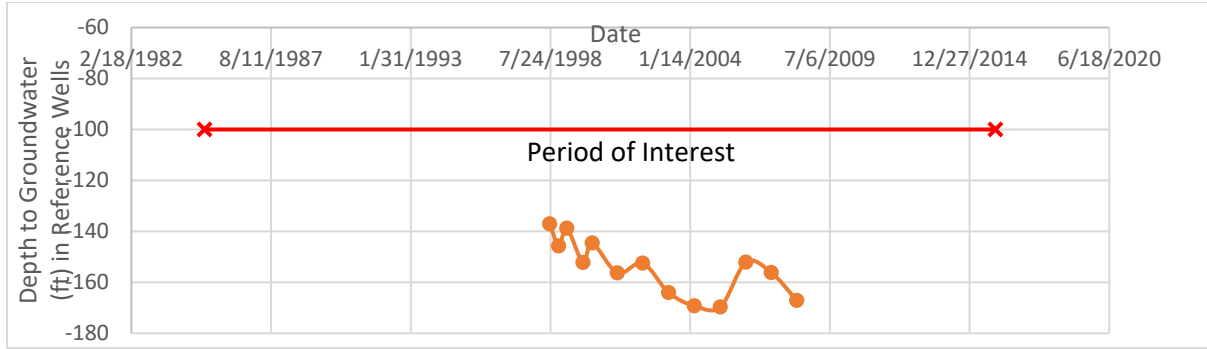
**Figure 2-12: Example of Well Time Series that does not Cover Period of Interest**

The first step in this method is to construct a single data frame, using the Pandas Python library (McKinney, 2010), containing the time series information for every well in the aquifer. This data frame includes an index of regular 3-month intervals with the time series observations of each well resampled to these regular 3-month intervals by means of a PCHIP interpolation. If a well does not have data within a 3-month interval, then the data frame contains a null value for that well at that time step. Next, those wells which contain data spanning the time period of interest are identified as "reference wells." After these reference wells, which contain full time series data for the period of interest, are identified, the Pearson Correlation Coefficient is calculated between the well with missing time series data and each of the reference wells. This correlation coefficient $r_{XY}$ between the target well $X$ and each reference well $Y$ for $n$ data points is calculated by Equation (2-1).

$$r_{XY} = \frac{\sum_{i=1}^{n}(X_i - \bar{X})(Y_i - \bar{Y})}{\sqrt{\sum_{i=1}^{n}(X_i - \bar{X})^2}\sqrt{\sum_{i=1}^{n}(Y_i - \bar{Y})^2}} \tag{2-1}$$

Data from the reference wells $Y$ with the five highest correlation values $r_{XY}$ are used as inputs for the process of multi-linear regression. Figure 2-13 shows the time series data for the

target well with missing time series data along with the 5 most correlated wells in the aquifer. The area within the red rectangle shows the data that will be used to train the multi-linear regression model to predict the target well's missing time series values.
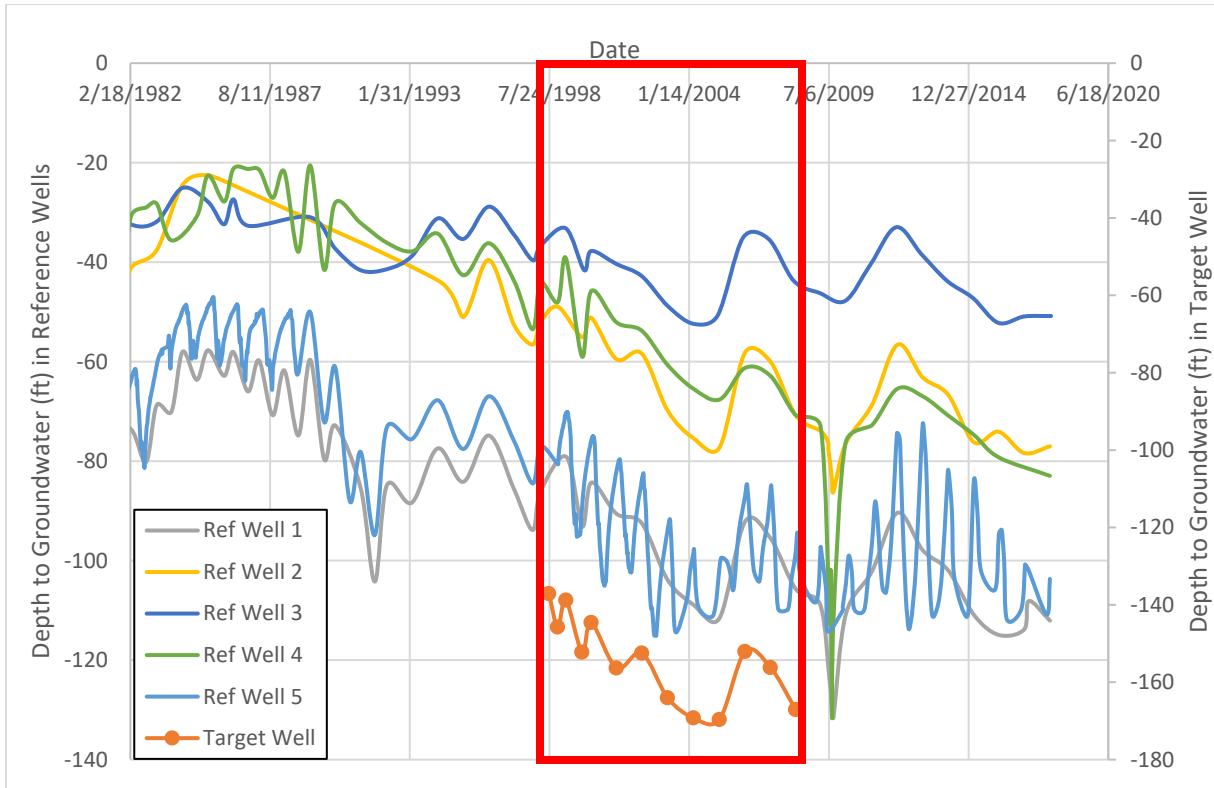


**Figure 2-13: Well with Missing Data Plotted with Correlated Reference Wells**

To effectively estimate the missing values of the target well, it is necessary to normalize the data. Notice from Figure 2-13 the similar shape, but differing depths of each of the wells. This normalization transforms the data so that all the wells are in the same range, which allows prediction based on the similar shapes of the data rather than the differing magnitudes of the data. Data from the target and reference wells are normalized such that all values within the training data set are between 0 and 1. Let Y represent the target well, and $R^1$, $R^2$, $R^3$, $R^4$, and $R^5$ represent the five reference wells. The training data subsets will be represented as $Y^{train}$ for the

www.manaraa.com

target well, and $R^{train1}$, $R^{train2}$, …, $R^{train5}$ for the five reference wells. The values of each well $i$ are normalized as shown in Equation (2-2).

$$R^{normi} = \frac{R^i - \min(R^{traini})}{\max(R^{traini}) - \min(R^{traini})}$$

(2-2)

These normalized data sets are plotted in Figure 2-14, with the normalized training set again bounded in red. The reference wells are normalized using the minimum and maximum values of the training subset, rather than the entire data set, because this provides a more skilled prediction, especially when predicting time series values outside the scope of the training data.
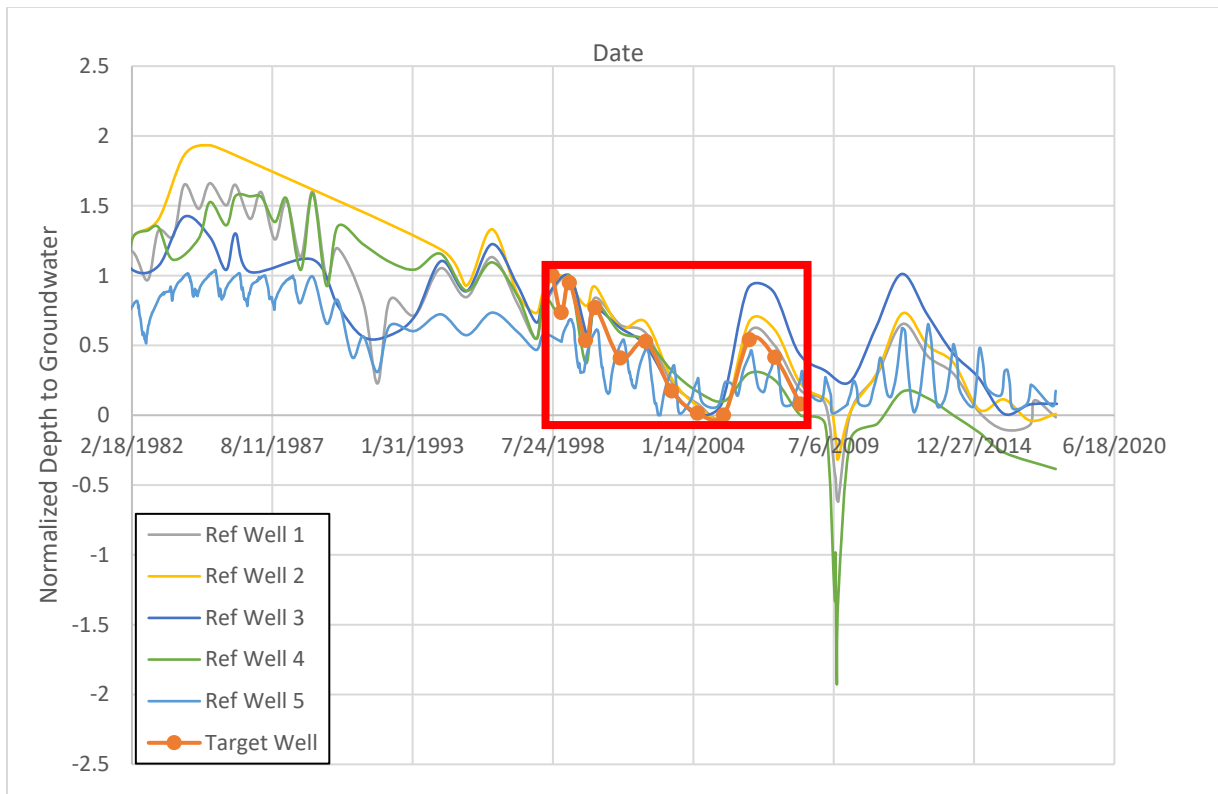


**Figure 2-14: Normalized Target Well with Normalized Correlated Reference Wells**

The normalized time series data of the target well is assumed to be a linear combination of the normalized time series data of the five reference wells. At each time (t), the normalized

value of depth to groundwater at the target well ($Y_t$) is approximated as a linear combination of the normalized depth to water table at time (t) of the reference wells ($R_t$). The equation for $Y_t$ is shown in Equation (2-3), where $e$ is an error residual term.

$$Y_t = R_t^1\beta_1 + R_t^2\beta_2 + R_t^3\beta_3 + R_t^4\beta_4 + R_t^5\beta_5 + e \tag{2-3}$$

Equation (2-3) can be rewritten in matrix form as Equation (2-4).

$$\vec{Y_t} = \boldsymbol{R}_t\vec{\beta} + \boldsymbol{e} \tag{2-4}$$

The $\vec{\beta}$ term represents weights determined by regularized least-squares fit using the training data subset, such that the sum of the squared residuals $e$ is minimized. These weights $\vec{\beta}$ are obtained by solving Equation (2-5), where $\lambda$ is a regularization term, and $\boldsymbol{I}$ is the identity matrix. This process is carried out in the app by using the regularized least squares solver in the Statsmodels Python library.

$$\boldsymbol{R}_{train}{}^T\vec{Y}_{train} = [\boldsymbol{R}_{train}{}^T\boldsymbol{R}_{train} + \lambda\boldsymbol{I}]\,\vec{\beta} \tag{2-5}$$

When using a high complexity estimator, such as multi-linear regression, the bias error is generally small, and the variance very large. Bias error is an error that causes the estimator algorithm to miss relevant relations between features and target outputs, thereby under fitting the data. Variance is an error from sensitivity to small fluctuations in the training set, which can cause the model to train to random noise in the training data, rather than actual correlations, thereby overfitting the data. The introduction of $\lambda$ increases the bias of the estimate, but significantly decreases the variance, preventing overfitting and generally yielding a more accurate estimate. The method of regularization used here is Tikhonov or Ridge regularization (Tikhonov & Arsenin, 1977).

Once $\vec{\beta}$ has been obtained by means of the regularized least squares model using the training data subset, the unknown Y terms may be estimated for each time step t by solving Equation (2-3). Once the Y terms have been obtained, they must be unscaled to their original extent, yielding Y_estimate. This is accomplished by applying Equation (2-6).

$$\vec{Y}_{estimate} = \vec{Y} * \left[\max(\vec{Y}^{train}) - \min(\vec{Y}^{train})\right] + \min(\vec{Y}^{train}) \qquad (2\text{-}6)$$

The process is now complete for estimating missing time series values for the target well. The estimated time series $\vec{Y}_{estimate}$ modelled using Multi-Linear Regression Harnessing Correlated Wells is shown in Figure 2-15, together with the original recorded data.
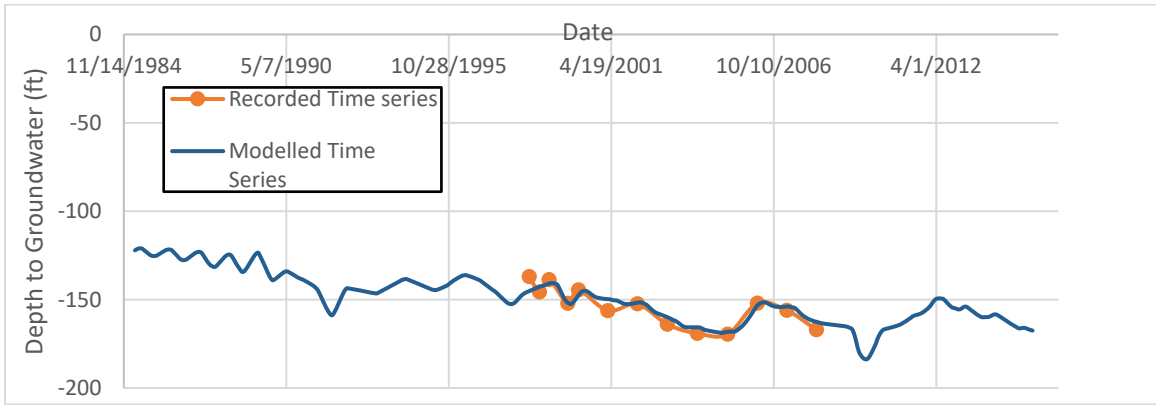


**Figure 2-15: Well Time Series Modelled by Multi-Linear Regression**

### 2.2.3   Extreme Learning Machine Harnessing Earth Observations

In some areas of the world, groundwater data are extremely scarce. To fill gaps in the data in these areas, where no thoroughly sampled wells exist to enable the Multi-Linear Regression technique, I have developed another time series extension technique using an Extreme Learning Machine Harnessing Earth Observations. This method is based on the assumption that groundwater levels are correlated with climatic factors such as drought and soil moisture, both of

www.manaraa.com

which can be measured using hydrological models with satellite Earth observations and land based observations as inputs. Figure 2-16 through Figure 2-19 show this correlation. All three wells see an increase in groundwater levels in early 2005, which corresponds to a period of increased soil moisture simulated by GLDAS from late 2004 to early 2005. This period of interest is highlighted in yellow on each of the figures.
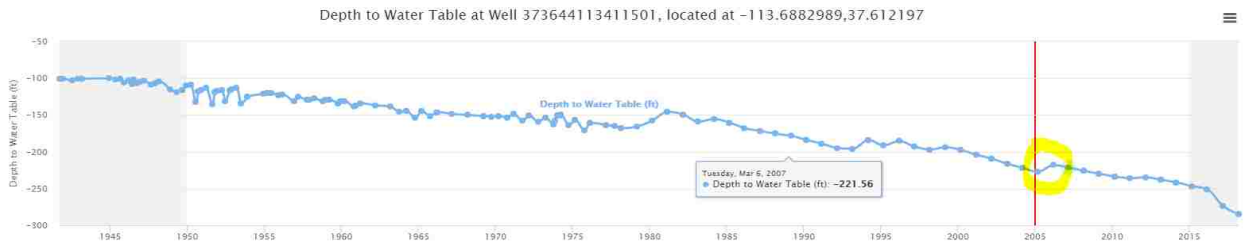


**Figure 2-16: Depth to Groundwater at Well 373644113411501 near Beryl, Utah**



**Figure 2-17: Depth to Groundwater at Well 37349113434201 near Beryl, Utah**
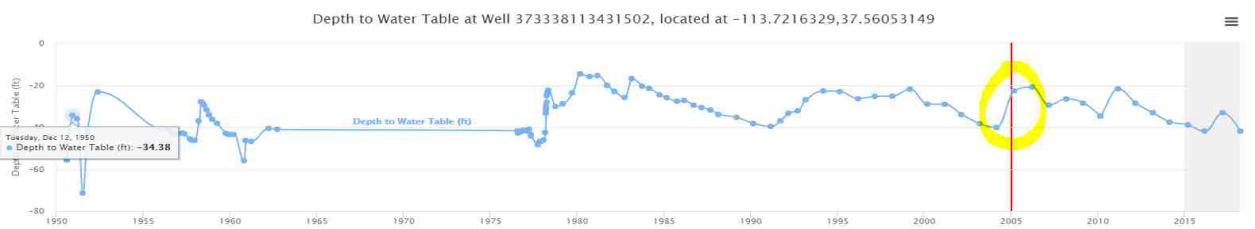


**Figure 2-18: Depth to Groundwater at Well 37349113434201 near Beryl, Utah**
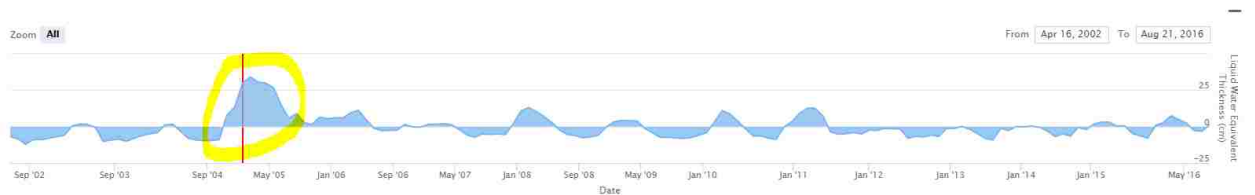


**Figure 2-19: Soil Moisture Simulated by GLDAS near Beryl, Utah**

22

There exists a correlation between soil moisture and groundwater levels, but this correlation is highly non-linear. In order to fill gaps in groundwater data using satellite observations, I employed a neural network using the Palmer Drought Severity Index (PDSI) and Soil Moisture liquid water equivalent thickness simulated from two different models as inputs.

The PDSI uses readily available temperature and precipitation data to estimate relative dryness. It is a standardized index that spans from -10 (dry) to +10 (wet) (Dai, 2019). The PDSI is available in NetCDF format on a THREDDS server hosted by NOAA. This global dataset is available at 0.5-degree resolution from 1850-2015 at monthly frequency.

The Soil Moisture liquid water equivalent thickness is estimated using a one-layer hydrological model which uses precipitation and temperature Earth observations as inputs (J. Huang et al., 1996). These data are available globally at 0.5-degree resolution from 1948 onwards at monthly frequency from NOAA's Climate Prediction Center (CPC) in NetCDF format on a THREDDS server hosted by NOAA. This soil moisture model uses monthly data from the CPC PRECipitation REConstruction over Land (Chen, Xie, Janowiak, & Arkin, 2002) and the CPC Global Land Surface Air Temperature Analysis (Fan & Van den Dool, 2008) datasets as inputs. Both of these datasets are derived from station observations collected from the Global Historical Climatology Network version 2 and the Climate Anomaly Monitoring System

The second soil moisture dataset used is simulated by the Global Land Data Assimilation System (GLDAS) model. GLDAS "is a global, high-resolution, offline (uncoupled to the atmosphere) terrestrial modeling system that incorporates satellite- and ground-based observations in order to produce optimal fields of land surface states and fluxes in near-real time" (Rodell et al., 2004). GLDAS incorporates hundreds of observations, including vegetation, land cover, soil, elevation, precipitation, and temperature information derived from or measured

23

by various satellites (AVHRR aboard *NOAA-15* satellite, MODIS aboard NASA's *Terra* satellite, EOS aboard NASA's *Aqua* satellite). Using this vast array of inputs, GLDAS simulates soil moisture, which is used as an input for the Groundwater Level Mapping Tool.

These datasets were used as inputs because they displayed the best correlation with observed groundwater levels when compared against other air temperature, earth temperature, and precipitation datasets. The best correlation between Earth observations and observed groundwater levels was obtained using Total Water Storage data from the GRACE mission. Although these data displayed the best correlation, they were not used in this research because the GRACE data are only available from 2002 onwards, which severely limited the amount of data available for testing and training datasets.

I developed a Python script to estimate missing groundwater level measurements for a well, using the PDSI and two Soil Moisture datasets. The monthly data for these three datasets at the location of the target well are extracted directly from the NOAA THREDDS server where the data are hosted. The data are then resampled using a PCHIP interpolation so that all measurements are at the same monthly resolution. The 1, 3, 5, and 10 year rolling averages for the PDSI and both of the Soil Moisture datasets are then calculated. These rolling average terms improve the accuracy of this estimation method because the varying window lengths help to capture the effects of both long- and short-term climatic events which contribute to changes in groundwater levels. Often, groundwater levels increase fairly quickly following an extremely wet month or year. These changes are captured in the model by incorporating the 1-year average and the original monthly data. When moisture levels are slightly below normal for extended periods of time, this generally causes a period of slow decline in groundwater levels. This phenomenon is captured well by the 5 and 10-year rolling averages. In addition to these rolling

average datasets, two dummy linear datasets are incorporated into the model. Together, these two linear datasets allow the model to capture any constant underlying linear trends in groundwater levels not modelled by the Earth observations. These two datasets are especially important in cases where the groundwater is being constantly over pumped because it allows the model to capture this near linear decrease in the water table cause by continuous over pumping. Thus, a total of 16 data sets, the two monthly sets, the two linear dummy sets, plus twelve additional rolling average datasets, are used in the model.

To accurately estimate missing groundwater measurements using a neural network, it is necessary to first normalize the data, scaling it to a range between 0 and 1. This normalization is achieved for each input dataset and for the available target well data following the pattern laid out in Section 2.2.2, using Equation (2-2).

The normalized depth measurements of the target well Y, and the normalized input data X for the time period where measurements are available for Y are used as the training dataset. The training data are then used to train a feedforward neural network with one hidden layer known as an extreme learning machine (ELM). ELMs have been shown to train up to thousands of times faster than networks trained using backpropagation, and have also outperformed Support Vector Machines (SVMs) in some instances (G.-B. Huang, 2015). Because of its high performance and fast training time, an ELM was selected for use in this research.

The basic assumption upon which ELMs are built is shown in Equation (2-7), where $W_1$ is the matrix of input-to-hidden-layer weights, $\sigma$ is an activation function, $\vec{b}$ is a bias vector, and $W_2$ is the matrix of hidden-to-output layer weights. The rectifier activation function is used for

$\sigma$, the rectifier function is shown in Equation (2-8). This process is summarized in Figure 2-20, where $a_1 \ldots a_N$ represent the rows of the matrix $\boldsymbol{W_1}$.

$$\vec{Y} = \boldsymbol{W_2} * \sigma(\boldsymbol{W_1}X + \vec{b}) \tag{2-7}$$

$$\sigma(x) = \max(0, x) \tag{2-8}$$
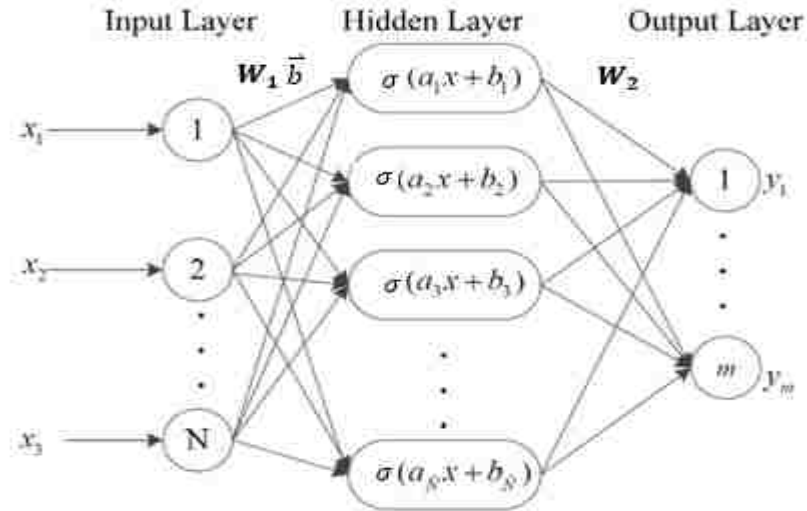


**Figure 2-20: Schematic of Extreme Learning Machine**

This method of using an ELM to estimate unknown groundwater levels using correlated Earth observations was developed because the ELM enables the non-linear relationship between drought index, soil moisture, and groundwater levels to be used to infer missing data. The ELM maps non-linear relationships by means of the random weight matrix $\boldsymbol{W_1}$ and the rectifier activation function $\sigma$. The algorithm for the ELM proceeds as follows:

1. Fill $\boldsymbol{W_1}$ and $\vec{b}$ with random values

2. Use the rectifier activation function for $\sigma$, shown in Equation (2-8)

3. Estimate $\boldsymbol{W_2}$ by least-squares fit to a vector of response variables $\vec{Y}$

Using these basic steps, the use of an ELM to infer missing groundwater data $Y_{estimate}$, using training data $Y_{train}$ and $X_{train}$ is accomplished as follows.

Let:

$M_{train}$= the number of sampled time-steps belonging to the training data set

$M_{test}$= the number of time-steps for which the ELM will estimate groundwater depth

N= the number of input variables used to infer groundwater measurements. In our case, N=17 (monthly, yearly, 3, 5, and 10-year averages of the PDSI and the two soil moisture datasets, plus two linear dummy variables).

$\vec{Y}_{train}$= a vector of length $M_{train}$, containing observed monthly groundwater levels at a well

$X_{train}$= an $M_{train}$ x N matrix of data used to infer groundwater depth ($\vec{Y}_{train}$)

$\vec{Y}_{estimate}$= a vector of length $M_{test}$, that will contain estimated groundwater levels for a well

$X_{test}$= an $M_{test}$ x N matrix of data used to infer groundwater depth ($\vec{Y}_{test}$)

h= the number of nodes in the hidden layer of the extreme learning machine

$\vec{b}$= a random vector of length h used as a bias variable in the ELM

$W_1$= an N x H matrix of random values to be used in the ELM

$\sigma =$ the rectifier function as shown in Equation (2-8)

The matrix $W_1$ is populated with random values using the random function available from the Numpy Python library. With $W_1$ populated, the next step is to solve for $W_2$.

Let $A_{train}$ be defined as shown in Equation (2-9).

27

$$A_{train} = \sigma(W_1 X_{train} + \vec{b}) \tag{2-9}$$

After solving for $\mathbf{A_{train}}$, Equation (2-10) is used to determine $W_2$ which minimizes the error $e$.

$$\vec{Y}_{train} = W_2 A_{train} + e \tag{2-10}$$

The unknown matrix of hidden-to-output weights $W_2$ is estimated using regularized least squares as shown in Equation (2-11), where $\lambda$ is a regularization parameter. $W_2$ is obtained by solving Equation (2-11) using the least squares function in the Numpy Python library.

$$A_{train}{}^T \vec{Y}_{train} = [A_{train}{}^T A_{train} + \lambda I] W_2 \tag{2-11}$$

Now that $W_2$ has been computed, it is straightforward to use the ELM to solve for $\vec{Y}_{test}$ as shown in Equation (2-12).

$$\vec{Y}_{test} = W_2 \sigma(W_1 X_{test} + \vec{b}) \tag{2-12}$$

Now, $\vec{Y}_{test}$ must be rescaled to its original extent, yielding the depth to groundwater estimates $\vec{Y}_{estimate}$ by implementing Equation (2-13).

$$\vec{Y}_{estimate} = \vec{Y}_{test} * \left[ \max(\vec{Y}_{train}) - \min(\vec{Y}_{train}) \right] + \min(\vec{Y}_{train}) \tag{2-13}$$

## 2.3 Spatial Interpolation Techniques

Once the depth to groundwater data measurements have been resampled, interpolated, and/or extended using the techniques in Section 2.2, the Groundwater Level Mapping Tool now maps these water levels throughout the aquifer by implementing spatial interpolation. Upon completion of temporal interpolation, depth to water table measurements are available as point data at each observation well for each desired time step. These data can be represented as shown in Figure 2-21, where point representations of depth to groundwater in December, 2014 are shown for the Sevier Desert in western Utah. After completing spatial interpolation, these same

28

data are represented as shown in Figure 2-22. This spatial interpolation provides a much better visual representation of the state of groundwater in the aquifer, and it allows quantification of groundwater storage volume throughout the aquifer.
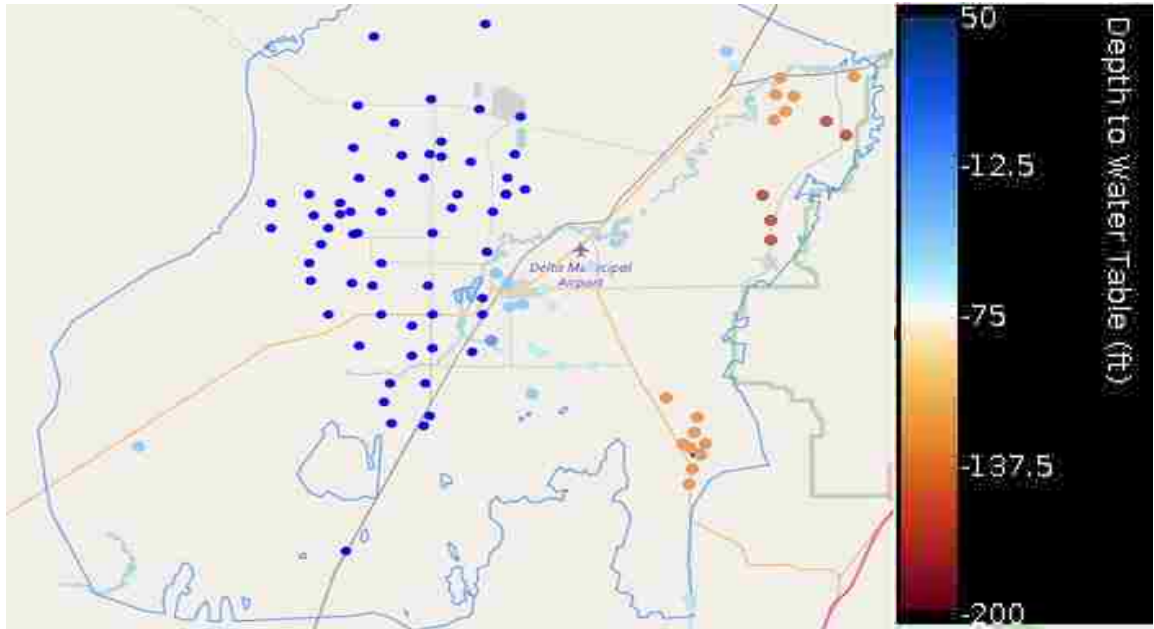


**Figure 2-21: Point Measurements of Depth to Groundwater near Delta, UT**
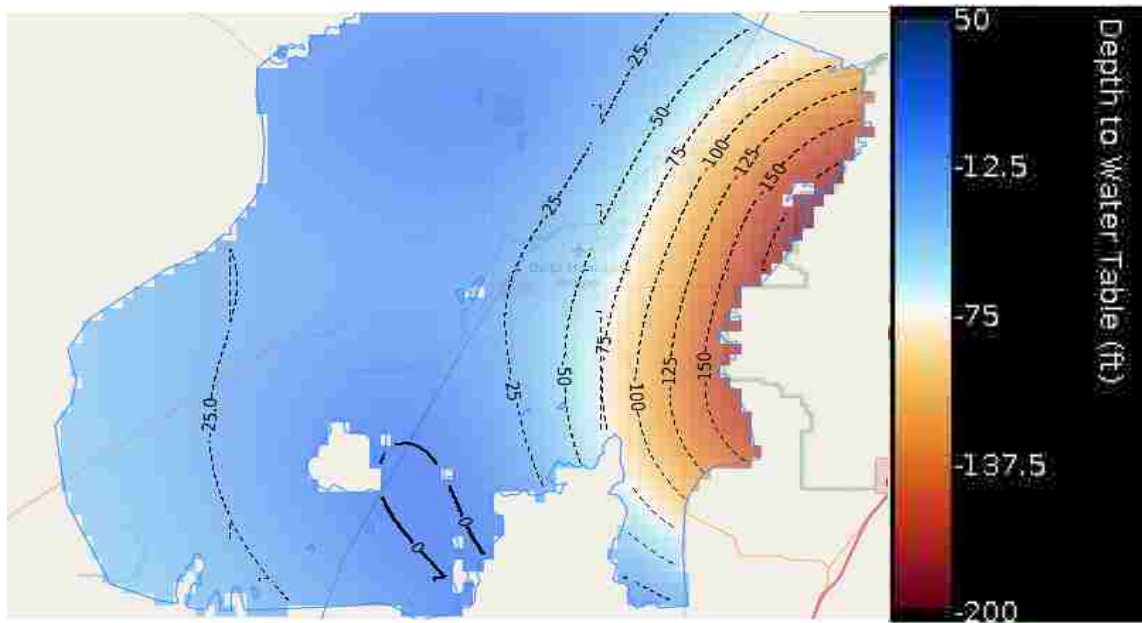


**Figure 2-22: Kriging Spatial Interpolation of Depth to Groundwater near Delta, UT**

29

The app employs two different methods of spatial interpolation. In both methods, the app determines weights and then estimates the value at a point using those weights. The procedure is continued on a regular grid at a user specified resolution for each point within the aquifer.

### 2.3.1   Inverse Distance Weighted Interpolation

The simplest method of spatial interpolation employed by the Groundwater Level Mapping Tool is inverse distance weighted interpolation. The equation of this interpolating function is shown in Equation (2-14), where $n$ is the number of points used to interpolate, $f_i$ are the dataset values at those points, and $w_i$ are the weight values assigned to each point.

$$F(x, y) = \sum_{i=1}^{n} w_i f_i \tag{2-14}$$

The weight values $w_i$ are assigned for each point by means of the weight function shown in Equation (2-15), where $R$ is the distance from the interpolation location to the most distant point, and $n$ is the number of points. $h_i$ is the Euclidean distance from the interpolation location to the point $i$ as defined by Equation (2-16), where $(x, y)$ are the coordinates of the interpolation location and $(x_i, y_i)$ are the coordinates of each point. Equation (2-15) is used as the weight function because it was found to give superior results to the classical weight function typically used in Shepard's Method (Franke & Nielson, 1980).

$$w_i = \frac{\left[\dfrac{R - h_i}{R h_i}\right]^2}{\sum_{j=1}^{n} \left[\dfrac{R - h_i}{R h_i}\right]^2} \tag{2-15}$$

$$h_i = \sqrt{(x - x_i)^2 + (y - y_i)^2} \tag{2-16}$$

The weight functions are normalized so that the weights sum to a value of one. Each weight $w_i$ varies from a value of one at the interpolation point to a value approaching zero as the distance from the interpolation point increases.

This method of interpolation is used in the Groundwater Level Mapping Tool for its simplicity and ease of implementation. Interpolated values can be computed using this IDW method quicker than using the Kriging method, and the IDW interpolation can always be computed. In cases where the Kriging interpolation method fails, then the Groundwater Level Mapping Tool reverts to using the IDW interpolation for those areas of failure. In this way, the Groundwater Level Mapping Tool still supplies the user with a map or animation of groundwater levels throughout the aquifer.

### 2.3.2 Kriging Interpolation

The Groundwater Level Mapping Tool utilizes the Kriging interpolation method in order to achieve the app's most accurate spatial interpolation. Similar to the IDW interpolation, the Kriging method assumes that the value $Z_*$ at location $(x_*, y_*)$, can be estimated using Equation (2-17), where $n$ is the number of points used to interpolate, $Z_i$ are the dataset values at those points, and $\lambda_i$ are the weight values assigned to each point.

$$Z_*(x_*, y_*) = \sum_{i=1}^{n} \lambda_i Z_i \qquad (2\text{-}17)$$

The weights $\lambda_i$ for each point are determined by the development and use of a model variogram function. A model variogram is developed by first creating and plotting the experimental variogram from the available point data. The experimental variogram is a function of the Euclidean distance $d(i,j)$, and the semivariance $V(i,j)$ between each pair of points $(i,j)$

31

in the dataset. The Euclidean distance $d(i,j)$ between a pair of points $(i,j)$ with coordinates $(x_i, y_i)$ and $(x_j, y_j)$ is calculated for each pair of points in the dataset using Equation (2-18).

$$d(i,j) = \sqrt{(x_i - x_j)^2 + (y_i - y_j)^2}$$ (2-18)

The semivariance $V(i,j)$ between a pair of points $(i,j)$ with data values $Z_i$ and $Z_j$ is calculated for each pair of points in the dataset using Equation (2-19).

$$V(i,j) = \frac{(z_i - z_j)^2}{2}$$ (2-19)

An ordered pair $(d(i,j), V(i,j))$ of distance and semivariance is created for each pair of points in the dataset. These ordered pairs are sorted plotted as shown in Figure 2-23. This set of ordered pairs are used to compose the experimental variogram for the data.
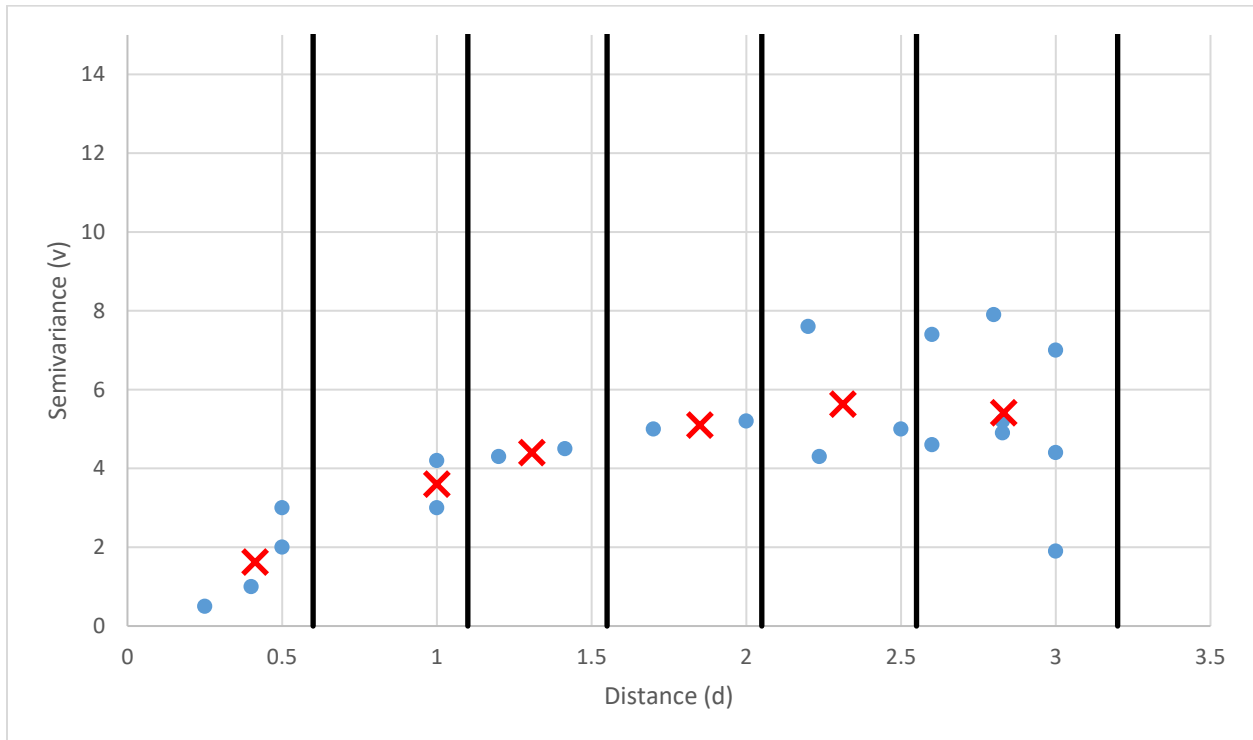


**Figure 2-23: Example of Experimental Variogram**

The next step is to fit a variogram model to the experimental variogram. This is an important step in Kriging interpolation. The selection and fitting of a proper variogram model greatly influences the accuracy of estimation. To interpolate groundwater levels, I used a spherical variogram model, which was found to produce the best results by several researchers, as well as from initial inspection of preliminary test case results (Gundogdu & Guney, 2007; Nikroo, Kompani-Zare, Sepaskhah, & Shamsi, 2010). The spherical variogram model $V(d)$ is a function of the distance $d$ of an observation point from the interpolation point and is given by Equation (2-20), defined by the Nugget ($n$), Range ($r$), and Sill ($s$), where the Partial Sill ($p$) is the difference between the sill and the nugget..

$$V(d) = \begin{cases} n + p\left(1.5\frac{d}{r} - .5\left(\frac{d}{r}\right)^3\right) & d \leq r \\ p + n & d > r \end{cases} \tag{2-20}$$

Equation (2-20) is known as the semivariance function. I developed a method to automatically fit a semivariance function with the appropriate Nugget, Range, and Sill parameters to the experimental variogram. In this method, the ordered pairs of distance and semi-variance $(d(i,j), V(i,j))$ are sorted into ten bins of equal intervals based on distance $d(i,j)$. The range of these bins extends from the minimum distance between two observation points in the aquifer to the sum of the minimum distance and the half the maximum distance between observation points in the aquifer. This approach of eliminating extremely distant points from the bins produces a more accurate estimation because the smallest distances are the most important for developing a proper variogram for accurate estimation (Kitanidis, 1997). The use of the distant observations skews the automatic variogram fitting routine towards the large variances of the distant observations, which negatively impacts the estimation.

Once the ordered pairs are sorted into the ten bins spanning equal intervals, the mean distance $d$ and semivariance $V$ are computed within each bin. These ten pairs of $(d, V)$ are then used to fit a spherical variogram model. The model is fit using a least squares optimization, by minimizing the residuals of the spherical variogram model compared to the ten ordered pairs. In this optimization, the residuals are weighted using a logistic function so that weights vary from a value approaching one at distance zero to a value approaching zero as the distance increases. This weighting allows the least squares optimization to fit the data better at closer distances, producing a better variogram for estimation (Kitanidis, 1997). The Nugget, Range, and Sill are determined using the least squares optimization. Figure 2-24 shows an example of the semivariance function automatically generated using this least squares technique, plotted with the original ordered pair data and the experimental variogram (red Xs).
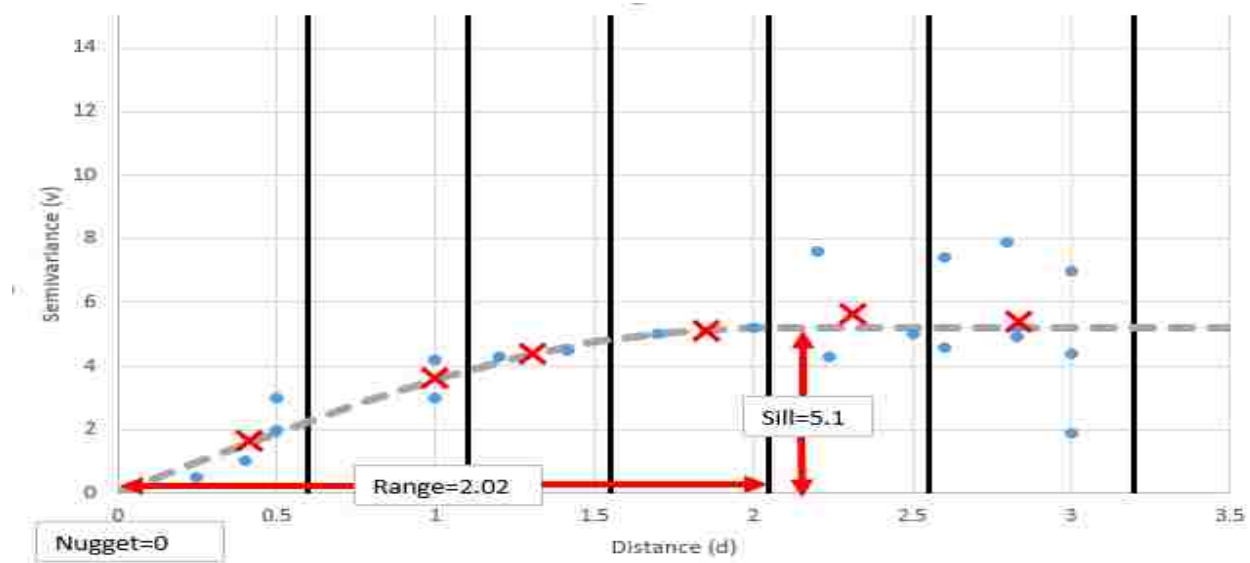


**Figure 2-24: Example of Semivariance Function fitted to Experimental Variogram**

With the semivariance function defined, the next step is to solve the Kriging system at each interpolation point. The matrix Equation (2-21) shows the format of this Kriging System.

34

$$\begin{bmatrix} V(1,1) & \cdots & V(1,n) & 1 \\ \vdots & \ddots & \vdots & 1 \\ V(n,1) & \cdots & V(n,n) & 1 \\ 1 & 1 & 1 & 0 \end{bmatrix} * \begin{bmatrix} \lambda_1 \\ \vdots \\ \lambda_{n+1} \end{bmatrix} = \begin{bmatrix} V(*,1) \\ \vdots \\ V(*,n) \\ 1 \end{bmatrix}$$

Equation (2-21) is solved for each of the $n + 1$ weights $\lambda_i$. With the weights determined, it is now straightforward to estimate $Z_*$ at each location $(x_*, y_*)$ using Equation (2-17). This Kriging interpolation is carried out at a user specified spatial resolution throughout the aquifer using the GSLIB FORTRAN code developed at Stanford University (Deutsch & Journel, 1992). This code provides a very well optimized, accurate, and complete version of Kriging estimation, which can be quickly performed throughout the entire aquifer. In some cases, the data may yield a singular matrix in Equation (2-21), so the GSLIB code cannot provide a solution. In these cases, the Groundwater Level Mapping Tool reverts to an IDW interpolation for the singular points, as detailed in Section 2.3.1.

## 2.4 Calculation of Aquifer Storage

With the results of the temporal and then spatial interpolation, it is possible to calculate changes in total aquifer storage volume based on an estimate of aquifer porosity. This is accomplished by performing mathematic operations on $n$ series of raster datasets $R$ of groundwater levels at specific times produced during the spatial interpolation phase. The first dataset (corresponding to the earliest time step in the series) is known as $R_0$ and serves as the baseline from which changes in aquifer storage are measured.

These changes are calculated by first calculating the drawdown $D_i$ from the bases case for each time step in the raster series. The drawdown $D_i$ is calculated on a cell-by-cell basis by

applying Equation (2-22) for each of the $n$ timesteps, resulting in a new set of $n - 1$ raster datasets of drawdown.

$$\forall i \in \{1, \dots, n\} \ D_i = R_i - R_0 \tag{2-22}$$

Aquifer-wide storage changes $C_i$ are then calculated  fore each time step by multiplying the drawdown $D_i^j$ at each grid cell $j$ by the average aquifer storage coefficient $p$ and the grid cell area $A_j$, and summing over all grid cells in the aquifer, as shown in Equation (2-23). The aquifer storage coefficient $p$ will be either the specific storage (for a confined aquifer) or the specific yield (for an unconfined aquifer), which is close to, but typically a little smaller than the porosity. These values may vary throughout an aquifer, and an aquifer may even be partially confined, partially unconfined. This tool is meant to produce a rough estimate of storage volume and so employs a rough average of the storage coefficient over the aquifer. To determine a more accurate estimate where storage coefficients are known in detail, the aquifer could be split into several sections based on storage coefficients, and the storage volume calculated separately and then summed together over the sections.

$$\forall i \in \{1, \dots, n\} \ C_i = \sum_{j=1}^{Aquifer} D_i^j p A_j \tag{2-23}$$

The area $A_j$ is not constant for each grid cell over the dataset, since the grids are defined at a specified latitude and longitude resolution. Each cell has constant height, but the cell width is dependent on the cell latitude. Cells closer to the equator will have larger widths than those nearer the poles. The area of each grid cell $A_j$ in the aquifer is calculated based on the resolution of the grid $g$, the mean radius of the Earth $R$, and the latitude $l_j$ of the center of each grid cell $j$ as shown in Equation (2-24).

$$\forall j \in \{Aquifer\} \; A_j = R^2 \sin g * \left| \sin(l_j + \frac{g}{2}) - \sin(l_j - \frac{g}{2}) \right| \tag{2-24}$$

When the Groundwater Level Mapping Tool is in metric mode, the mean radius of the Earth $R$ is 6,371,000 meters (Moritz, 1980). The aquifer storage is calculated in cubic meters, since the depth to groundwater measurements and therefore drawdown $D_i$ is also in meters. In imperial units, the Groundwater Level Mapping Tool reports changes in aquifer storage volume in Acre-ft. The app uses a mean Radius of the Earth $R$ of 3,959 miles. In this case, the result of Equation (2-23) is in square mile-ft, which is converted to acre-ft by multiplying by 640. An example of the output of this storage volume calculation procedure for the Cedar Valley, UT Aquifer is shown in Figure 2-25.
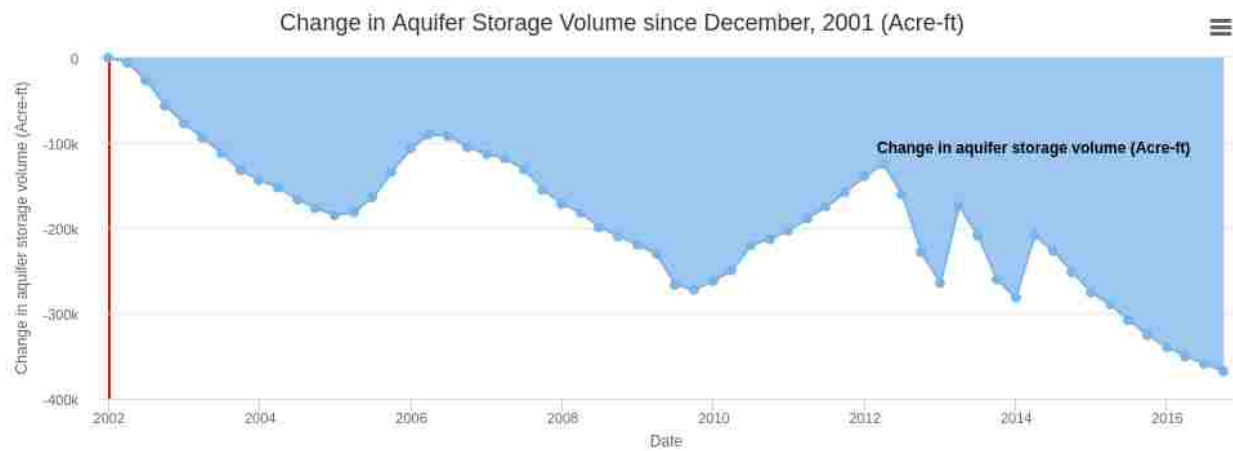


**Figure 2-25: Example Output of Aquifer Storage Volume**

## 3 RESULTS

The Groundwater Level Mapping Tool has been implemented in Utah, Texas, The Dominican Republic, South Africa, and Colombia. This wide range of application demonstrates the versatility of this new tool, which will enable water managers world-wide to take better stewardship over groundwater resources.

### 3.1 Utah

I used the Groundwater Level Mapping Tool to analyze 18 aquifer systems throughout the State of Utah, using data hosted on the USGS NWIS site. The Utah aquifers were useful in validating the results of the application because the USGS published a report on the groundwater conditions in Utah in the spring of 2015. In this report, aquifer groundwater levels in 2015 were compared to those 30 years earlier in 1985 (Burden, 2015). To validate the interpolation techniques described in the previous chapter, I compared maps of aquifer drawdown from 1985 to 2015 produced by the Groundwater Level Mapping Tool to those produced by the USGS. Figure 3-1 shows a side-by-side comparison of this 30-yr drawdown mapped by the app (on the left) and by the USGS (on the right) for the Tooele Valley near Tooele, UT. Figure 3-2 shows a similar comparison for the Escalante Valley near Milford, UT, Figure 3-3 for the Escalante Valley near Beryl, UT, and Figure 3-4 for the Juab Valley near Nephi, UT.

**Figure 3-1: Comparison for Tooele Valley, near Tooele, UT**
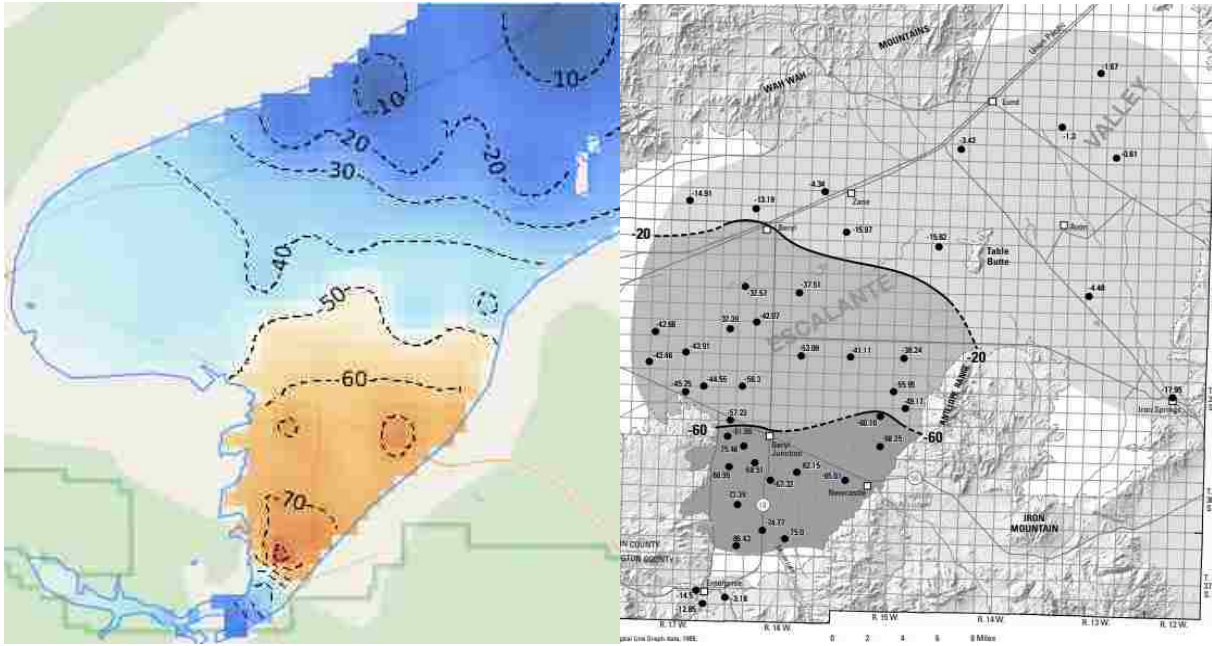


**Figure 3-2: Comparison for Escalante Valley near Milford, UT**

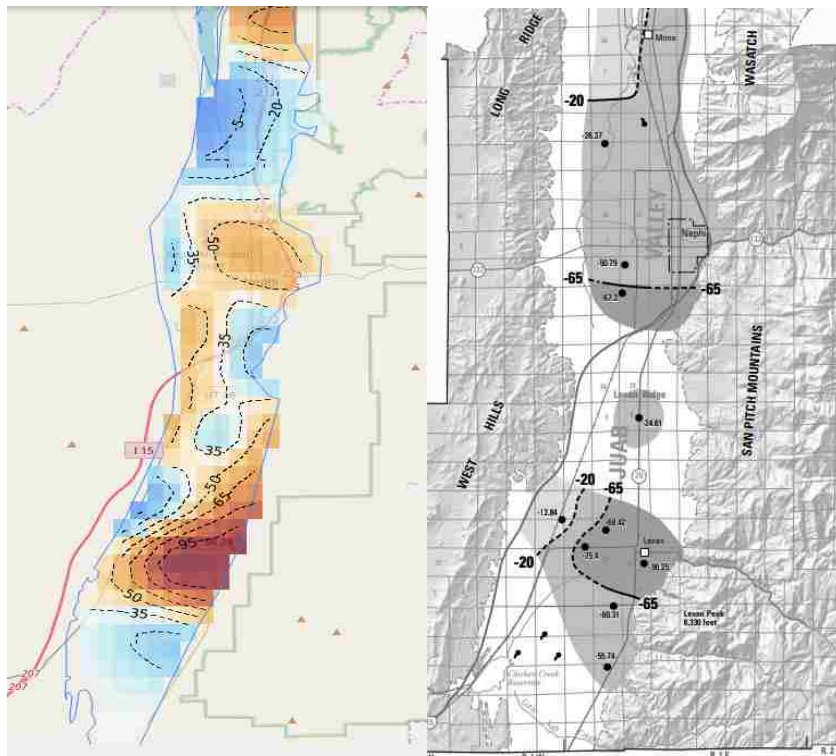**Figure 3-3: Comparison for Escalante Valley near Beryl, UT**



**Figure 3-4: Comparison for Juab Valley near Nephi, UT**

40

The contours generated by the app are reasonably similar to those mapped by the USGS. This shows the utility of the app for mapping groundwater throughout aquifers.

### 3.1.1  Testing of Multi-Linear Regression Harnessing Correlated Wells in Utah

The method of time series extension by Multi-Linear Regression Harnessing Correlated Wells detailed in Section 2.2.2 was tested using a set of ten wells from the Cedar Valley Aquifer each containing data from 1980 – 2015. The locations of these 10 wells are shown in Figure 3-5. The Cedar Valley Aquifer was chosen as a test case because it contains several wells with a sufficiently long and detailed period of groundwater measurements and because the wells in this aquifer exhibit trends and patterns that pose significant difficulties to time series analysis. The time series in this aquifer are non-stationary, and neither increase or decrease at constant rates. The measurements taken from 1980-1995 were used to train the dataset, then the model predictions were compared to the actual data for measurements taken after 1995, thus testing the model. Both the training and testing datasets include significant peaks and valleys in the data, and cannot be predicted easily using classical time series analysis methods. The testing dataset also includes values well outside the scope of the training dataset. The newly developed MLR method of time series extension was used to make predictions at each well, and then compared against a naïve prediction, where the groundwater was assumed to remain constant after 1995, and a linear least squares prediction. The results of these model predictions are shown in Figure 3-6 through Figure 3-15, with the training data (green), the measured data (solid red), the MLR prediction (dashed red), the naïve prediction (dashed blue), and the least squares prediction (dashed yellow) for each of the ten wells.

41
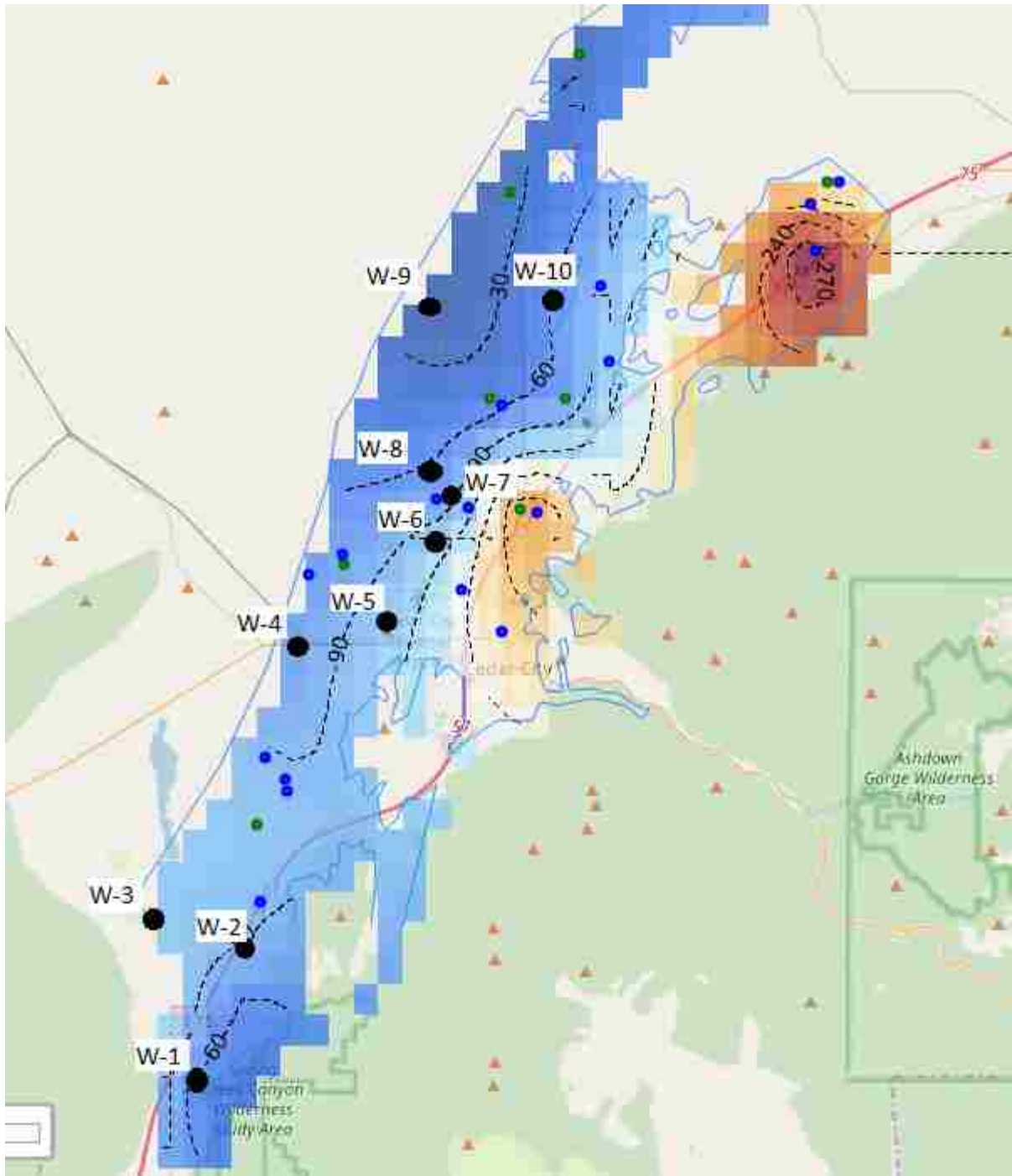
**Figure 3-5: Location of 10 Testing Wells for MLR in Cedar Valley Aquifer**
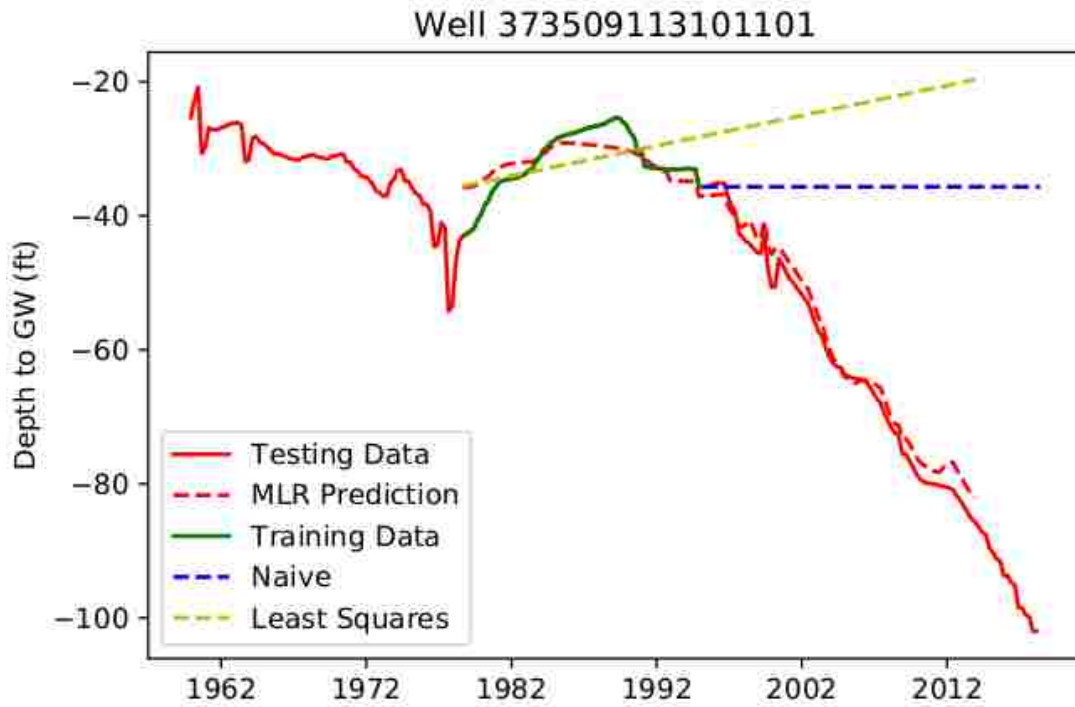
**Figure 3-6: Time Series Model for Well 373509113101101**
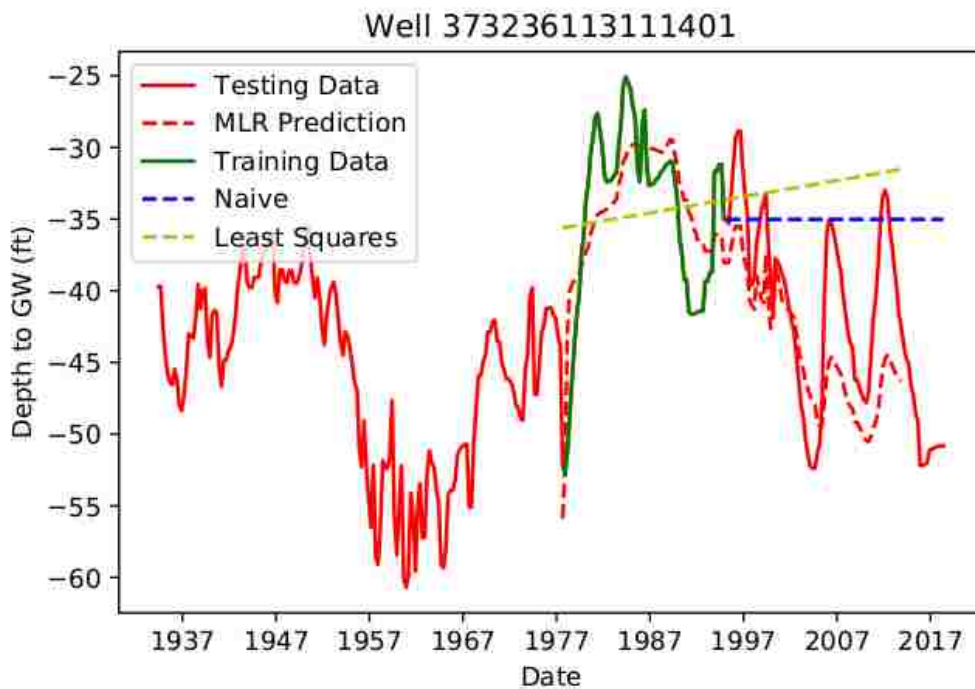


**Figure 3-7: Time Series Model for Well 373236113111401**
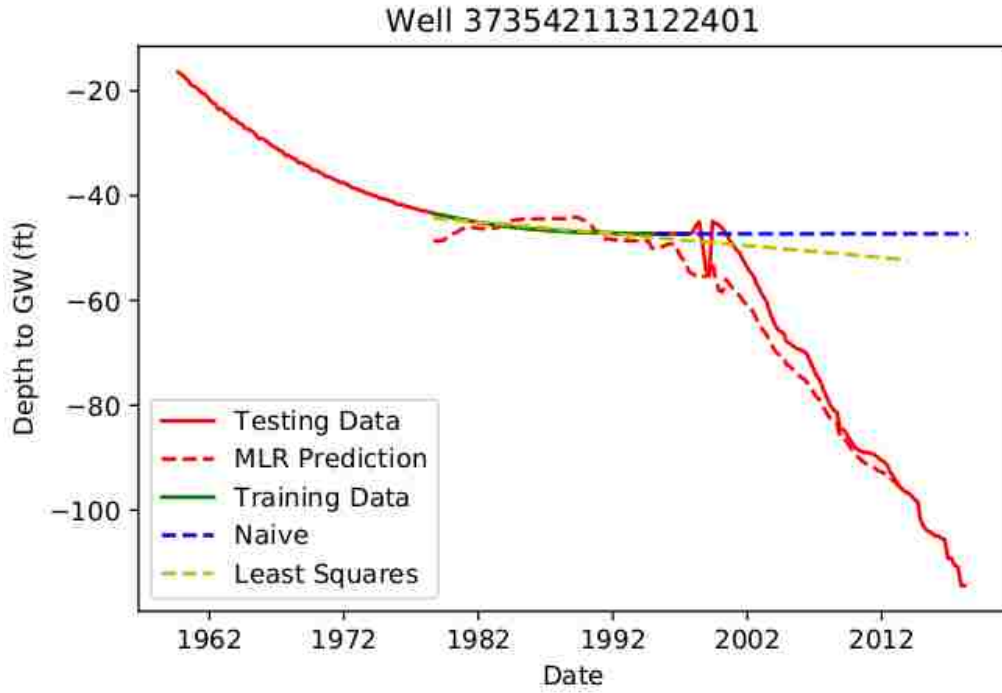
**Figure 3-8: Time Series Model for Well 373542113122401**
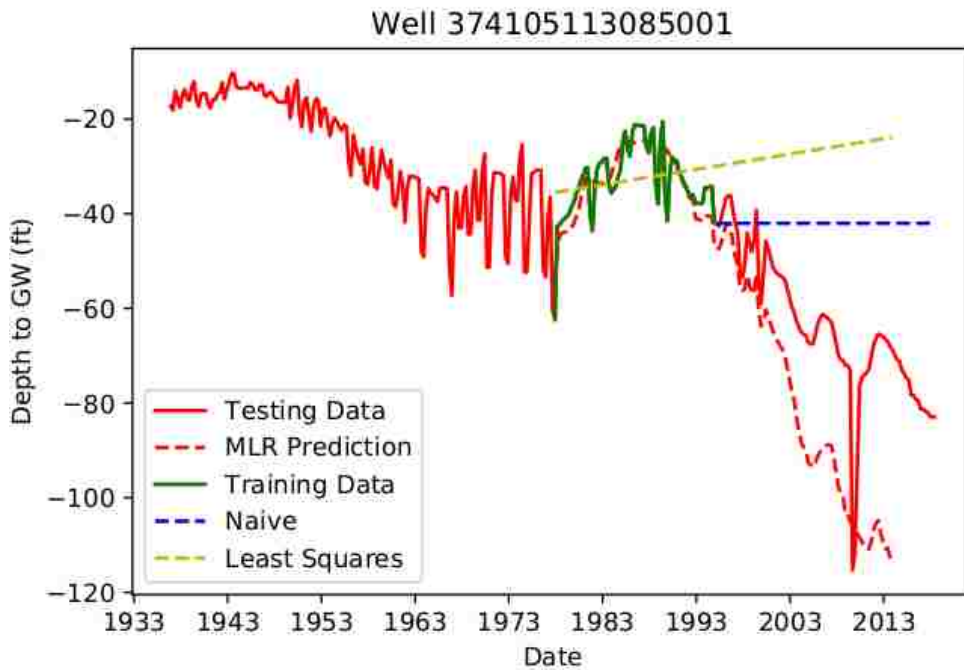


**Figure 3-9: Time Series Model for Well 374105113085001**
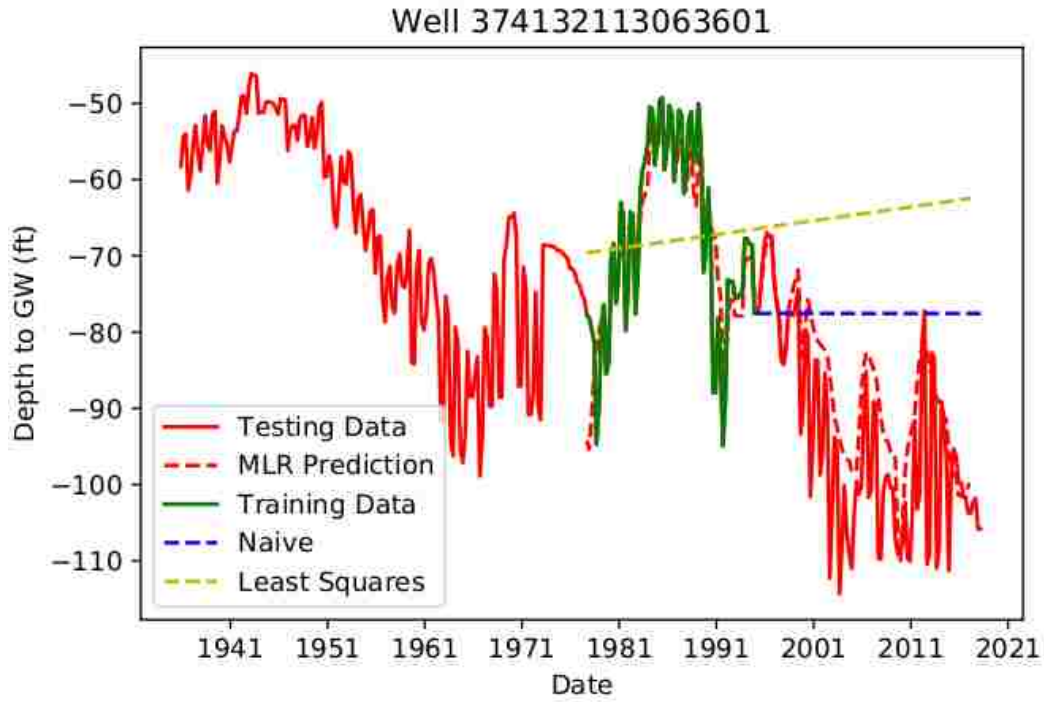
**Figure 3-10: Time Series Model for Well 374132113063601**
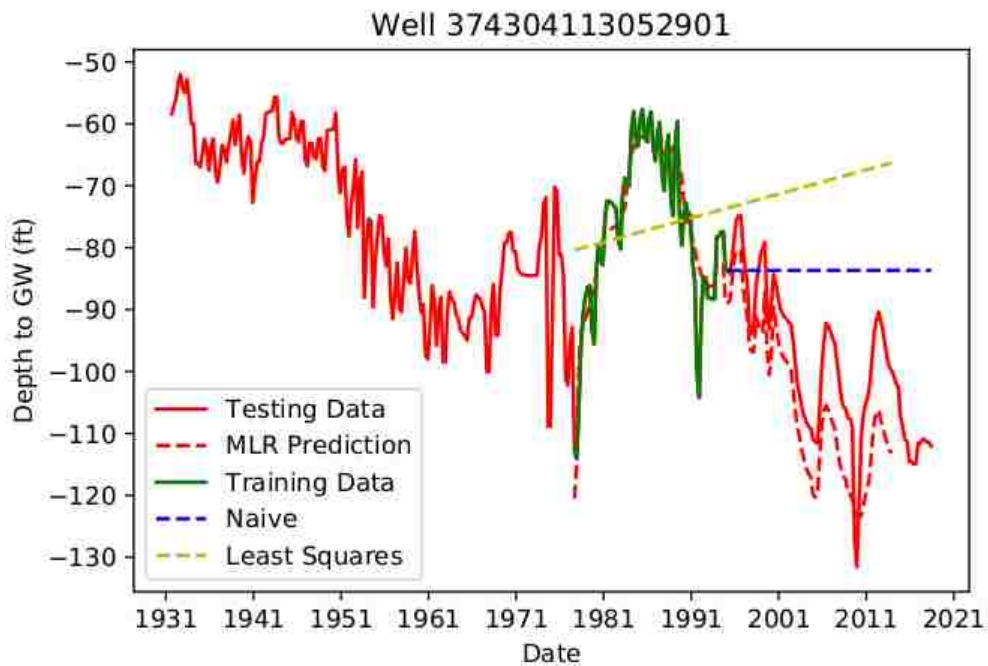


**Figure 3-11: Time Series Model for Well 374304113052901**
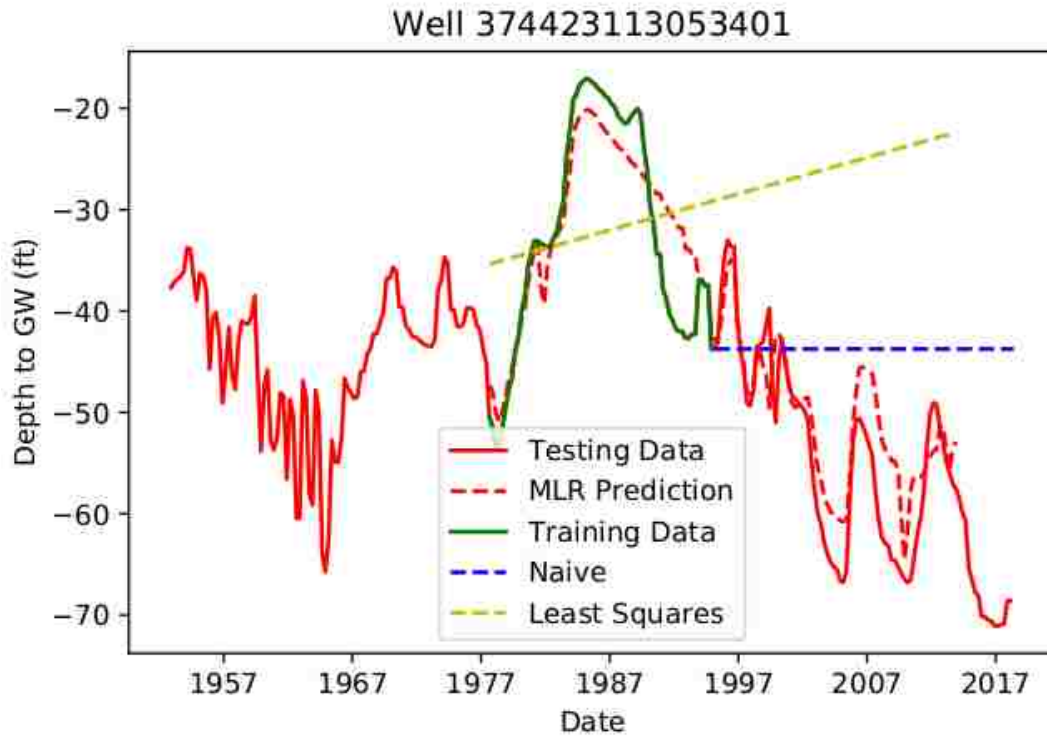
**Figure 3-12: Time Series Model for Well 374423113053401**
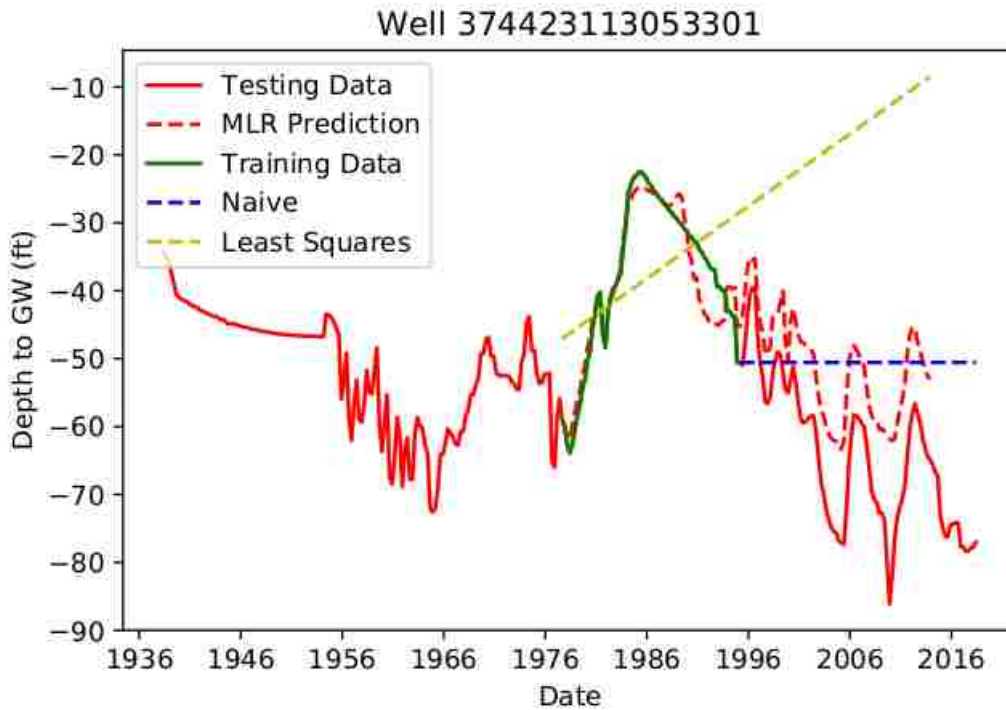


**Figure 3-13: Time Series Model for Well 374423113053301**
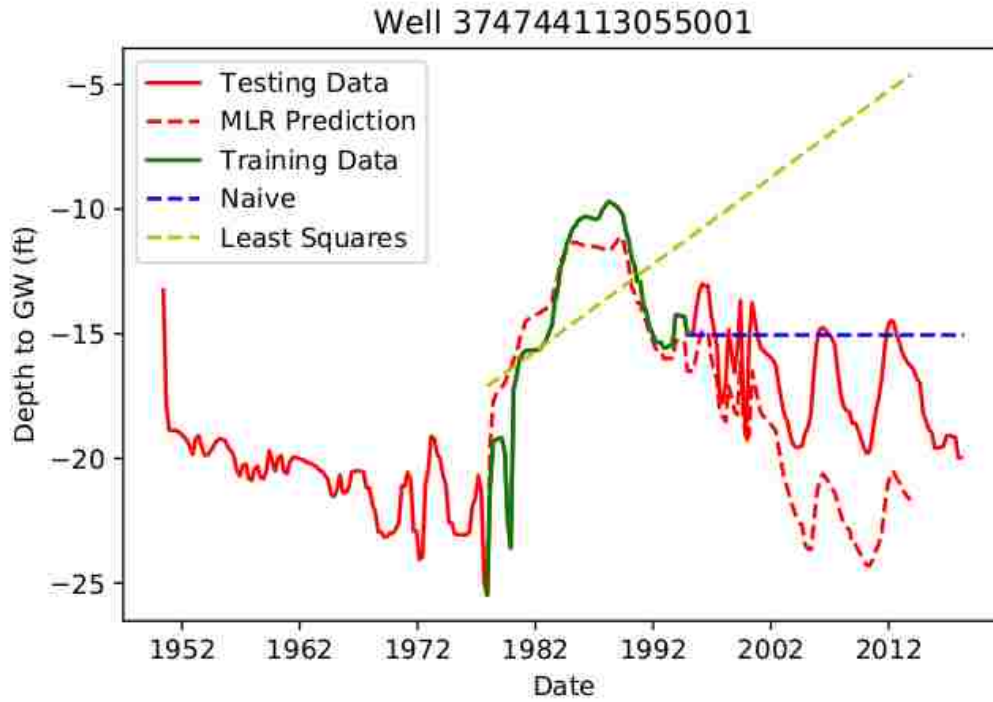
**Figure 3-14: Time Series Model for Well 374744113055001**
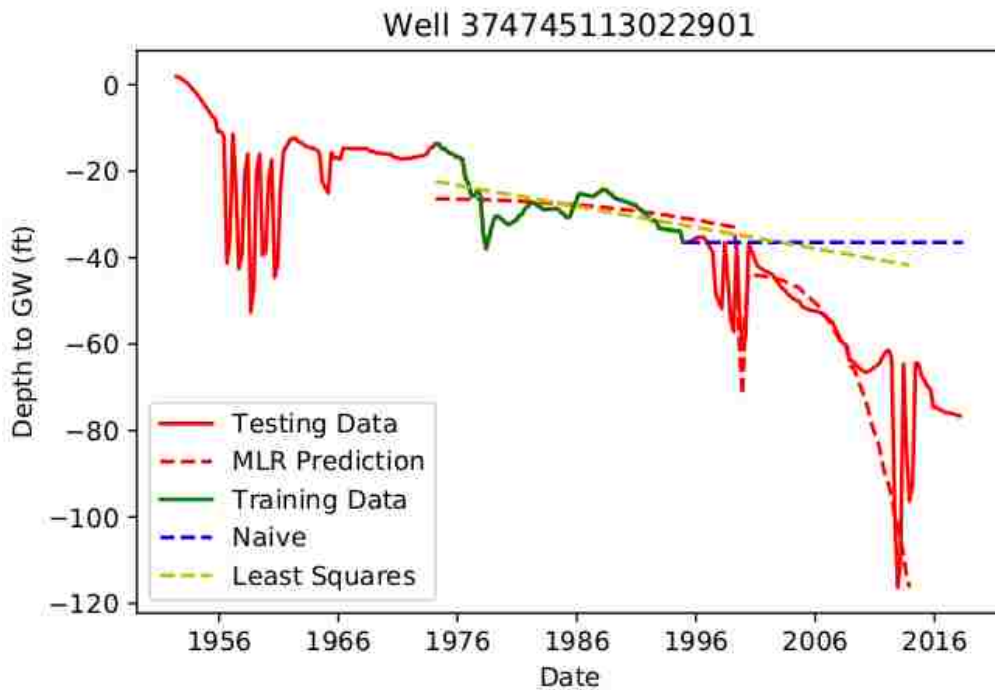


**Figure 3-15: Time Series Model for Well 3745113022901**

As demonstrated by Figure 3-6 through Figure 3-15, the MLR method outperformed the naïve and least squares estimation methods for each well (with the exception of Well 374744113055001). Table 3-1 shows the RMSE value for each of the ten wells in the Cedar Valley study area for the MLR, naïve, and least squares prediction methods. The MLR method decreased the RMSE value by an average of 57% from the naïve method, and 68% from the least squares method.

**Table 3-1: RMSE Values for Time Series Prediction
for Ten Wells in Cedar Valley Aquifer**

| Map ID | Well ID | RMSE Value for Various Methods | | |
|--------|---------|------|------|---------------|
| | | MLR | Naïve | Least Squares |
| W-1 | Well 373236113111401 | 5.67 | 9.63 | 9.89 |
| W-2 | Well 373509113101101 | 2.33 | 36.64 | 41.00 |
| W-3 | Well 373542113122401 | 5.29 | 34.58 | 23.45 |
| W-4 | Well 374105113085001 | 24.57 | 26.29 | 37.09 |
| W-5 | Well 374132113063601 | 10.33 | 21.16 | 32.59 |
| W-6 | Well 374304113052901 | 10.06 | 19.37 | 29.38 |
| W-7 | Well 374423113053301 | 11.33 | 17.43 | 45.88 |
| W-8 | Well 374423113053401 | 4.98 | 15.79 | 29.46 |
| W-9 | Well 374744113055001 | 4.14 | 2.73 | 9.20 |
| W-10 | Well 374745113022901 | 11.97 | 27.06 | 22.15 |

The method of time series extension using Multi-Linear Regression Harnessing Correlated Wells was also tested for accuracy against Kriging spatial interpolation, using a jackknife approach. This testing was carried out for ten wells in the Cedar Valley Aquifer. The depth to groundwater on December 31, 2014 was estimated at each testing well by implementing the PCHIP and then Kriging interpolation, omitting the measured depth at the testing well from the interpolation. The depth to groundwater on December 31, 2014 was then estimated at each testing well by implementing the MLR technique, using data from 1985-1995 as the training set, and then estimating twenty years of groundwater depths from 1995-2015. The results of both of

48

these estimates, the actual measurement, and the % error for each estimate are displayed in Table 3-2 for each of the ten tested wells.

**Table 3-2: Error Values for MLR Estimate Compared to Kriging Estimate
for Ten Wells in Cedar Valley Aquifer**

| Map ID | Well ID | Measured Value Depth to GW (ft) | MLR Estimate Depth to GW (ft) | (% error) | Kriging Estimate Depth to GW (ft) | (% error) |
|---|---|---|---|---|---|---|
| W-1 | Well 373236113111401 | -47.6 | -49.9 | -(4.8%) | -66.8 | -(40.3%) |
| W-2 | Well 373509113101101 | -90.6 | -92.1 | -(1.7%) | -89.3 | (1.4%) |
| W-3 | Well 373542113122401 | -103.7 | -101.4 | (2.2%) | -88.6 | (14.6%) |
| W-4 | Well 374105113085001 | -74 | -79.1 | -(6.9%) | -88.6 | -(19.7%) |
| W-5 | Well 374132113063601 | -93.5 | -96.2 | -(2.9%) | -100.8 | -(7.8%) |
| W-6 | Well 374304113052901 | -109.7 | -113.8 | -(3.7%) | -77.4 | (29.4%) |
| W-7 | Well 374423113053301 | -75.6 | -60 | (20.6%) | -80.8 | -(6.9%) |
| W-8 | Well 374423113053401 | -67 | -67.2 | -(0.3%) | -61.8 | (7.8%) |
| W-9 | Well 374744113055001 | -18.6 | -20.2 | -(8.6%) | -30.3 | -(62.9%) |
| W-10 | Well 374745113022901 | -68.9 | -69.4 | -(0.7%) | -58.3 | (15.4%) |

The MLR produced relatively accurate results, with seven of the ten tested wells exhibiting less than 5% error, and nine of the wells exhibiting less than 10% error. Errors are significantly smaller for the MLR estimate than the Kriging estimate with the exception of W-2, where the error is practically the same, and W-7, where the MLR error is greater than Kriging. Kriging produces a better estimate at this well for two reasons: W-7 is quite close to W-6 and W-8 (see Figure 3-5), which decreases the variance of the Kriging interpolation; and the time series for W-7 contains only four points in its training dataset from 1985-1995 as shown in Figure 3-16, which decreases the accuracy of the MLR method. With these factors, it is unsurprising that Kriging outperformed MLR in this instance. These results demonstrate that in most cases where data are available from a different time period than desired, it is more accurate to interpolate temporally using MLR referencing other wells than to interpolate spatially from other wells. This

49

is significant, since researchers using different temporal interpolation methods have previously concluded that "spatial structure was a little bit stronger than temporal structure"(Ahmadi & Sedghamiz, 2007).



**Figure 3-16: Time Series for W-7 in Cedar Valley Aquifer**

### 3.1.2 Testing of ELM Harnessing Earth Observations in Cedar Valley, Utah

I tested the ELM method in Utah's Cedar Valley Aquifer. Data from 1958-199 were used as training data for the model, and data from 2000-2015 were used as the testing data set. This test was performed on five wells within the aquifer. These wells are shown in Figure 3-17. The Map ID for each corresponding Well ID is shown in Table 3-3.

**Table 3-3: Map IDs for 5 Wells**
**in Cedar Valley Aquifer**

| Map ID | Well ID |
|--------|---------|
| E-1 | Well 373236113111401 |
| E-2 | Well 374132113063601 |
| E-3 | Well 374304113052901 |
| E-4 | Well 374423113053301 |
| E-5 | Well 374927113033401 |

50
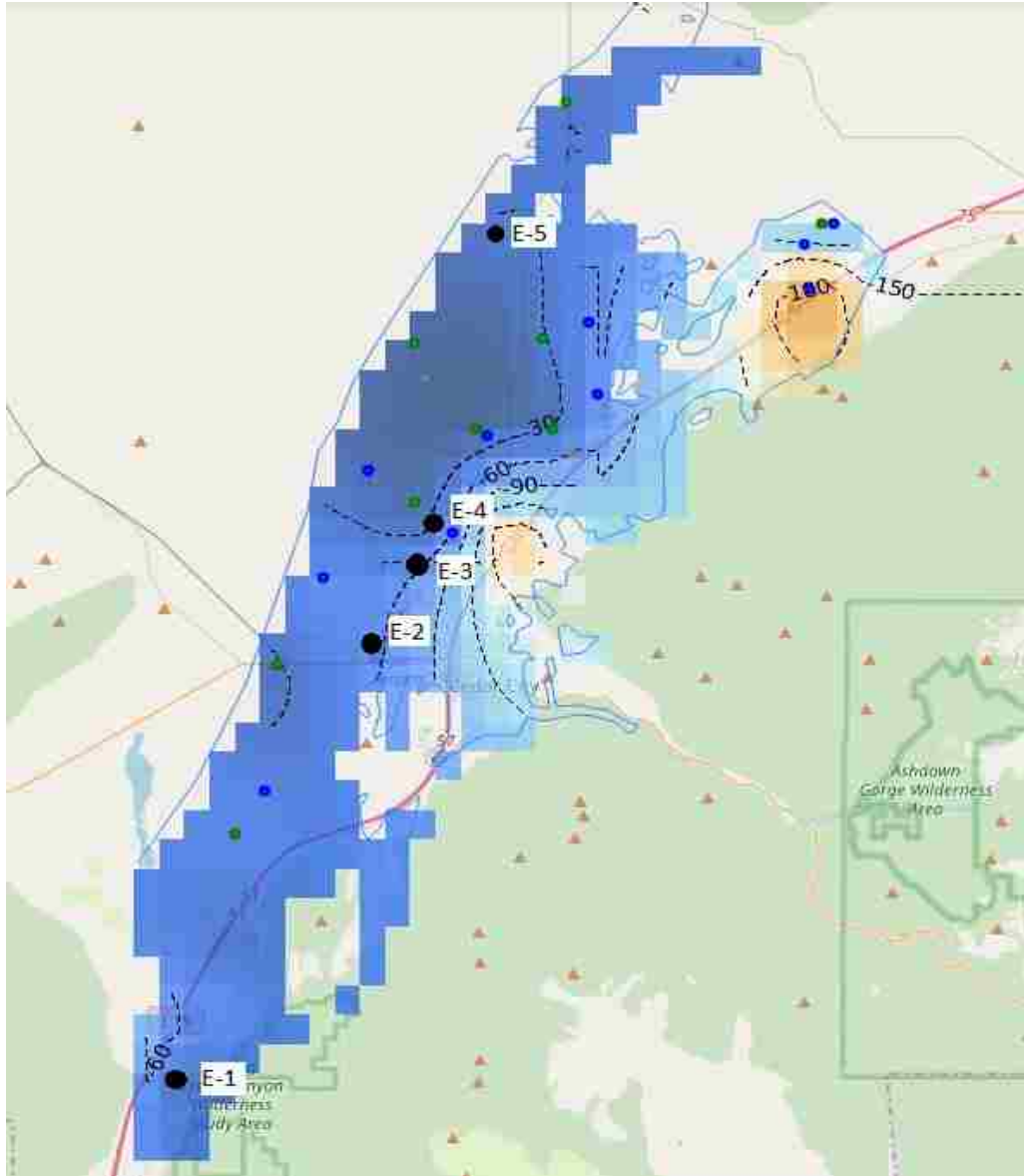
**Figure 3-17: Location of 5 Testing Wells for ELM in Cedar Valley Aquifer**

Figure 3-18 shows the modelled (blue) and the measured (orange) depth to groundwater (ft) with the testing period denoted by the red bounding box for Well 37236113111401 (E-1), which is located just west of Kanarraville, Utah in the Cedar Valley. The depth to groundwater over the observation period at this well varies between 25 and 60 ft. The modelled depth to groundwater values match the measured data very well for the testing period.

**Figure 3-18: ELM Results for Well 373236113111401 (E-1)**

Figure 3-19 shows the results for Well 37430113052901 (E-3), which is located just North of the Cedar City Regional Airport in Utah's Cedar Valley. Again, the results are quite good, with modelled depth to groundwater matching the shape and approximating the magnitude of the measured depth to groundwater. This well is deeper than the first well, with depths varying between 60 and 130 ft.



**Figure 3-19: ELM Results for Well 374113052901 (E-3)**

Figure 3-20 shows the results from Well 374423113053301 (E-4), which is located North of the previous well. The results of this model are good, but this model shows a trend of overestimating the groundwater levels, a trend also present in the first two wells, but to a smaller extent. This consistent overestimation possibly occurs because of human pumping activity, which is not explicitly represented in the model. The PDSI variables attempt to represent pumping, since pumping will likely increase during times of relative dryness, but this is not sufficient to adequately represent all pumping activity.
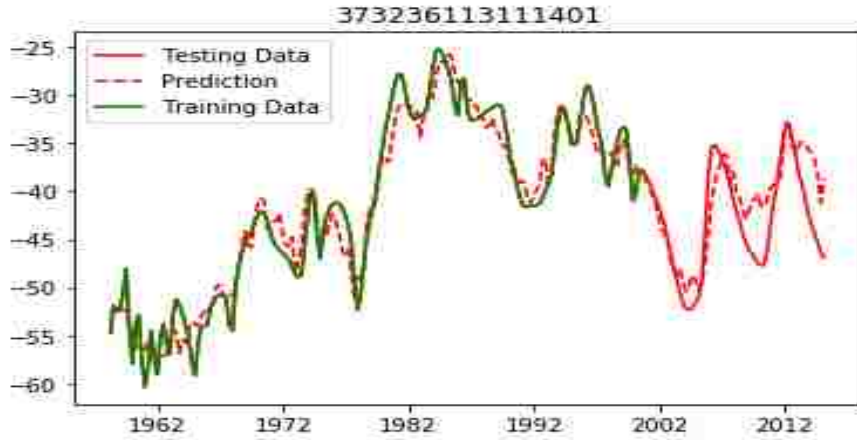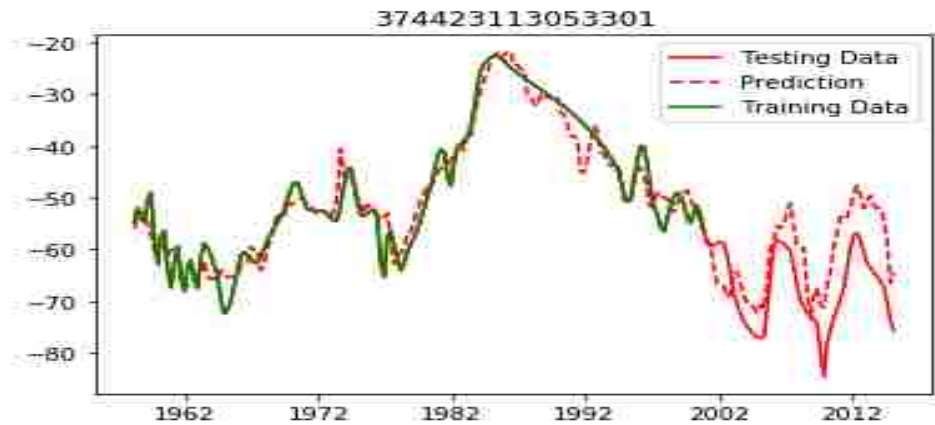


**Figure 3-20: ELM Results for Well 374423113053301 (E-4)**

Figure 3-21 shows the results for Well 374132113063601 (E-2), which is located just West of the Cedar City Regional Airport. The ELM model results are quite good here as well. The model captures the general trends of the groundwater, following a course matching the general average depth to groundwater. However, this model fails to properly capture the magnitude of the seasonal variation of the water table throughout the year. This most likely occurred because of the inconsistent sampling rate of the well. In some cases throughout the training period, it was

sampled at monthly frequency, but not for the duration. This mixture of higher and lower sampling rates negatively impacted the model.
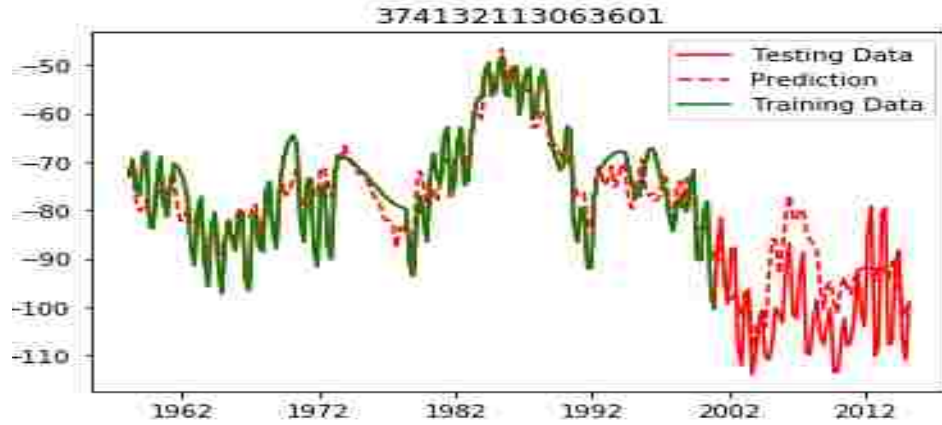


**Figure 3-21: ELM Results for Well 374132113063601 (E-2)**

The worst results obtained were for Well 374927113033401 (E-5), located at the northern end of the aquifer. The model failed to accurately capture the general shape of the time series, as shown in Figure 3-22. It is possible that this failure occurred because of the low resolution of the Earth observation data, which does not accurately reflect conditions in this area at the northern end of the aquifer.
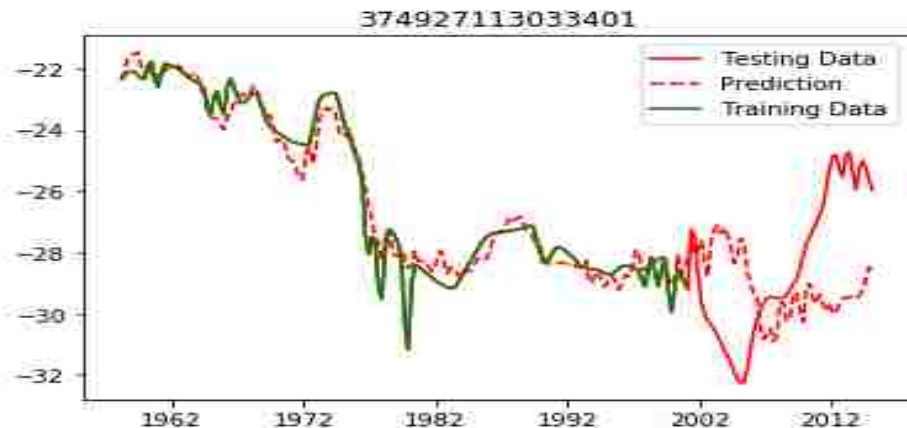


**Figure 3-22: ELM Results for Well 374927113033401 (E-5)**

Results obtained from the ELM method were compared against the naïve and least squares predictions using the RMSE and NRMSE error metrics. The NRMSE is akin to the RMSE method, but normalized by the range of the data. This helps make better comparisons between results for different wells. For example, Well 374927113033401 has a very small range of data compared to Well 374304113052901, so the RMSE for the first well is lower than that of the second, even though the model fits better for the second well. The NRMSE is much lower for the second well than the first, since this error metric takes the range of the data into account. The RMSE measurements for each well are given in Table 3-4, while the NRMSE values are given in Table 3-5.

**Table 3-4: RMSE Values for ELM Time Series Prediction for Five Wells in Cedar Valley Aquifer**

| Map ID | Well ID | RMSE Value for Various Methods | | |
|--------|---------|------|-------|---------------|
| | | ELM | Naïve | Least Squares |
| E-1 | Well 373236113111401 | 2.96 | 12.69 | 14.93 |
| E-2 | Well 374132113063601 | 12.96 | 69.45 | 71.99 |
| E-3 | Well 374304113052901 | 10.44 | 70.94 | 73.49 |
| E-4 | Well 374423113053301 | 10.98 | 36.57 | 39.09 |
| E-5 | Well 374927113033401 | 4.81 | 4.29 | 2.38 |

**Table 3-5: NRMSE Values for ELM Time Series Prediction for Five Wells in Cedar Valley Aquifer**

| Map ID | Well ID | NRMSE Value for Various Methods | | |
|--------|---------|------|-------|---------------|
| | | ELM | Naïve | Least Squares |
| E-1 | Well 373236113111401 | 0.22 | 0.66 | 0.78 |
| E-2 | Well 374132113063601 | 0.31 | 1.99 | 2.07 |
| E-3 | Well 374304113052901 | 0.27 | 1.84 | 1.91 |
| E-4 | Well 374423113053301 | 0.29 | 1.31 | 1.40 |
| E-5 | Well 374927113033401 | 0.60 | 0.57 | 0.32 |

The ELM method produced a better prediction than both the naïve and least squares methods for four of the five wells. This method is not as accurate as the MLR prediction method and should only be used when no data from other wells is available. In some cases, the ELM fails to produce a good model.

### 3.1.3 Testing of ELM Harnessing Earth Observations in Beryl Enterprise, Utah

I tested this method again in the Beryl Enterprise area of southern Utah, which has experienced significant drawdown over the last century, especially in the southern portion of the aquifer. I chose ten wells in this aquifer for testing, as shown in Figure 3-23.
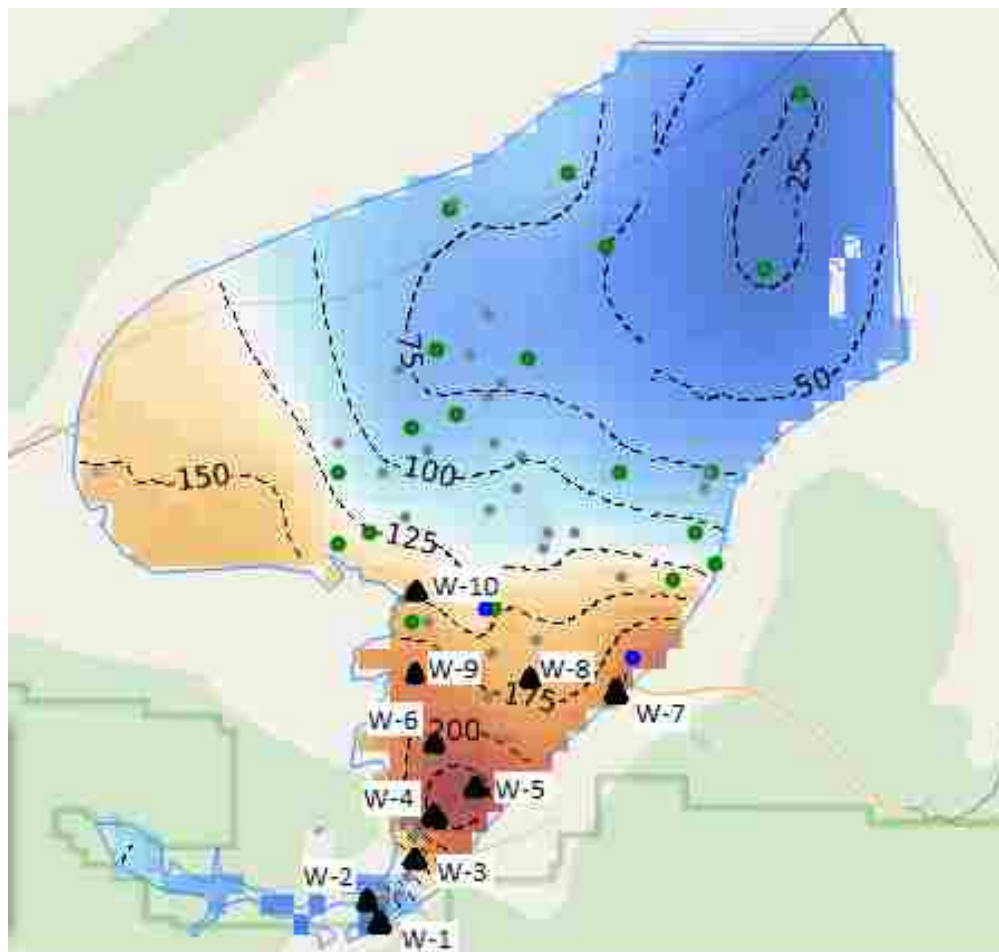


**Figure 3-23: Location of 10 Testing Wells for ELM in Beryl Enterprise Aquifer**

56

Well 373338113431502 (W-1), Well 373419113434201 (W-2), and Well

373527113415101 (W-3) displayed the best results, as shown in Figure 3-24, Figure 3-25, and

Figure 3-26 with the testing period from 2000 onwards shown in the red bounding box.
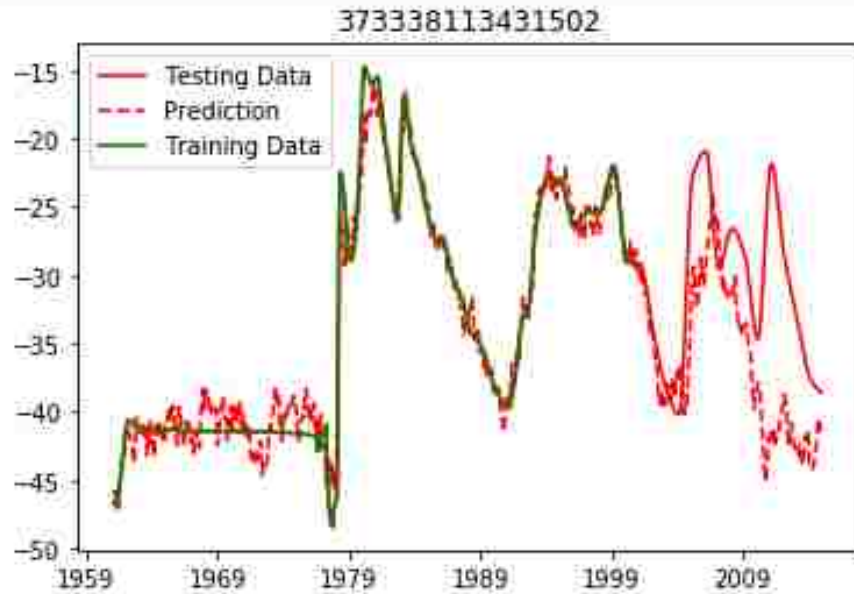


**Figure 3-24: ELM Results for Well 373338113431502 (E-1)**
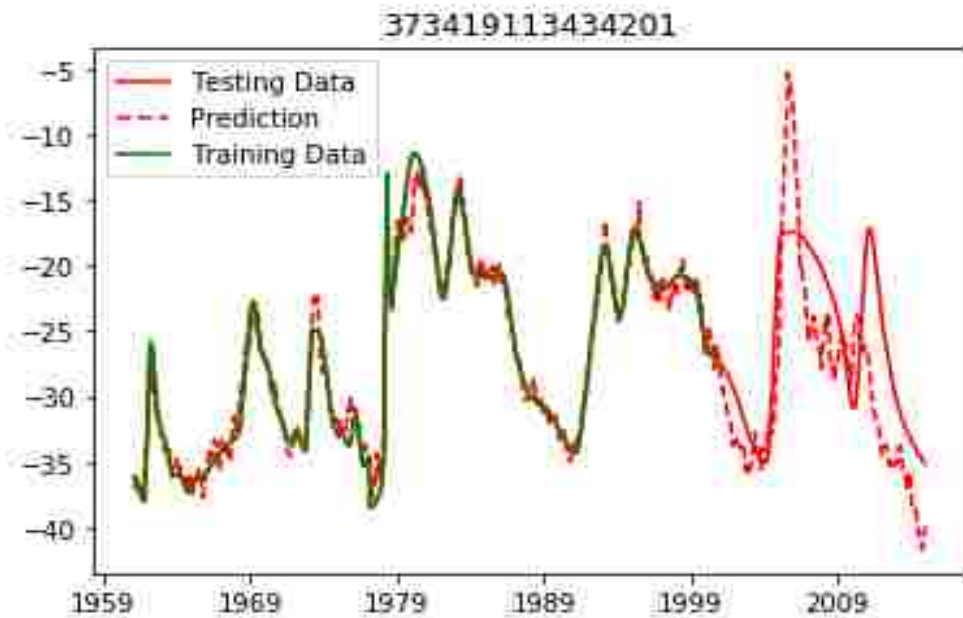


**Figure 3-25: ELM Results for Well 373419113434201 (E-2)**
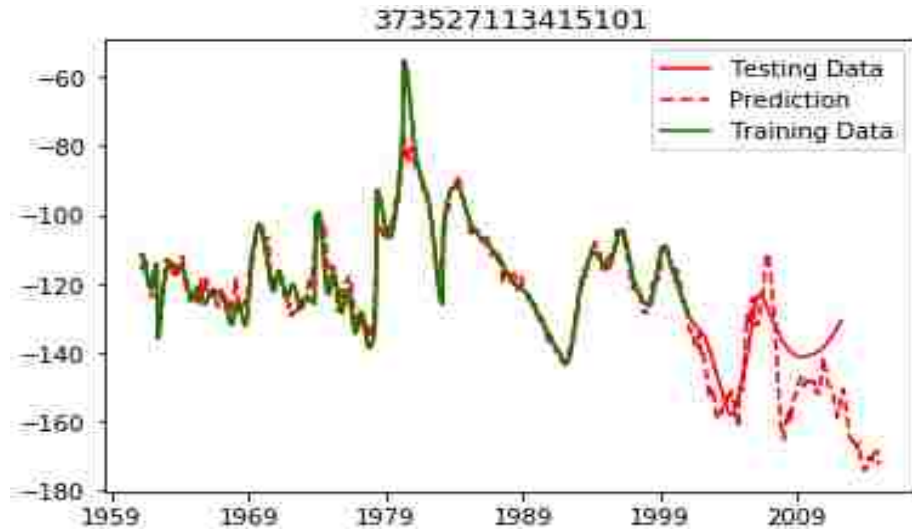
**Figure 3-26: ELM Results for Well 37327113415101 (E-3)**

Results for the other seven wells in the aquifer were not as good. In each case, the ELM model correctly identified periods of increase and decrease in water levels for each of the wells, but failed to properly estimate the magnitude of these changes, the result was an underestimation of drawdown for each of the tested wells. Figure 3-27 shows results typical for wells E-4 – E-10.
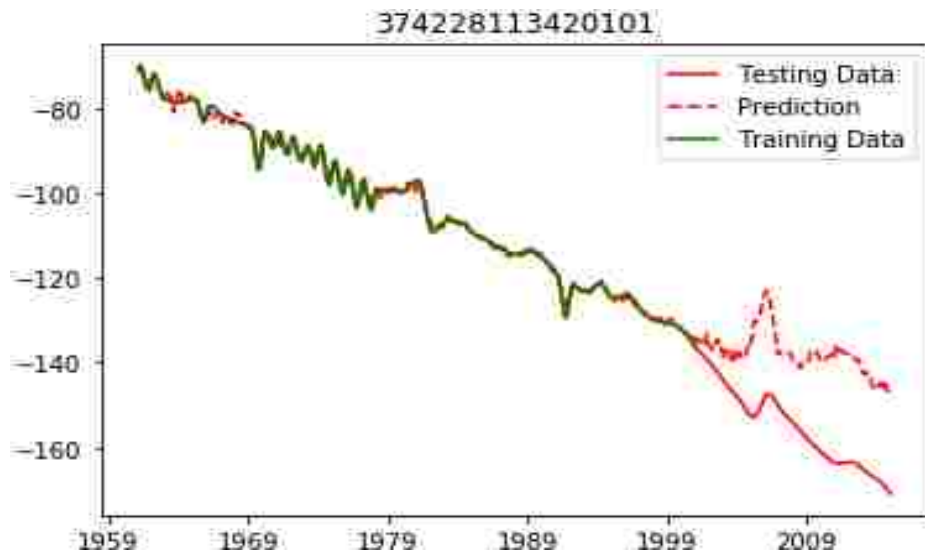


**Figure 3-27: ELM Results for Well 374228113420101 (E-4),**
**Typical of Wells E-4 to E-10**

58

Based on these results from the Cedar Valley and the Beryl Enterprise Aquifer, I concluded that the ELM method is less accurate for aquifers heavily influenced by human activity. The area around wells E-4 through E-10 is pumped excessively for irrigation purposes, which is not captured by the ELM model. The accuracy of this method would be significantly increased if the input parameters included a term accounting for pumped withdrawals. The method performs best in areas that are not subject to excessive pumping (wells E-1 – E-3). Table 3-6 shows the NRMSE values for each of the ten wells for the testing period from 2000-2015.

**Table 3-6: NRMSE Values for ELM Time Series Prediction
for Ten Wells in Beryl Enterprise Aquifer**

| Map ID | Well ID | NRMSE Error for Prediction | | |
| | | ELM | Least Squares | Naïve |
| --- | --- | --- | --- | --- |
| W-1 | 373338113431502 | 0.21 | 0.75 | 0.29 |
| W-2 | 373419113434201 | 0.28 | 0.64 | 0.31 |
| W-3 | 373527113415101 | 0.22 | 0.89 | 0.34 |
| W-4 | 373644113411501 | 0.42 | 0.60 | 0.54 |
| W-5 | 373735113393801 | 0.28 | 0.40 | 0.48 |
| W-6 | 373854113411501 | 0.37 | 0.52 | 0.52 |
| W-7 | 374020113343101 | 0.38 | 0.34 | 0.58 |
| W-8 | 374041113373501 | 0.31 | 0.44 | 0.54 |
| W-9 | 374053113415101 | 0.50 | 0.54 | 0.55 |
| W-10 | 374319113415201 | 0.38 | 0.36 | 0.51 |
| | **Average NRMSE Error** | **0.33** | **0.55** | **0.47** |

The ELM method produced the best results for the first 3 wells and outperformed the Naïve and Least Squares predictions in most cases.

### 3.1.4 Testing of Aquifer Storage Volume Estimation in Cedar Valley, Utah

The method of aquifer storage calculation described in Section 2.4 was tested and compared to various study results for the Cedar Valley Aquifer in Southern Utah. This aquifer

has recently experienced land subsidence, the opening of fissures, and some damage to infrastructure because of over pumping of the aquifer (Inkenbrandt, Lund, Lowe, Knudsen, & Bowman, 2014). The aquifer has been the subject of several studies. One difficulty of these studies is the development of an accurate water budget to estimate the storage change of the aquifer. For example, in the USGS conceptual water budget for the year 2000, aquifer recharge was estimated as 42,000 acre-ft/yr, while discharge was estimated at 38,000 acre-ft/yr, a 4,000 acre-ft/yr surplus. This estimated surplus is in direct conflict with observed drawdown of wells in the aquifer, as noted in the USGS report (Brooks & Mason, 2005). The USGS also estimated storage change in the aquifer using a groundwater model, which estimated annual recharge at 27,100 acre-ft/yr and discharge at 34,800 acre-ft/yr, a 7,700 acre-ft/yr deficit. This estimate seems more logical, as it matches the observed trends in lowering groundwater levels in the area. The USGS also estimated recharge in the aquifer using a Chloride mass-balance estimate, which yielded an estimated recharge of 20,800 acre-ft/yr. Last of all, the USGS employed a Basin Characterization Model (BCM) to estimate precipitation recharge throughout the basin. This model estimated recharge at 20,900 acre-ft/yr. The results of these studies, all carried out by the USGS, demonstrate the difficult nature of aquifer storage quantification (Heilweil & Brooks, 2010; Inkenbrandt et al., 2014; Thomas & Taylor, 1946). Based upon these reports and other studies, the Utah Division of Water Rights concluded that "the average annual groundwater deficit is probably about 7,600 acre-feet" over the last fifteen years for the Cedar Valley aquifer (D. P. E. Jones, 2016). Inkenbrandt et al. (2014) concluded that the deficit in 2000 was 10,700 acre-ft.

I used the Groundwater Level Mapping Tool to calculate aquifer storage change for the period from 2000 to 2015, corresponding to the same 15 year period studied by D. P. E. Jones

(2016). In this calculation, I used a specific yield value of 0.1, which was used by Bjorklund,
Sunsion, and Sandberg (1978) and by Inkenbrandt et al. (2014). Following the procedures
outlined in Section 2.2.2 (MLR) for temporal interpolation, Section 2.3.2 (Kriging) for spatial
interpolation, and Section 2.4 for the final calculation, I calculated the change in aquifer storage
volume in the Cedar Valley aquifer between March, 2000 and March, 2015. A time series plot
showing this aquifer depletion as calculated by the Groundwater Level Mapping Tool is
displayed in Figure 3-28.
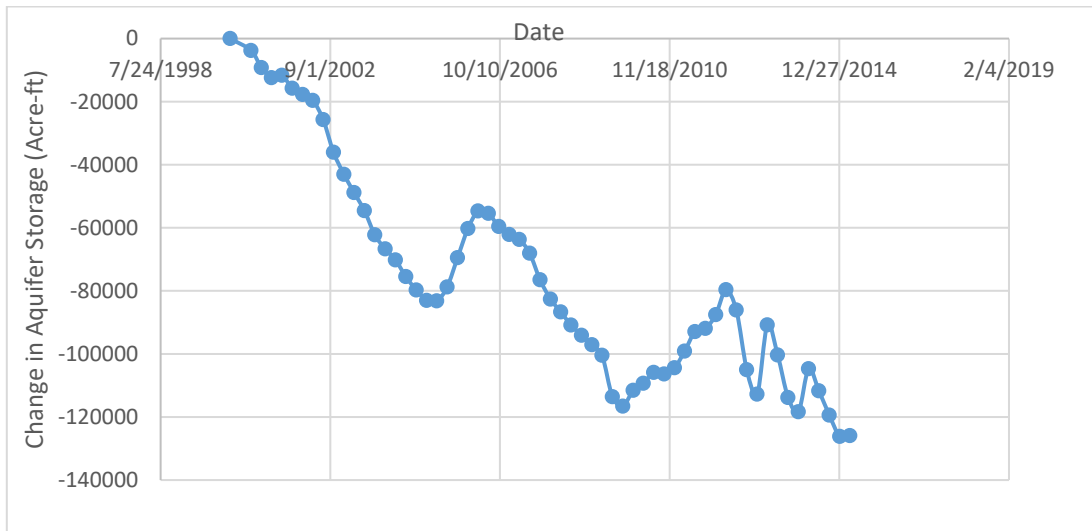


**Figure 3-28: Storage Change since March, 2000 in Cedar Valley Aquifer**

Over the 15-year period, the aquifer was depleted by 125,000 acre-feet, an average of
8,300 acre-feet per year. This value calculated using the Groundwater Level Mapping Tool is
comparable to the USGS/Utah Division of Water Rights calculated value of 7,600 acre-feet per
year. The Groundwater Level Mapping Tool also estimated a water budget deficit of 11,500
acre-feet per year for the year 2000, comparable to the Inkenbrandt et al. (2014) estimate of
10,700 acre-feet per year.

### 3.1.5 Testing of Aquifer Storage Volume Estimation in Beryl Enterprise Area, Utah

The Groundwater Level Mapping Tool was also used to calculate changes in water storage in the Beryl Enterprise Aquifer in southern Utah, shown in Figure 3-29.
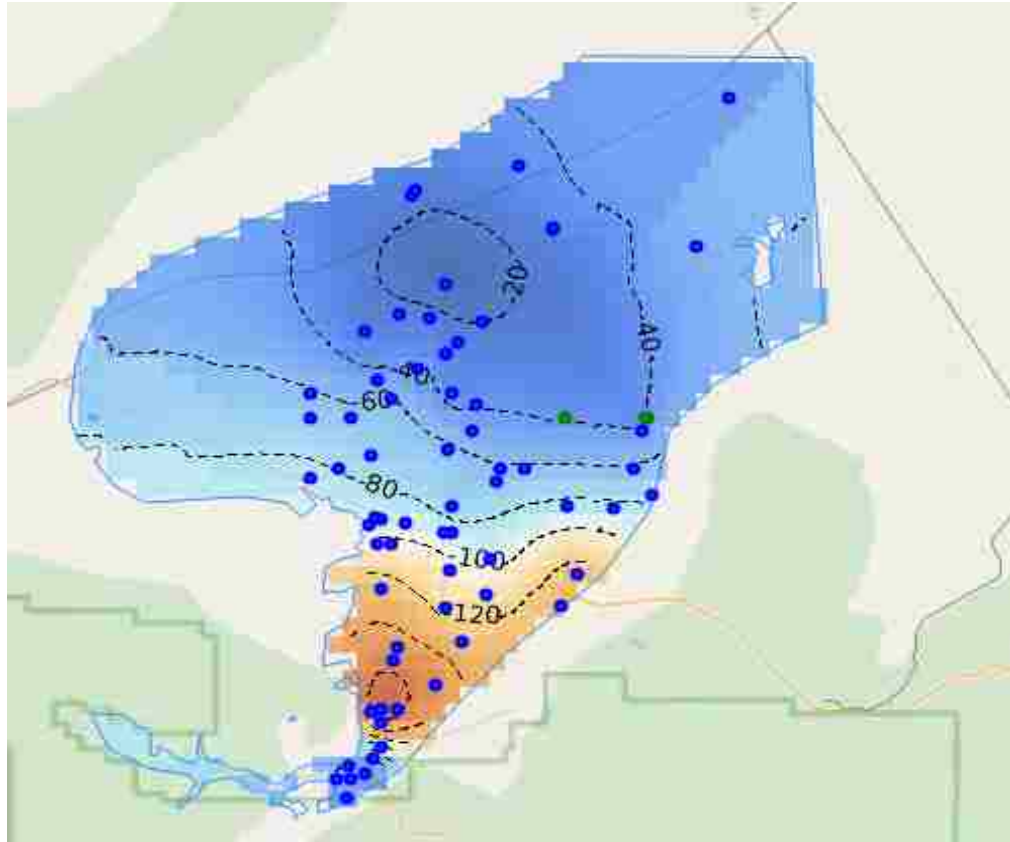


**Figure 3-29: Beryl Enterprise Aquifer in Southern Utah**

The results were compared against a study prepared by the United States Geological Survey in cooperation with the Utah Department of Natural Resources, Division of Water Rights, which concluded that between 1937 and 1978, the aquifer lost between 1.3 and 1.5 million acre-feet of storage (Mower & Sandberg, 1982). Using the USGS estimate of 0.2 as the storage coefficient, the Groundwater Level Mapping Tool calculated a storage loss of 1.45 million acre-feet between 1937 and 1978. The aquifer storage change is shown in Figure 3-30.
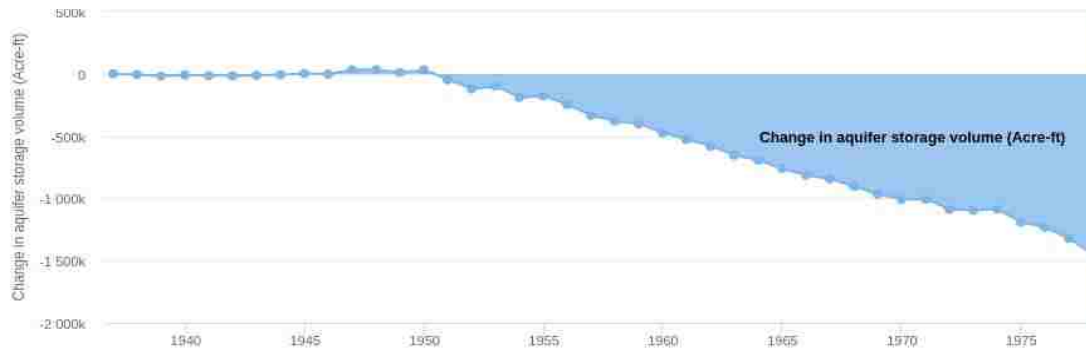
**Figure 3-30: Storage Change since March, 1937 in Beryl Enterprise Aquifer**

The Utah Division of Water Rights estimated that the annual depletion rate of this aquifer around the year 2012 was approximately 65,000 acre-feet per year (K. L. Jones, 2012). The Groundwater Level Mapping Tool estimates this rate as 66,000 acre-feet per year, using a storage coefficient of 0.2, as shown in Figure 3-31.



**Figure 3-31: Storage Loss since March, 2000 in Beryl Enterprise Aquifer**

## 3.2 Texas

I used the Groundwater Level Mapping Tool to analyze 31 aquifers throughout the state of Texas. This was useful for calibrating and validating the tool since the state contains thousands of wells, some with hundreds of depth to groundwater measurements.

### 3.2.1 Testing of Multi-Linear Regression Harnessing Correlated Wells in Texas

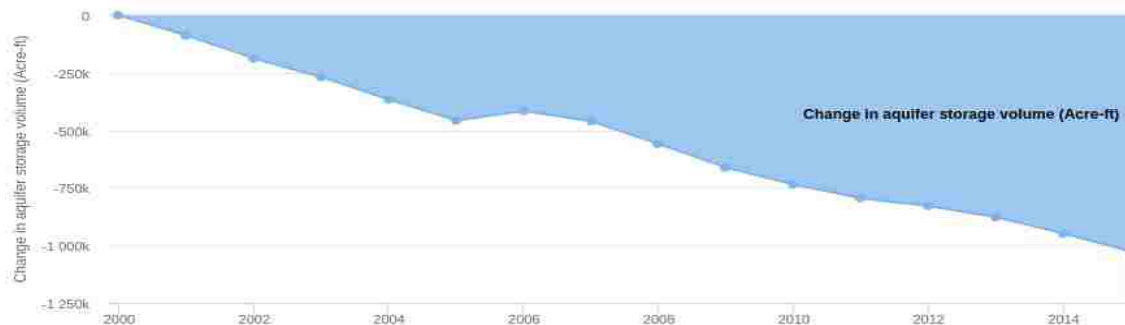The method of time series extension by Multi-Linear Regression Harnessing Correlated Wells (MLR) detailed in Section 2.2.2 was tested using 467 wells located in the Ogallala Aquifer in the Texas Panhandle, each containing data from 1960 – 2010. The area is shown in Figure 3-32. The time series observations from each of these wells were divided into a training set from 1960-1995, and a testing set from 1995-2010. The method of MLR was used to predict the values of depth to water table at each well from 1995-2010 and then compared against the actual values of the testing dataset. Some results of this prediction are shown in Figure 3-33, Figure 3-34, Figure 3-35, Figure 3-36, Figure 3-37, and Figure 3-38 with the training data (green), the measured data (solid red), the MLR prediction (dashed red), the naïve prediction (dashed blue), and the least squares prediction (dashed yellow) for each well.
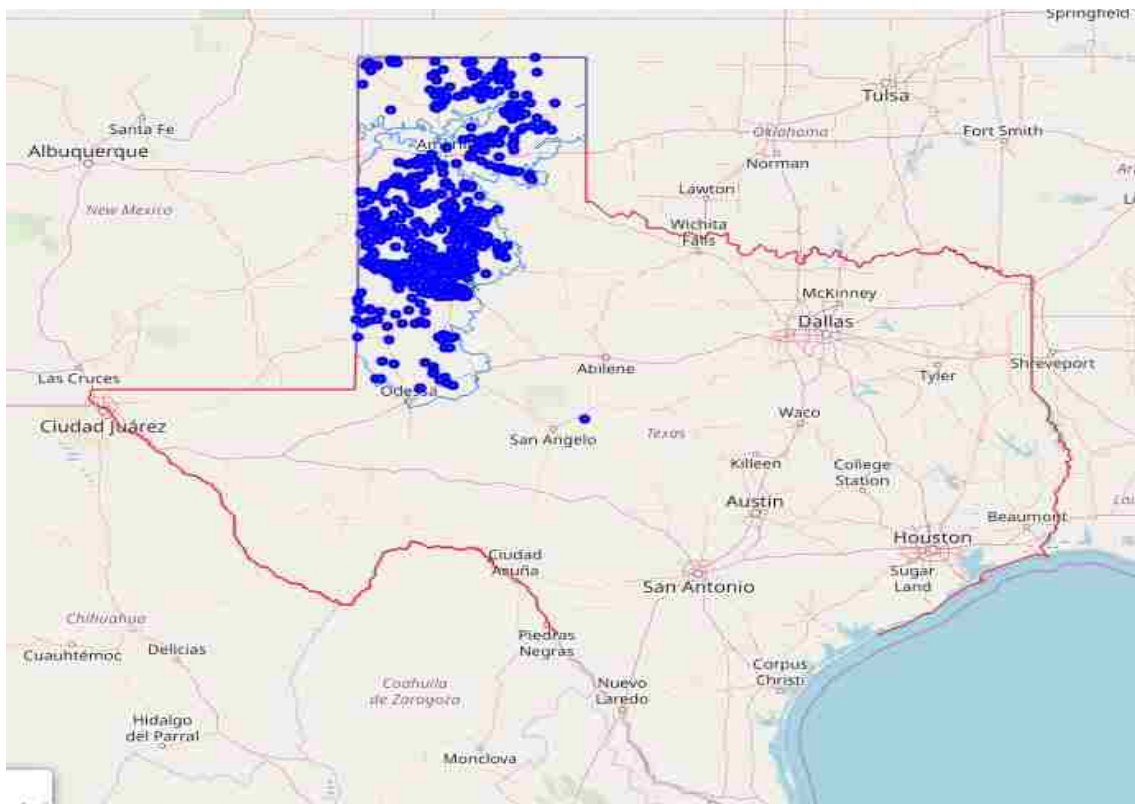


**Figure 3-32: Wells in the Ogallala Aquifer in the Texas Panhandle**

المنارة للاستشارات

www.manaraa.com

**Figure 3-33: Time Series Model for Well 2421301**
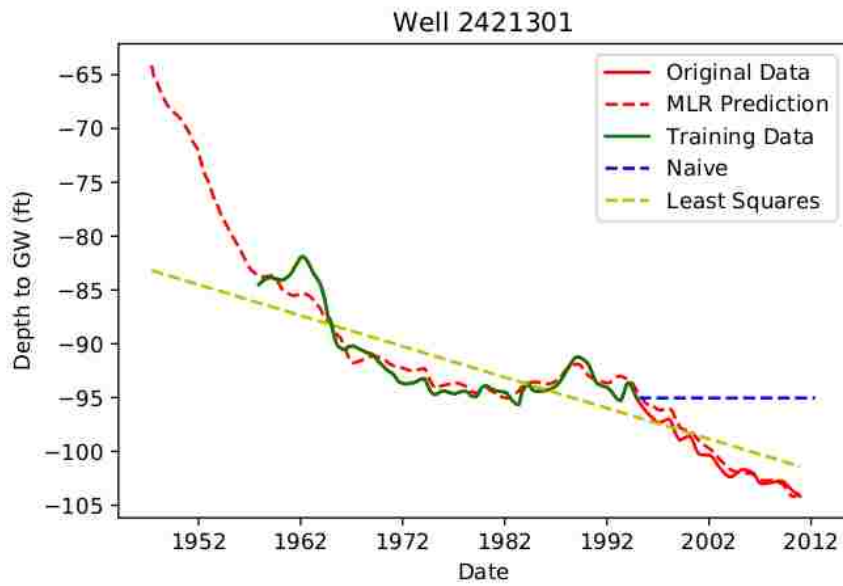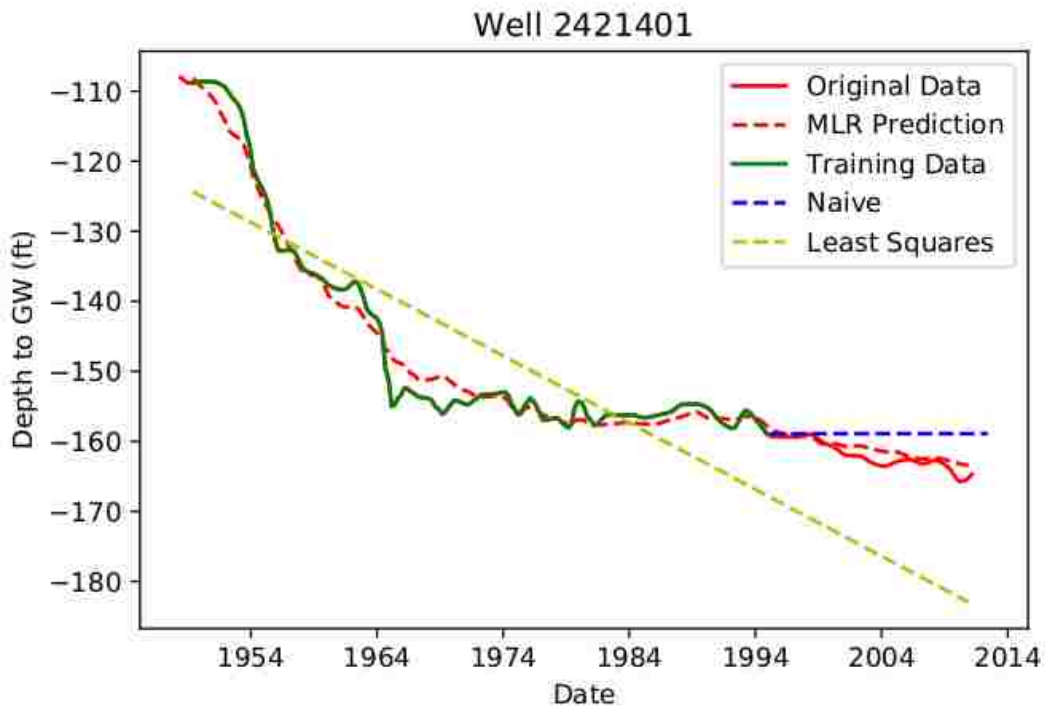


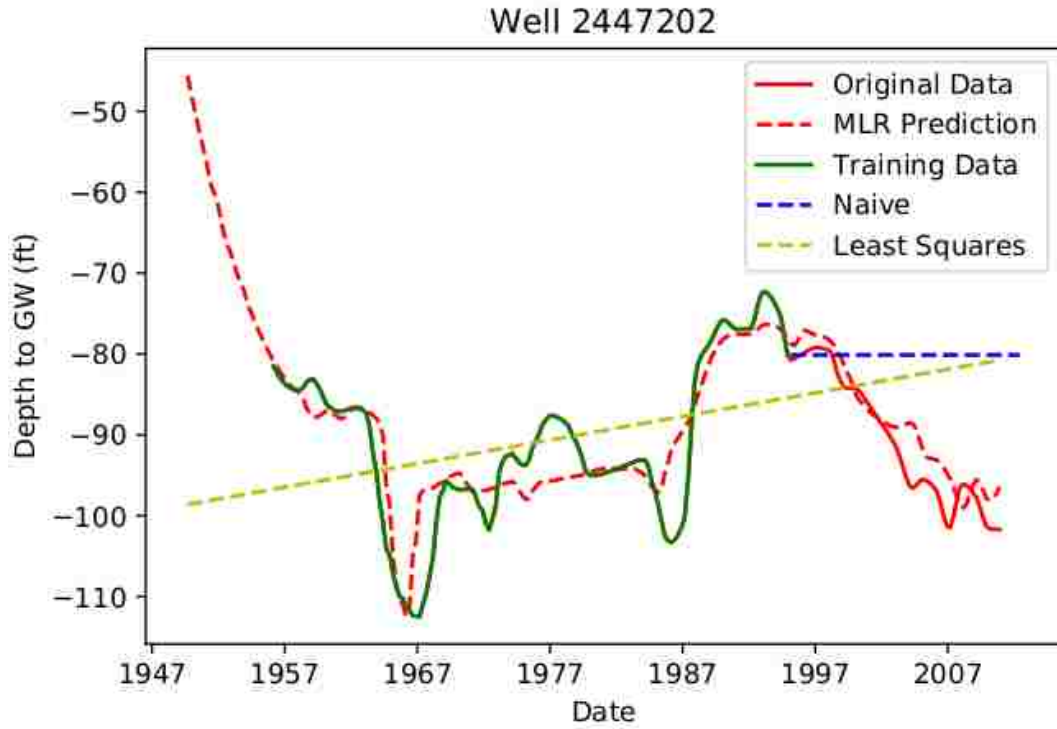**Figure 3-34: Time Series Model for Well 2421401**

65

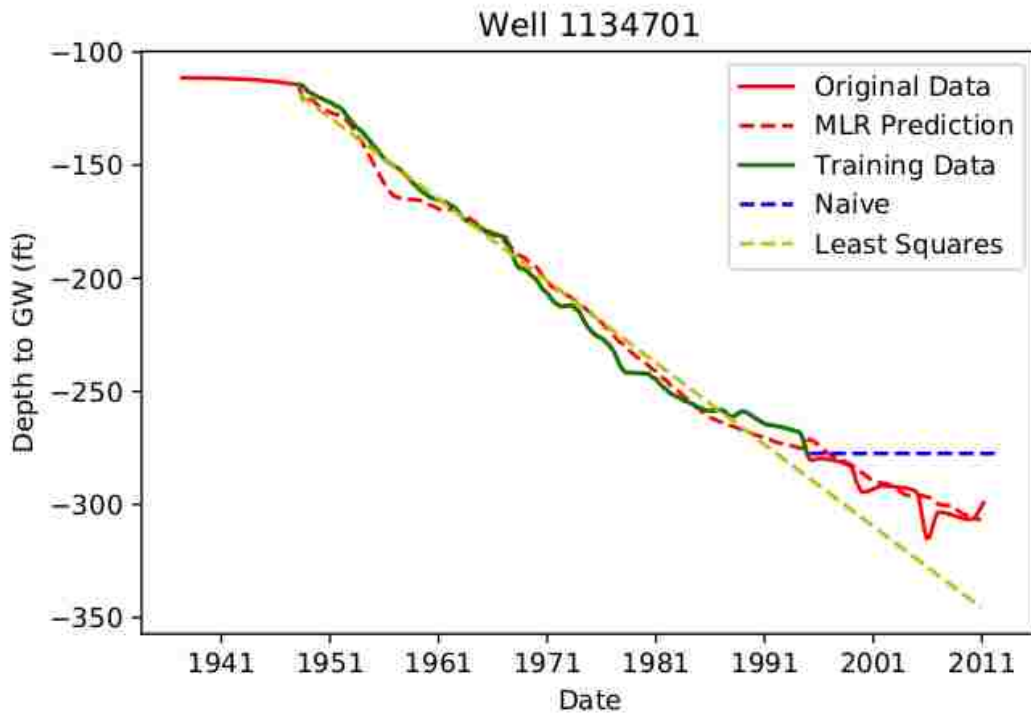**Figure 3-35: Time Series Model for Well 2447202**



**Figure 3-36: Time Series Model for Well 1134701**
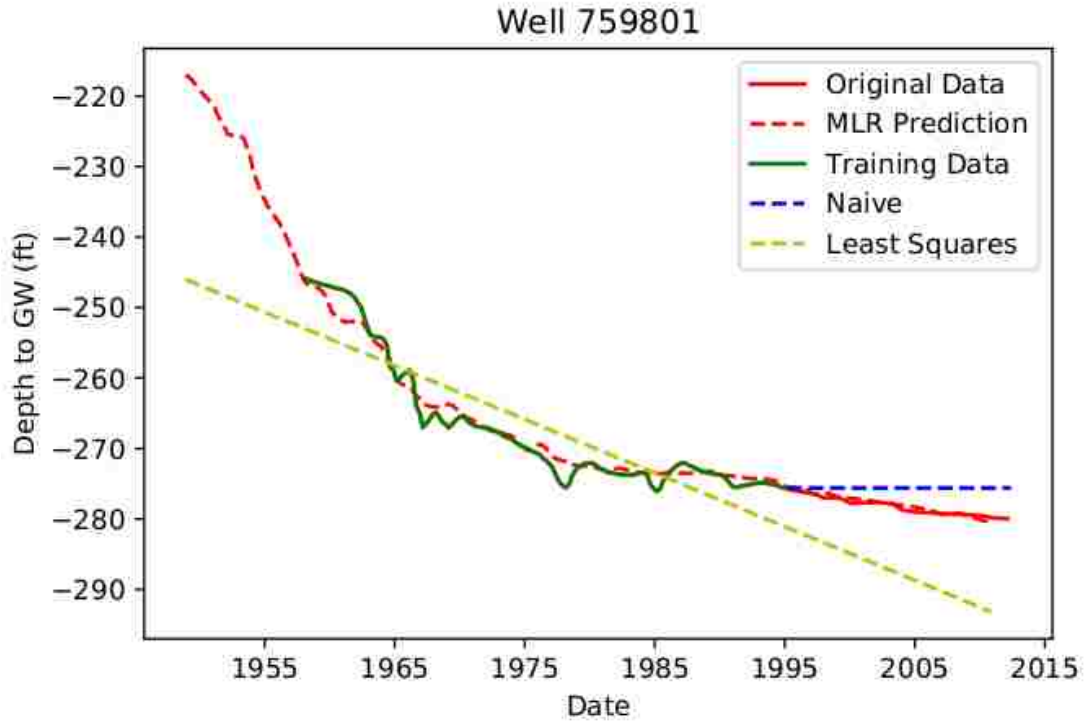
**Figure 3-37: Time Series Model for Well 759801**
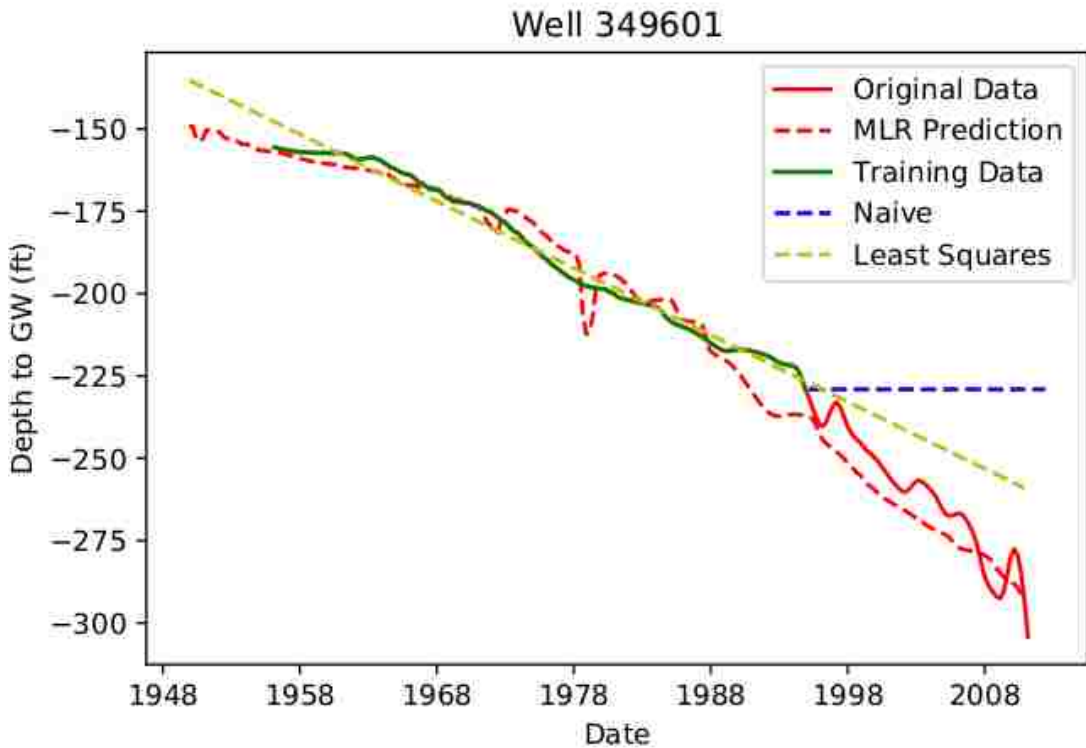


**Figure 3-38: Time Series Model for Well 349601**

As shown in the preceding figures, the MLR method generally outperformed the naïve and least squares methods. As shown in Figure 3-33, Figure 3-34, and Figure 3-35, this MLR method was able to capture a period of decrease in water table elevation following a period of increase, which could not be accomplished with the naïve or least squares method. As shown in Figure 3-36, the MLR model was able to correctly predict a variation from a basically constant decrease in water levels from 1950-1990, while the least-squares method simply continued along the same linear trend line. Figure 3-37 and Figure 3-38 also demonstrate the MLR method's ability to correctly model changes in aquifer depletion rate.

The results of the time series models were compared using the Range Normalized RMSE (NRMSE) method. Table 3-7 shows the mean and median normalized NRMSE values for the 467 tested wells.

**Table 3-7: NRMSE Values for Time Series Models
in the Ogallala Aquifer**

|  | MLR Model | Naïve Prediction | Least Squares Prediction |
|---|---|---|---|
| **Mean** | 0.108 | 0.181 | 0.250 |
| **Median** | 0.076 | 0.145 | 0.211 |

A box and whisker plot of the NRMSE values for the 467 wells is shown in Figure 3-39, with the MLR Model in blue, the Naïve Prediction in orange, and the Least Squares Prediction shown in grey. Overall, the MLR Model exhibited the best results.
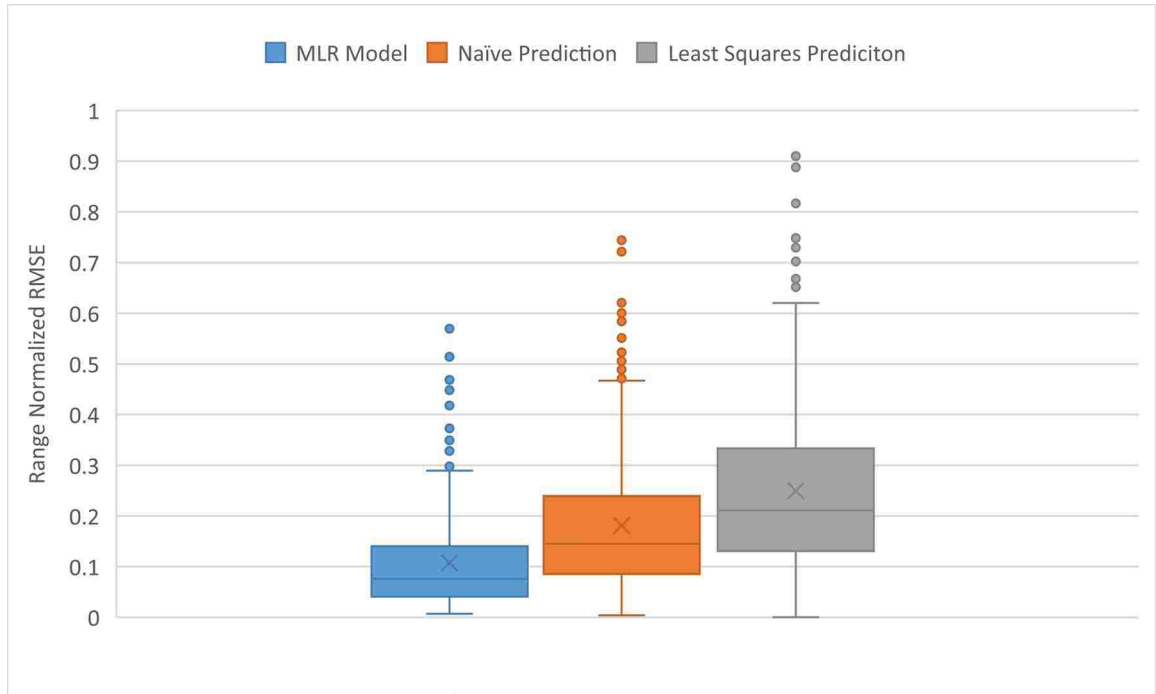
**Figure 3-39: Box and Whisker Plot of NRMSE Values in the Ogallala Aquifer**

The MLR method outperformed both the naïve and least squares method in 314 of the 467 tested wells (67%). In those cases where the naïve prediction outperformed the MLR method, it was generally by a small margin, as shown in Figure 3-40. In this case, the NRMSE value of the MLR model was 0.033, while that of the Naïve prediction was 0.026, both of which are acceptably small errors. The Least Squares method performed the best in those cases where the time series for the well was completely linear, as shown in Figure 3-41. In this case, the MLR method performs well, but with a higher error than the least squares prediction.

69
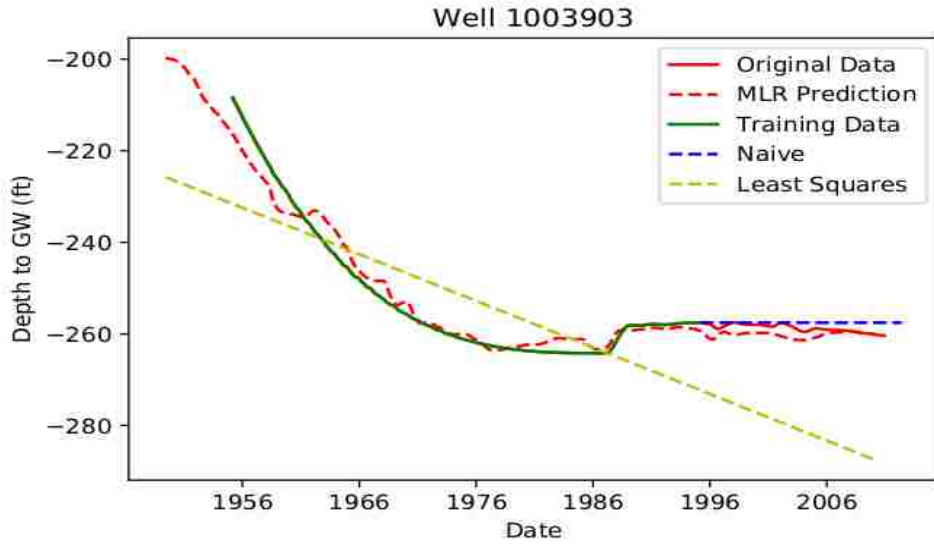
**Figure 3-40: Time Series Model for Well 1003903**
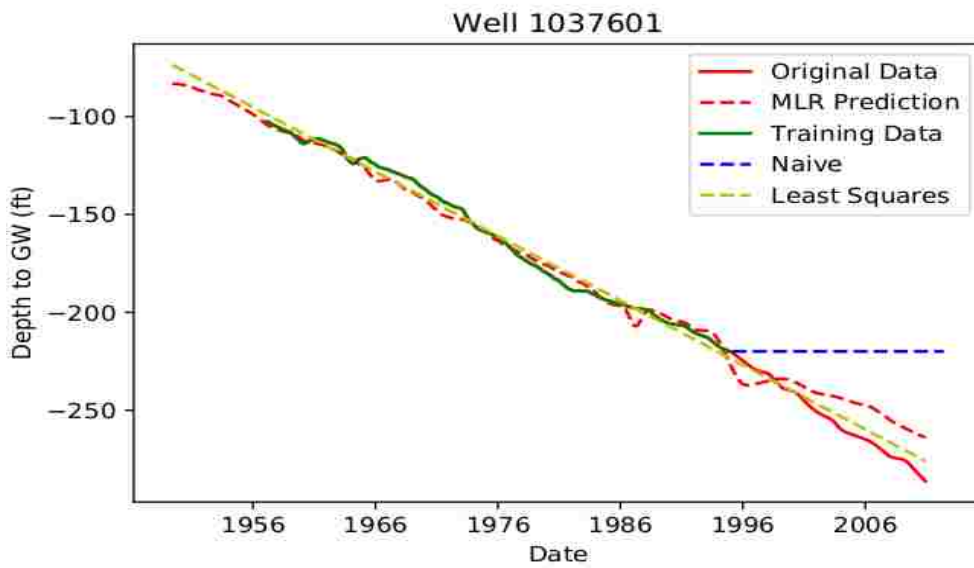


**Figure 3-41: Time Series Model for Well 1037601**

The method of time series extension using Multi-Linear Regression Harnessing Correlated

Wells was also tested for accuracy against Kriging spatial interpolation, using a jackknife

approach. This testing was carried out for 407 wells in the Ogallala Aquifer in the Texas

panhandle. These wells were selected because they each contained time series data from 1960 to

2010, which enabled comparison of the estimates to actual measured values. The depth to groundwater on December 31, 2009 was estimated at each testing well by implementing the PCHIP and then Kriging interpolation, omitting the measured depth at the testing well from the interpolation. The depth to groundwater on December 31, 2009 was then estimated at each testing well by implementing the MLR technique, using data from 1960-1995 as the training set, and then estimating fifteen years of groundwater depths from 1995-2010. The estimated depth to water table obtained from both of these methods were then compared to the measured value for the testing well, and the percent absolute error was measured. Figure 3-42 shows a box and whisker plot of the percent absolute error for both the MLR (blue) and Kriging (orange) methods for these 407 testing wells.
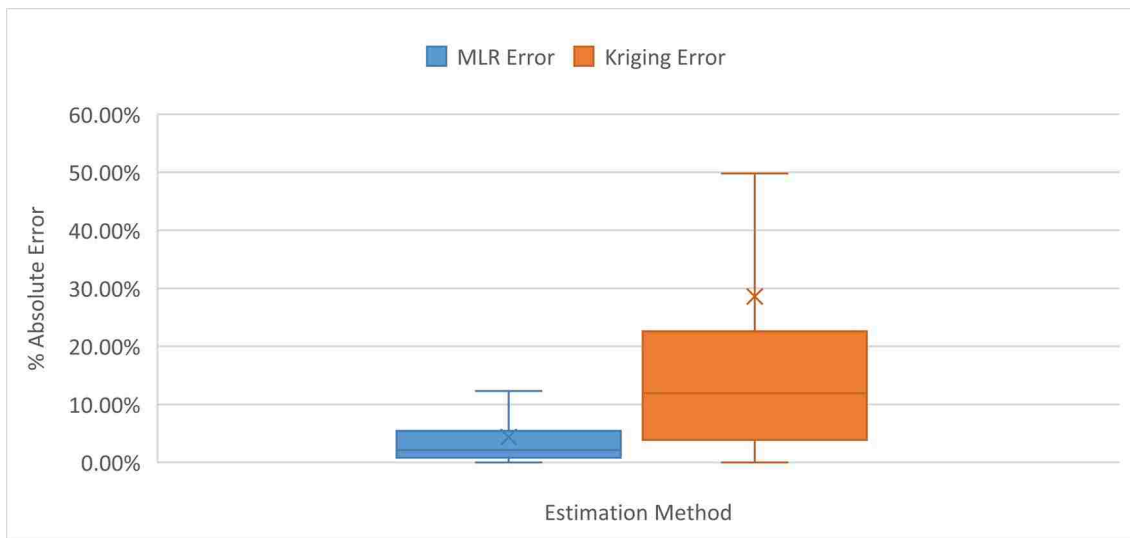


**Figure 3-42: Box and Whisker Plot of Percent Estimation Error in Ogallala Aquifer**

Table 3-8 shows the mean and median absolute percent error, and Table 3-9 shows the mean and median absolute error (ft) for the Kriging and MLR estimates for the 407 wells in the Ogallala Aquifer. The MLR method outperformed the Kriging method significantly. Out of the

71

407 tested wells, 340 estimates (80%) yielded lower error using the MLR method, while 67

(20%) yielded lower error using Kriging. Over 80% of the MLR estimated depths were within

ten feet of the actual measurements, which is quite accurate, considering the average depth to

groundwater in this area is approximately 200 feet.

**Table 3-8: Mean and Median Absolute Percent
Error for 417 Wells in the Ogallala Aquifer**

| Test Statistic | MLR Method | Kriging Method |
|---|---|---|
| Mean Absolute  Percent Error | 4.35% | 29.35% |
| Median Absolute Percent Error | 2.11% | 12.82% |

**Table 3-9: Mean and Median Absolute Error
for 417 Wells in the Ogallala Aquifer**

| Test Statistic | MLR Method | Kriging Method |
|---|---|---|
| Mean Absolute Error | 6.2 ft | 26.4 ft |
| Median Absolute Error | 3.5 ft | 19.1 ft |

### 3.2.2   Testing of Aquifer Storage Volume Estimation in Hueco Bolson, Texas

The method of aquifer storage calculation described in Section 2.4 was tested and

compared to a USGS report for the Texas portion of the Hueco Bolson near El Paso, Texas. The

Texas portion of the aquifer is shown in Figure 3-43.
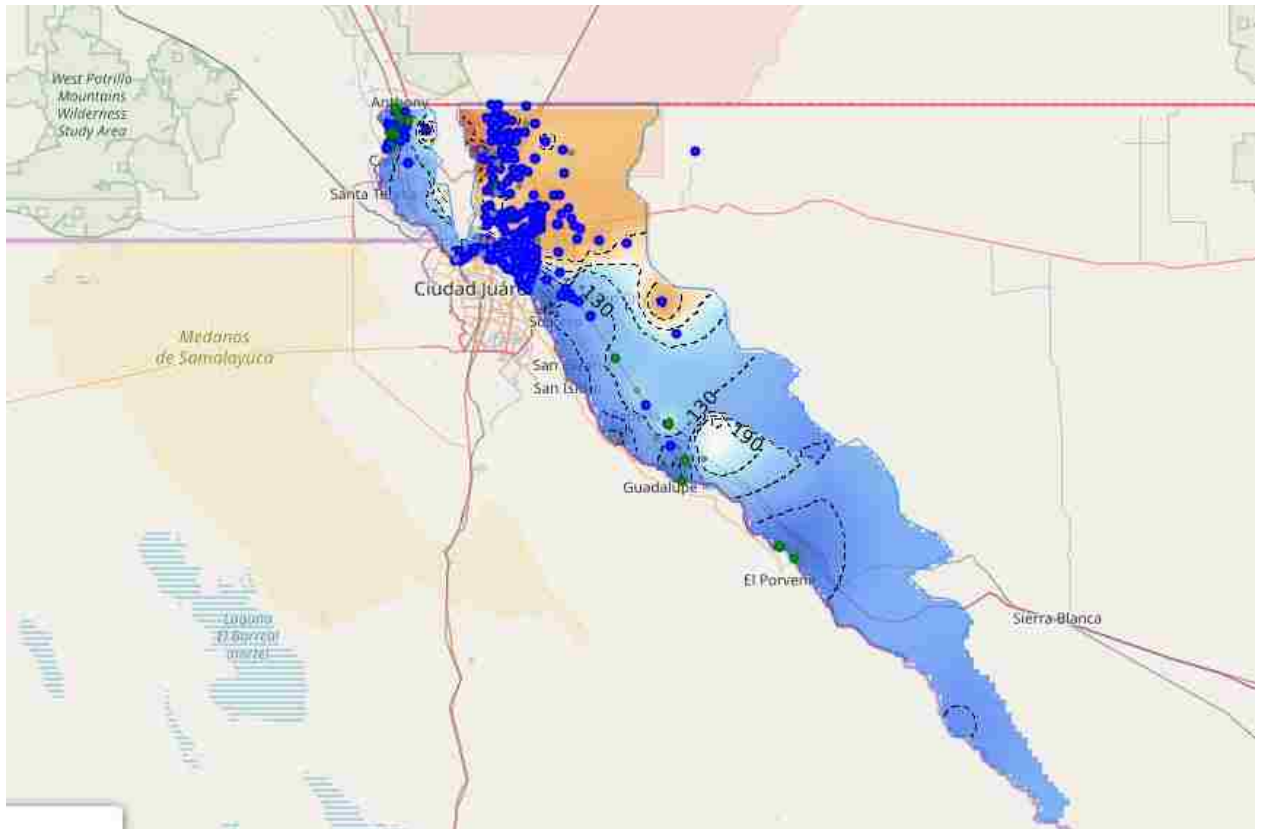
**Figure 3-43: Hueco Bolson near El Paso, Texas**

Based on a USGS model, Bredehoeft, Ford, Harden, Mace, and Rumbaugh III (2004) estimated the aquifer depletion rate of this Texas portion of the Hueco Bolson as between 18,000-33,000 acre-feet per year. The wide range implies the uncertainty of the estimate. The USGS determined that the specific yield of the aquifer was between 0.1 and 0.2, and calibrated their groundwater model with a specific yield of 0.178 for the unconfined portions, and a specific storage value of $7.6 * 10^{-5}$ per meter for the confined portions of the aquifer (Heywood & Yager, 2003). In my calculations using the Groundwater Level Mapping Tool, I used a storage coefficient of 0.15 to represent the aquifer. Using this value, I estimated the average aquifer depletion rate of the Hueco Bolson as 28,000 acre-feet per year. This depletion of the Hueco

73

Bolson determined using this storage coefficient is shown in Figure 3-44. This calculation is similar to the USGS estimate, indicating the utility of the Groundwater Level Mapping Tool for quickly estimating aquifer depletion. If the storage coefficient were adjusted to 0.1 or 0.2, then the aquifer depletion rate estimated using the Groundwater Level Mapping Tool becomes 18,000 acre-feet per year or 37,000 acre-feet per year, respectively (again, similar to the USGS estimate).



**Figure 3-44: Storage Change since December, 1994 in Hueco Bolson**

## 4 CONCLUSIONS

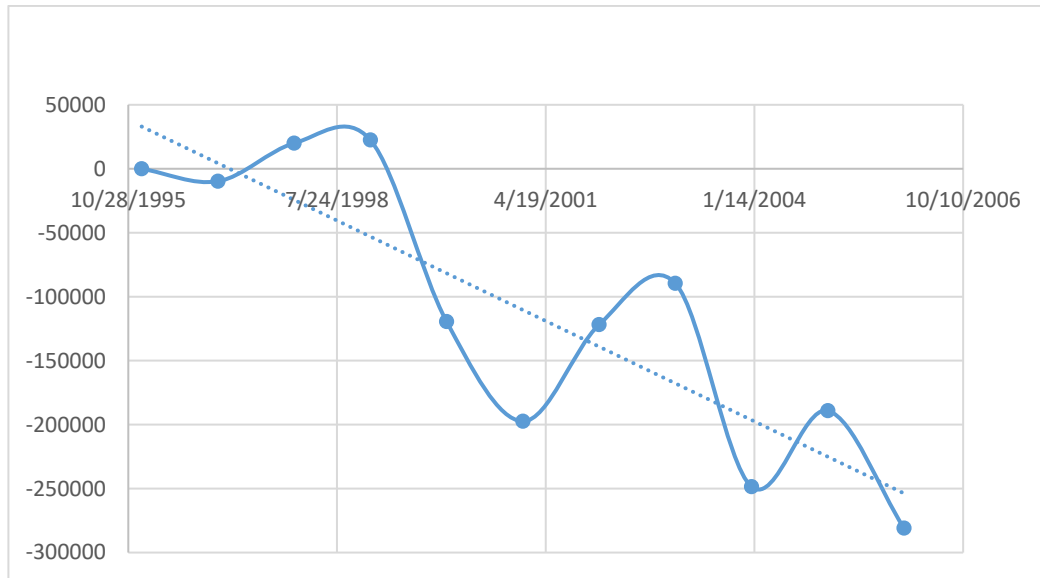The Groundwater Level Mapping Tool developed during this research has the potential for world-wide use, allowing water managers and other decision makers to quickly and easily view trends in aquifer storage levels. I developed the application to generate maps and animations of groundwater levels and drawdown which can be used to inform decision makers, enabling them to identify areas of concern and develop groundwater management plans to ensure the long term sustainability of aquifers.

In addition to these animations, I developed a quick, simple, automated method within the Groundwater Level Mapping Tool to estimate changes in total aquifer storage, which is typically a painstaking, laborious task. This automated method yielded results comparable to several detailed USGS studies in Utah's Cedar Valley, Utah's Beryl-Enterprise area, and Texas' Hueco Bolson. These aquifer storage estimates can be used to develop a water budget and identify the safe yield of water withdrawal at which aquifers can continue sustainably.

I improved the accuracy of these aquifer storage estimates by developing a new method of temporal interpolation, Multi-Linear Regression Harnessing Correlated Wells (MLR). This method of temporally extrapolating recorded data to unsampled time periods using data from other wells outperformed the typical Kriging spatial interpolation method. This is significant, since researchers using different temporal interpolation methods have previously concluded that

75

"spatial structure was a little bit stronger than temporal structure," and that it was more accurate to interpolate spatially than temporally (Ahmadi & Sedghamiz, 2007).

I also developed an experimental method for expanding time series data using PDSI and Soil Moisture models, driven by satellite Earth observations as well as land based observations. This method uses an extreme learning machine (ELM) to infer groundwater levels from these observations. Results from this method were not as good as from the MLR method, but I demonstrated that groundwater levels are correlated to, and can be inferred from Earth observations. This method was most accurate in areas not subject to excessive groundwater pumping. As the GRACE mission continues to make improvements and gather more data, this method will become more and more accurate and useful. This method could also be improved by incorporating a term to capture the aquifer pumping rate.

In conclusion, the Groundwater Level Mapping Tool developed during this research enables water managers to make informed decisions and implement wise management plans and regulations regarding the sustainable use of aquifers world-wide.

76

# REFERENCES

Abidin, H. Z., Andreas, H., Djaja, R., Darmawan, D., & Gamal, M. (2008). Land subsidence characteristics of Jakarta between 1997 and 2005, as estimated using GPS surveys. *Gps Solutions, 12*(1), 23-32.

Ahmadi, S. H., & Sedghamiz, A. (2007). Geostatistical analysis of spatial and temporal variations of groundwater level. *Environmental monitoring and assessment, 129*(1-3), 277-294.

Bidwell, V. J. (2005). Realistic forecasting of groundwater level, based on the eigenstructure of aquifer dynamics. *Mathematics and Computers in Simulation, 69*(1-2), 12-20.

Bjorklund, L. J., Sunsion, C., & Sandberg, G. W. (1978). *Ground-water resources of the Parowan-Cedar City drainage basin, Iron County, Utah*. Retrieved from Utah Department of Natural Resources, Division of Water Rights.

Boezio, M., Costa, J., & Koppe, J. J. A. E. S. (2006). Kriging with an external drift versus collocated cokriging for water table mapping. *115*(3), 103-112.

Bredehoeft, J., Ford, J., Harden, B., Mace, R., & Rumbaugh III, J. (2004). Review and Interpretation of the Hueco Bolson Groundwater Model. *El Paso Water Utilities*.

Brooks, L. E., & Mason, J. L. (2005). *Hydrology and simulation of ground-water flow in Cedar Valley, Iron County, Utah* (2328-0328). Retrieved from US Geological Survey.

Burden, C. B. (2015). *Groundwater conditions in Utah, spring of 2015*. Retrieved from Utah Department of Natural Resources, Division of Water Rights.

Chen, M., Xie, P., Janowiak, J. E., & Arkin, P. A. (2002). Global land precipitation: A 50-yr monthly analysis based on gauge observations. *Journal of Hydrometeorology, 3*(3), 249-266.

Dai, A. N. C. f. A. R. S. E. (2019). The Climate Data Guide: Palmer Drought Severity Index (PDSI). Retrieved from https://climatedataguide.ucar.edu/climate-data/palmer-drought-severity-index-pdsi

Deutsch, C. V., & Journel, A. (1992). GSLIB: geostatistical library and user's guide. In: NY, Oxford University Press.

Fan, Y., & Van den Dool, H. (2008). A global monthly land surface air temperature analysis for 1948–present. *Journal of Geophysical Research: Atmospheres, 113*(D1).

Franke, R., & Nielson, G. (1980). Smooth interpolation of large sets of scattered data. *International journal for numerical methods in engineering, 15*(11), 1691-1704.

Fritsch, F. N., & Carlson, R. E. (1980). Monotone piecewise cubic interpolation. *SIAM Journal on Numerical Analysis, 17*(2), 238-246.

Galloway, D., & Riley, F. S. (1999). San Joaquin Valley, California. *Land subsidence in the United States: US Geological Survey Circular, 1182*, 23-34.

Gleick, P. H. (1993). Water in crisis. *Pacific Institute for Studies in Dev., Environment & Security. Stockholm Env. Institute, Oxford Univ. Press. 473p, 9.*

Gundogdu, K. S., & Guney, I. J. J. o. E. S. S. (2007). Spatial analyses of groundwater levels using universal kriging. *116*(1), 49-55.

Heilweil, V. M., & Brooks, L. E. (2010). Conceptual model of the Great Basin carbonate and alluvial aquifer system. *US Geological Survey Scientific Investigations Report, 5193*(2011), 191.

Heywood, C. E., & Yager, R. M. (2003). Simulated groundwater flow in the Hueco Bolson, an alluvialbasin aquifer system near El Paso, Texas. *Water-Resources Investigations Report, 2*, 4108.

Huang, G.-B. (2015). What are extreme learning machines? Filling the gap between Frank Rosenblatt's dream and John von Neumann's puzzle. *Cognitive Computation, 7*(3), 263-278.

Huang, J., van den Dool, H. M., & Georgarakos, K. P. (1996). Analysis of model-calculated soil moisture over the United States (1931–1993) and applications to long-range temperature forecasts. *Journal of Climate, 9*(6), 1350-1362.

Inkenbrandt, P., Lund, W., Lowe, M., Knudsen, T., & Bowman, S. (2014). *Investigation of land subsidence and earth fissures in Cedar Valley, Iron County, Utah* (Vol. 150): Utah Geological Survey.

Jones, D. P. E. (2016). *Annual Recharge Estimate for Cedar City Valley*. Retrieved from Utah Department of Natural Resources: Division of Water Rights.

Jones, K. L. (2012). *Beryl Enterprise Groundwater Management Plan*. Retrieved from Utah Department of Natural Resources: Division of Water Rights.

Khorasani, M., Ehteshami, M., Ghadimi, H., & Salari, M. (2016). Simulation and analysis of temporal changes of groundwater depth using time series modeling. *Modeling Earth Systems and Environment, 2*(2), 90.

Kitanidis, P. K. (1997). *Introduction to geostatistics: applications in hydrogeology*: Cambridge University Press.

McKinney, W. (2010). *Data structures for statistical computing in python.* Paper presented at the Proceedings of the 9th Python in Science Conference.

Mirzavand, M., & Ghazavi, R. (2015). A stochastic modelling technique for groundwater level forecasting in an arid environment using time series methods. *Water Resources Management, 29*(4), 1315-1328.

Moritz, H. (1980). Geodetic reference system 1980. *Journal of Geodesy, 54*(3), 395-405.

Mower, R. W., & Sandberg, G. W. (1982). *Hydrology of the Beryl-Enterprise area, Escalante Desert, Utah, with emphasis on ground water; With a section on surface water*. Retrieved from Utah Department of Natural Resources, Division of Water Rights.

Nikroo, L., Kompani-Zare, M., Sepaskhah, A. R., & Shamsi, S. R. F. (2010). Groundwater depth and elevation interpolation by kriging methods in Mohr Basin of Fars province in Iran. *Environmental monitoring and assessment, 166*(1-4), 387-407.

Ortega-Guerrero, A., Rudolph, D. L., & Cherry, J. A. (1999). Analysis of long-term land subsidence near Mexico City: Field investigations and predictive modeling. *Water Resources Research, 35*(11), 3327-3341.

Rodell, M., Houser, P., Jambor, U., Gottschalck, J., Mitchell, K., Meng, C.-J., . . . Bosilovich, M. (2004). The global land data assimilation system. *Bulletin of the American Meteorological Society, 85*(3), 381-394.

Rouhani, S., & Wackernagel, H. J. W. R. R. (1990). Multivariate geostatistical approach to space-time data analysis. *26*(4), 585-591.

Sahoo, M., Dhar, A., Kasot, A., & Kar, A. J. J. o. H. E. (2018). Space-Time Cokriging Approach for Groundwater-Level Prediction with Multiattribute Multiresolution Satellite Data. *23*(7), 05018012.

Sahoo, S., & Jha, M. K. J. H. J. (2013). Groundwater-level prediction using multiple linear regression and artificial neural network techniques: a comparative assessment. *21*(8), 1865-1887.

Sethi, R. R., Kumar, A., Sharma, S., & Verma, H. (2010). Prediction of water table depth in a hard rock basin by using artificial neural network. *International Journal of Water Resources and Environmental Engineering, 4*(2), 95-102.

Sun, A. Y. (2013). Predicting groundwater level changes using GRACE data. *Water Resources Research, 49*(9), 5900-5912.

Swain, N. R., Christensen, S. D., Snow, A. D., Dolder, H., Espinoza-Dávalos, G., Goharian, E., . . . Burian, S. J. (2016). A new open source platform for lowering the barrier for environmental web app development. *Environmental modelling & software, 85*, 11-26.

Swenson, S., Wahr, J., & Milly, P. (2003). Estimated accuracies of regional water storage variations inferred from the Gravity Recovery and Climate Experiment (GRACE). *Water Resources Research, 39*(8).

Tapley, B. D., Bettadpur, S., Ries, J. C., Thompson, P. F., & Watkins, M. M. (2004). GRACE measurements of mass variability in the Earth system. *Science, 305*(5683), 503-505.

Thomas, H. E., & Taylor, G. H. (1946). *Geology and ground-water resources of Cedar City and Parowan Valleys, Iron County, Utah*. Retrieved from Utah Department of Natural Resources, Division of Water Rights.

Tikhonov, A. N., & Arsenin, V. I. (1977). *Solutions of ill-posed problems* (Vol. 14): Winston, Washington, DC.

Zhu, W., Miao, J., & Qing, L. (2014). *Constrained extreme learning machine: a novel highly discriminative random feedforward neural network.* Paper presented at the 2014 International Joint Conference on Neural Networks (IJCNN).